DEVELOPMENT AND CHARACTERIZATION OF DNA APTAMER AND MICROFLUIDIC PAPER BASED PLATFORM FOR DETECTION OF HEART TYPE FATTY ACID BINDING PROTEIN

A thesis

Submitted by

ANKANA KAKOTI

For the award of the degree

of

Doctor of Philosophy

DEPARTMENT OF BIOSCIENCES AND BIOENGINEERING

INDIAN INSTITUTE OF TECHNOLOGY GUWAHATI

GUWAHATI-781039, ASSAM, INDIA

JUNE 2016

Dedicated to my family and all those who encouraged me to fly toward my dreams.

INDIAN INSTITUTE OF TECHNOLOGY GUWAHATI
Department of Biosciences and Bioengineering
Guwahati-781039

STATEMENT

I do hereby declare that the matter embodied in this thesis is the result of investigations carried out by me in the Department of Biosciences and Bioengineering, Indian Institute of Technology Guwahati, Assam, India, under the guidance of Prof. Pranab Goswami.

In keeping with the general practice of reporting scientific observations, due acknowledgements have been made wherever the work described is based on the findings of other investigators.

June, 2016 Ankana Kakoti

INDIAN INSTITUTE OF TECHNOLOGY GUWAHATI
Department of Biosciences and Bioengineering
Guwahati-781039

CERTIFICATE

It is certified that the work described in this thesis, entitled "*Development and characterization of DNA aptamer and microfluidic paper based platform for detection of heart type fatty acid binding protein*", done by Miss. Ankana Kakoti (Roll No. 10610610) for the award of degree of Doctor of Philosophy is an authentic record of the results obtained from the research work carried out under my supervision in the Department of Biosciences and Bioengineering, Indian Institute of Technology Guwahati, India.

The results embodied in this thesis have not been submitted to any other University or Institute for the award of any degree.

June, 2016

Prof. Pranab Goswami

(Supervisor)

ACKNOWLEDGEMENT

Finally at the end of a seemingly endless journey towards producing this thesis, I get a leaf for expressing my heartfelt gratitude to all those persons whose comments, questions, criticism, support and encouragement, personal as well as academic, have left a mark on this work. As opposed to what I had perceived, putting into words the deep appreciation for everyone turned out to be the most difficult part of my thesis. My efforts might not be enough to thank everyone involved and inevitably this list would be incomplete, however, I hope that they accept my sincere appreciation of their influence in my work.

First and foremost, I would like to express my deepest gratitude to my Ph.D. supervisor Prof. Pranab Goswami for providing me with all the freedom to explore on my own and at the same time guidance whenever I faltered. I would always be thankful to him for providing me with the opportunity to conduct my research work in his lab which was a stimulating experience. I would always be indebted for the conviction you showed on my abilities and teaching me the art of patience. Thank you Sir for keeping your cool when I had lost mine.

Next, I would like to acknowledge the members of my doctoral committee Dr. Anil Mukund Limaye, Prof. Aiyagari Ramesh and Prof. Sunil K Khijwania for their constructive criticism and helpful suggestions during the course of my thesis work. I would also like to acknowledge all the former and present Heads of the Department, faculty members and all the staff members of the Department of Biosciences and Bioengineering, IIT Guwahati for providing me with their immeasurable help and assistance. I would also like to thank the Central Instruments Facility,

IITG and Centre for Energy for providing access to various instrumentation facilities without which this work would not have been possible.

The influence of those who inspired me to take up research and provided me with the foundations for fulfilling my aims, continues to be significant. Prof. Alak Kr Buragohain finds special mention for his contribution in inspiring me at a time when I had lost my way. I am indebted to Dr. Laishram I Singha and Dr. Mostaque A Laskar for their guidance and support during my Masters and inculcating in me good research cultures.

I would like to extend my thanks to the Biosensors group members for equally sharing my trials and tribulations as well as my successes. Special thanks to the senior members Preety Vatsyayan, Urmila Saxena, Seraj Ahmad, Mitun Chakraborty, Somasekhar Reddy, Madhuri Das and Adepu Kiran Kumar for their guidance and support during the initial stages of the work. I sincerely thank my wonderful lab fellows Santhosh, Priyamvada, Babina, Naveen, Phurpa, Mrinal, Priyanki, Sharbani, Abdul, Vinay and Smita for providing such a fun loving environment in the research lab that working in the lab was one of the best times spent in IITG. I am grateful to Mr. Farhan Siddiqui (M.Tech project student) for his significant contributions in carrying out the microfluidics section of my thesis.

This acknowledgement would be incomplete without the mention of my friends who made my stay in IITG a fulfilling one. The tea parties, outings, card games, discussions over coffee, cooking, crafts, the long walks we took were the actual stressbusters. Thank you Gauri, Debamitra, Priyamvada, Babina and Phurpa for the great times in the campus. I would also like to thank my batchmates Tulsi, Ankita, Arghya and Nand Kishor for their help as well as for the "whining sessions" that we shared so intimately. A special thanks to my decade old friends Ifti, Munmee,

Parama, Archi, Tabha, Anusree, Madhurima, and Fahmin for making my life worthwhile. Thank you for being this crazy bunch without whom my life would be so mundane.

Finally, I express my deepest gratitude to my parents for their unconditional support and love. If not for their encouragement and freedom, I would never have achieved this milestone. "I want to thank you for always understanding the things I said, the things I didn't say and the things I never planned on telling you. Thank you for understanding me always." A special thanks to my siblings for holding the fort while I was gone and sharing my bit of responsibilities. I would also like to thank Himangshu for his love, support and understanding throughout these years.

Above all, I thank God for giving me the strength to go on through the storms as well as the sunshine.

Ankana Kakoti

June, 2016

Contents

Abstract

The current investigation is centered on the development of specific aptamers against human heart type fatty acid binding protein (FABP3), a novel early marker for detection of acute myocardial infarction (AMI). It also encompasses the detection of FABP3 using the developed aptamers on a specially designed paper based microfluidic device (µPAD). For generating specific aptamers for FABP3, recombinant FABP3 was selected as the target while recombinant FABP1, FABP4 and FABP7 were chosen as controls. The coding sequences of all the four proteins were separately sub cloned into the pGEX-4T2 expression vector and transformed into BL21 (DE3) cells. Recombinant FABP3, FABP1 and FABP4 expression was induced at an IPTG concentration of 100 µM for 12 hrs at 37 ^{o}C, while expression of FABP7 was accomplished at an IPTG concentration of 50 µM for 12 hrs at 30 ^{o}C. The recombinant proteins were purified using glutathione agarose affinity chromatography and confirmed by SDS-PAGE and Western blots. All the recombinant proteins retained their correct secondary structures suggested by their CD spectra which were dominated by β-sheets. Systematic Evolution of Ligands by Exponential Enrichment (SELEX) was employed to generate aptamers against FABP3. A total of 20 SELEX cycles were performed, out of which 8 were counter SELEX cycles incorporating the control proteins. The enriched pool was cloned into TA vectors and the positive clones were selected on the basis of blue-white screening and restriction enzyme digestion. Sequencing and alignment studies of 50 positive clones revealed seven sequences were enriched at levels more than the others. EMSA and CD studies in the presence of FABP3 and the control proteins were conducted to study the specificity of the enriched sequences. Out of the seven aptamers, two aptamers (N13 and N53) were found to bind FABP3

specifically with dissociation constants (K_d) 0.0743 ± 0.0142 µM and 0.3337 ± 0.1485 µM, respectively. Both the aptamers shared a stem loop structure as predicted by Mfold which was confirmed through CD studies. Aptamer stability studies were performed to evaluate its behavior at different pH, temperature and ionic strength. Both the aptamers were stable at high salt concentrations in the settings of the binding buffer. Additionally at neutral and slightly alkaline pH, the aptamers were stable, however at acidic and highly alkaline conditions, the CD spectra of the aptamers deviated from the normal. Both the aptamers were thermally stable with melting temperatures of 60.7 ± 0.9 ^{o}C and 53 ± 8.0 ^{o}C for N13 and N53, respectively. Furthermore, singular value decomposition (SVD) analysis of 3D melting curves indicated that both the aptamers exist in a simple two state form without the formation of higher ordered structures. The evolved aptamers though showed comparable specificity towards the target, a significant sequence variation between them and their different binding affinity to the target prompted to explore the distribution pattern of diverse chemical forces involved in these interactions to corroborate the bindings. Considering the large sizes of the aptamers, limited proteolysis of the aptamer-protein complex was performed to map the amino acids involved in binding, which was then used to screen docked structures. The N13 aptamer led interaction with stronger affinity, involving more salt bridges (three) and fewer hydrogen bonds (two), whereas N53 had less number of salt bridges (two) with higher number of hydrogen (eight) and hydrophobic interactions. It is suggested that the greater footprint of N53 incited synergistic conformational changes in N53 and FABP3 leading to decrease in binding affinity during the recognition.

To utilize the aptamers so developed as a bio recognition element on a µPAD for FABP3 detection, we designed a microfluidic platform using a modified negative photolithography technique. The modified technique allowed the partial polymerization of photoresist on the rear of

the device, which acts a leak proof layer. The presence of the partial photoresist layer was confirmed through AFM, FESEM and normal imaging under a microscope. This modification reduces the cost of laminating both sides of the device thereby reducing the overall device cost to $ 0.048 (as on Dec. 2014). The partial layer of photoresist on the device channel limits sample volume to 7 ± 0.2 µl as compared to devices without the partial photoresist layer which requires a larger sample volume of 10 ± 0.1 µl. The partially laminated device was then coupled with an externally fabricated test zone that allowed controlled loading of reagents as well as modification steps for incorporating reagents covalently without any spillage to the other zones of the device. In the coupled device the wicking speed was reduced to 1.8 ± 0.9 mm/min compared to the completely laminated device with an inbuilt test zone (3.3 ± 1.2 mm/min), thus extending the reaction time between the analyte and the reagents in the test zone. The efficacy of the prepared device was studied with colorimetric assays for the non-specific detection of protein by tetrabromophenol blue, acid/base with phenolphthalein indicator, and specific detection of proteins using the HRP-DAB chemistry. Finally, for the detection of FABP3 on the developed µPAD, using the aptamers generated, the principle of salt induced aggregation of gold nanoparticles was exploited. The detection served as a Yes/No format for FABP3 presence with a minimum detection limit of 54 ng/ml.

List of Abbreviations and symbols

ΔH	Enthalpy change
µPAD	Microfluidic paper based analytical device/ paper based microfluidic device
ACS	Acute coronary syndrome
AFM	Atomic force microscopy
AKD	Alkyl ketene dimer
AMI	Acute myocardial infarction
AP	Alkaline phosphatase
APBS	Adaptive Poisson-Boltzmann Solver
ATP	Adenosine triphosphate
AUC	Area under the receiver operating characteristic
AuNP	Gold nanoparticle
bp	Base pair
BSA	Bovine serum albumin
CBB	Coomassie Brilliant Blue
CD	Circular dichroism
CK-MB	Creatine kinase-MB
Cm	Centimeter
CMYK	Cyan, magenta, yellow, and key (black)
CT	Computerized tomography
cTnI	Cardiac troponin I
cTnT	Cardiac troponin T
CV	Coefficients of variation
CVD	Cardiovascular diseases
DAB	3, 3'-Diaminobenzidine tetrahydrochloride hydrate
DNA	Deoxyribonucleic acid
DVS	Divinylsulfone

e	Charge of an electron
ECG	Electrocardiography
ED	Emergency department
EDTA	Ethylenediaminetetraacetic acid
ELISA	Enzyme-linked immunosorbent assay
EMSA	Electrophoretic mobility shift assay
FA	Fatty acid
FABP1	Liver type fatty acid binding protein
FABP2	Intestinal type fatty acid binding protein
FABP3	Heart type fatty acid binding protein
FABP4	Adipocyte type fatty acid binding protein
FABP5	Epidermal type fatty acid binding protein
FABP6	Ileal type fatty acid binding protein
FABP7	Brain type fatty acid binding protein
FABP8	Myelin type fatty acid binding protein
FABP9	Testis type fatty acid binding protein
FESEM	Field Emission Scanning Electron Microscopy
FITC	Fluorescein isothiocyanate
FLASH	Fast Lithographic Activation of Sheets
GOD	Glucose oxidase
GPBB	Glycogen phosphorylase BB
GST	Glutathione S-transferase
hr	Hour
HRP	Horse radish peroxidase
HSA	Human serum albumin
IPTG	β-D-thiogalactopyranoside
ITC	Isothermal titration calorimetry
K	Boltzmann's constant
Kb	Kilo base
K_d	Dissociation constant
kDa	Kilo Dalton

kV	Kilo Volt
L	Liter
LB	Luria Bertani
m/z	Mass by charge
mA	Milli ampere
MALDI	Matrix-assisted laser desorption/ionization
Mb	Myoglobin
MDGI	Mammary derived growth inhibitor
mg	Milligram
min	Minute
mL	Milliliter
mM	Mill molar
mm	Millimeter
MS	Mass spectrometry
mV	Milli Volt
mΩ	Milli Ohm
ng	Nano gram
nL	Nano liter
nM	Nano molar
nm	Nano meter
nmole	Nano mole
NMR	Nuclear magnetic resonance
O.D.	Optical density
PART	Personal Analyzer for Rapid Tests
PBS	Phosphate buffered saline
PBS-T	Phosphate buffered saline-Tween 20
PCR	Polymerase chain reaction
PDGF	Platelet-derived growth factor
PDMS	Polydimethylsiloxane
PGMEA	Propylene glycol monomethyl ether acetate
PLIP	Protein-ligand interaction profiler

pmol	Pico moles
QCM	Quartz crystal microbalance
QGRS	Quadruplex forming G-Rich Sequences
R^2	Regression coefficient
RMS	Root mean square
RNA	Ribonucleic acid
ROC	Receiver operating characteristic
rpm	Revolutions per minute
RT-PCR	Reverse transcription polymerase chain reaction
s	Second
SAXS	Small angle X-ray scattering
SD	Standard deviation
SDS-PAGE	Sodium dodecyl sulfate polyacrylamide gel electrophoresis
SELEX	Systematic Evolution of Ligands by EXponential enrichment
SPB	Sodium phosphate buffer
SPRS	Surface plasmon resonance spectroscopy
ssDNA	Single stranded deoxyribonucleic acid
SVD	Singular value decomposition
T	Temperature in Kelvin
TAE	Tris-acetate-EDTA
TBPB	Tetrabromophenol blue
TFA	Trifluoroacetic acid
T_m	Melting temperature
TSS	Transformation and storage solution
U	Unit
URL	Upper reference limit
UV	Ultraviolet
V	Volt
v/v	Volume by volume
W	Watt
w/v	Weight by volume

w/w	Weight by weight
WHO	World Health Organization
x g	Relative centrifugal force
X-Gal	5-bromo-4-chloro-3-indolyl-*β*-d-galactopyranoside
mg	Microgram
ml	Microliter
µM	Micro molar
µm	Micro meter

List of Figures

List of Tables

Introduction

Introduction

Cardiovascular diseases are the single greatest cause of adult mortality globally, constituting about 31% of all global deaths (WHO report, 2012). Lifestyles, lack of early detection systems, high incidences of misdiagnosis and lack of clearly defined risk assessment criteria contribute to this problem equally. Though many advances have been made in the early detection, prevention and treatment of these conditions, they still persist as the leading cause of death worldwide with reports indicating an increase in mortality each passing year. Detection of cardiovascular diseases has thus emerged as not only a social and clinical issue but also as an economic one. Early stratification of patients with high risk of acute myocardial infarction is of immense importance as it can help in reducing costs by screening the hospital admission process and by streamlining resources to those that are specifically at risk. The current diagnostic methods being routinely used includes electrocardiography, chest X-ray, echocardiography, cardiac catheterization, CT heart scan and blood tests for detection of cardiac biomarkers. Among the cardiac biomarkers, troponins, creatine kinase MB and myoglobin are established markers. However, these biomarkers are moderately successful in the emergency department owing to different drawbacks. For example, troponins are late markers appearing in the bloodstream only after 12 hrs of symptom onset, while creatine kinase-MB and myoglobin are not totally cardiospecific. Among the novel early markers being investigated, heart type fatty acid binding protein (FABP3) finds importance as a potential

candidate. It is a small cytoplasmic protein which is 20 times more specific to heart muscle than myoglobin and 10 fold lower in the skeletal muscle. It is rapidly released into the bloodstream following myocardial damage, appearing as early as 90 mins and peaks within 6 hrs. These parameters of kinetic release make it an ideal candidate for assessment and exclusion of acute myocardial infarction and also for measurement of recurrent infarctions (Kakoti *et al*., 2013). The studies by Okamoto *et al* have demonstrated the superior sensitivity and specificity of FABP3 over myoglobin for clinical detection of acute myocardial infarction within 12 hr of symptom onset. Similarly, the prognostic utility of FABP3 has also been highlighted by several other studies. Detection of FABP3 in clinical settings are mainly performed by immunoassays incorporating both monoclonal as well as polyclonal antibodies (Pelsers *et al*., 1999; Wodzig *et al*., 1997a, 1997b). Various modifications of the standard assay have since been reported with reduced assay time and increased sensitivity (Tanaka *et al*., 1991, Ohkaru *et al*., 1995). However, long total assay time, requirement for dilution of sample prior to use, need for a skilled technician and elaborate testing and detection with sophisticated instruments contribute to its limitations. The field of bioanalytical detection of FABP3 has seen the development of various types of biosensors (Siegmann-Thoss *et al*., 1996, Schreiber *et al*., 1997, Kroger *et al*., 1998, Gallardo *et al*., 2002, O'Regan *et al*., 2002). Biosensors mainly involve a biorecognition element in conjunction with a transducer, which converts the biological signal into a quantifiable electronic one. Similarly different point of care (POC) assays have been developed to meet the criteria of fast and low cost detection (Ren *et al*., 2012, Mion *et al*., 2007, Wang *et al*., 2009a,b,c,). However, the immunotests as well as the biosensors developed so far are still at the higher end of cost which makes them moderately

successful in remote areas. Furthermore, all the detection mechanisms are based on the use of antibodies as the biorecognition element, which suffer from various drawbacks like thermal instability, laborious and limited methods for chemical modification, batch to batch variations and high production cost.

According to the World Health Organization, one third of the deaths due to cardiovascular diseases occur in the low and middle income countries. Therefore, for affordable early detection of the disease, low cost sensing platforms are a prerequisite for detection and management of the disease. In this regard, use of alternate biorecognition elements like aptamers have found great importance for various advantages over antibodies. Nucleic acid aptamers are single stranded DNA or RNA sequences that can bind to their target with the same or enhanced specificity and affinity of antibodies (Ellington *et al.*, 1990, Tuerk *et al.*, 1990). Additionally, nucleic acid aptamers have the following advantages: thermal stability, low cost production, rapid mass scale synthesis and chemical modification capability (Radom *et al.*, 2013). Another development in the field of low cost detection has been the incorporation of paper based microfluidic systems for lab on a chip detection (Martinez *et al.*, 2010). These systems offer the benefit of rapid analysis, less expensive, multiplexing potential, small sample volume and little or no external equipment or power. However, in the context of detection of FABP3, no such strategy has been developed so far.

Considering the importance of affordable detection of cardiovascular diseases at an early stage, the present investigation aims to develop an alternative biorecognition element for the biomarker FABP3 in the form of a specific DNA aptamer. This study also intends to characterize the aptamers developed and elucidate the interaction between the aptamer and the target. Another,

proposed objective is the development of a suitable paper based microfluidic device for detection of FABP3.

Based on the proposed plan, the thesis has been divided into five chapters. At the end a brief section entitled "Conclusion and future scope of research" is also included to apprise the readers on the major findings of the current work and the important gaps that need to be bridged to attain a low cost commercially viable sensing platform.

Chapter 1: Literature review

The objective of this chapter is to summarize the current status and progress in the area of detection of FABP3. The chapter highlights the importance of FABP3 as a biomarker for cardiovascular diseases and discusses in detail the various immunosensors and immunotests developed for FABP3 detection. Special emphasis has been given on discussing technical importance, performance, benefits and limitations of different types of detection mechanisms. This section also discusses the potential of aptamers as an alternative biorecognition element and methods for studying its interaction with targets. Finally, a background on the development of paper based microfluidic devices have been incorporated.

Chapter 2: Cloning, expression and purification of FABP3, FABP1, FABP4 and FABP7

In this chapter, cloning of the coding sequence, expression and purification of recombinant FABP3, FABP1, FABP4 and FABP7 have been described. Analysis of the integrity of the

recombinant proteins was also studied through Western blot and Circular Dichroism (CD).

Chapter 3: Development of aptamer specific for human FABP3 and its characterization

This chapter entails the generation of DNA aptamers specific for FABP3 through Systematic Evolution of Ligands by Exponential enrichment. Characterization of the selected aptamers were performed using electrophoretic mobility shift assays and CD studies. The dissociation constants were determined though CD studies, while structure predictions were done using Mfold, CD studies, multidimensional melting studies and Singular value deposition analysis. Stability of the aptamers were also studied at different temperature, pH and ionic strengths.

Chapter 4: Aptamer-FABP3 interaction studies

Studies in this chapter involve the elucidation of DNA aptamer target interaction using a combinatorial approach. Mass spectrometry, CD spectroscopy and molecular docking studies were carried out to predict the possible interactions and residues involved in maintaining aptamer-protein synergy.

Chapter 5: Development of a paper-based microfluidic platform for detection of FABP3

This chapter discusses the designing and fabrication of a paper based microfluidic device using a modified photolithography technique. Characterization of the constructed device was performed using Atomic Force Microscopy (AFM) and Field Emission Scanning Electron Microscopy

(FESEM). Validation of the constructed device was confirmed through colorimetric assays for protein and base. Detection of FABP3 on the device was performed based on a gold nanoparticle aggregation assay.

1

Literature review

CHAPTER 1

Literature review

Cardiovascular diseases (CVDs) are globally the single greatest cause of adult mortality. According to the World Health Organization report (2012), an estimated 17.5 million people died from CVDs in 2012 representing 31 % of all global deaths. Of these deaths, an estimated 7.4 million were due to coronary heart disease and 6.7 million were due to stroke. Acute coronary syndromes (ACS) constitute a varied array of clinical symptoms appearing after coronary plaque disruption. Normally, the inner lining of the coronary artery is smooth and free from obstruction. However, with age or in persons with hypercholesterolemia, due to endothelial dysfunction, lipids and fatty substances penetrate the arterial wall and accumulate within the endothelium. Oxidation of these lipoproteins by free radicals triggers an inflammatory response in which monocytes migrate into the arterial wall, differentiate into macrophages and ingest the oxidized lipoproteins. Accumulation of lipoproteins within the macrophages convert them into foam cells that deposit within the endothelium. This is followed by the proliferation of smooth muscle cells around the foam cells forming a fibrous cap. This lesion is called and atherosclerotic plaque. The pathogenesis of ACS roots from the rupture or disruption of such an atherosclerotic plaque, which in itself may

be self-limiting or progressive, occurring rapidly or over a long period of time (Davies, 1996) (Fig. 1.1).

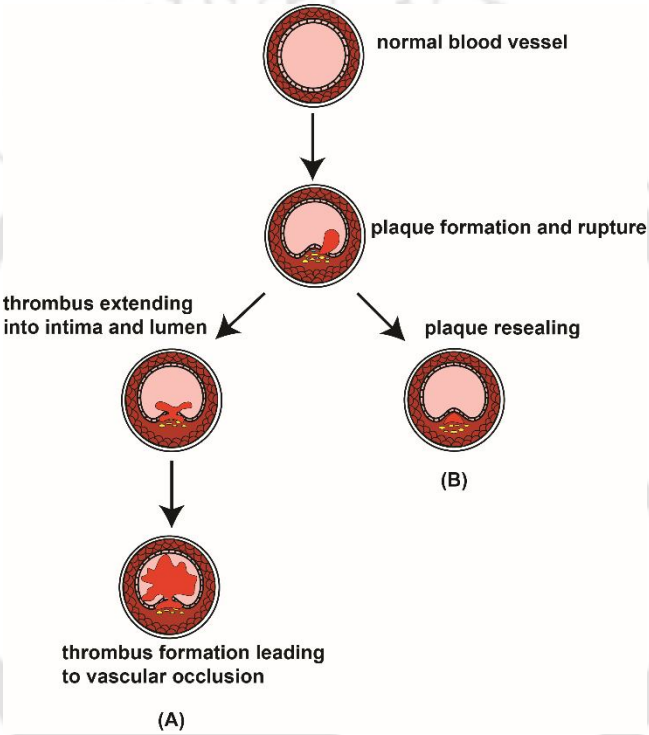

Figure 1.1: Plaque rupture—the two outcomes: (A) progressive or (B) self-limiting.

Exposure of the plaque core activates the clotting cascade which in turn triggers thrombosis resulting in the aggregation of platelets. This can damage the myocardium in three ways: (i) intraluminal platelet aggregation may lead to vascular occlusion, which can lead to ischemia (during partial occlusion) or necrosis (during complete occlusion) (ii) release of platelet

microaggregates may embolise small vessels causing ischemia and localized infarction and (iii) formation of thrombus and triggering of the clotting cascade will lead to partial or total occlusion of the vessel resulting in ischemia or necrosis. The whole lineage from plaque rupture to subsequent vascular occlusion can be divided into three phases: initial phase of myocardial ischemia followed by necrosis and finally a phase of repair and vascular remodeling (Fig 1.2) (Collinson and Gaze, 2007).

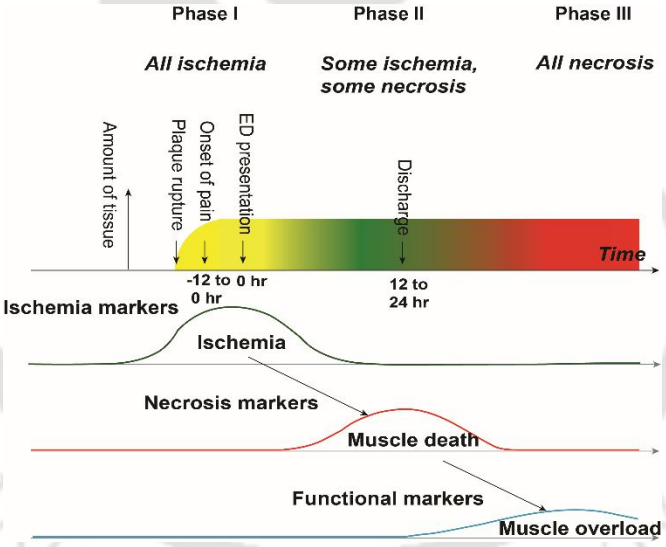

Figure 1.2: Three phases of plaque rupture and vascular occlusion. (ED: emergency department).

This may ultimately lead to unstable angina or myocardial infarction, depending upon the location and amount of blockage. Detection of myocardial infarction is of immense importance considering its consequence leading to high mortality when left untreated. Early treatments of myocardial

ischemia to prevent necrosis are available, but in order for such treatments to be of maximal benefit, early diagnosis is crucial. The current diagnostic methods routinely used for ACS detection are electrocardiography (ECG), chest X-ray, echocardiography, cardiac catheterization, CT heart scan and blood tests. However, these methods are time consuming and are difficult to use in resource limiting and point of care settings. Here point of care tests for cardiac biomarkers can be of great use by delivering test results within minutes and thus helping in quick decision making and patient management in emergency settings.

Biomarkers play a vital role in improving diagnostic accuracy of the disease as well as risk stratification of patients and prognosis. Cardiac biomarkers are defined as biological analytes that are released into the bloodstream at detectable levels during the continuum of CVD or immediately after myocardial damage. Presently, cardiac troponins (late markers) are the gold standards utilized as biomarkers of myocardial damage as they are highly specific for myocardial tissue. When used in combination with creatine kinase-MB (CK-MB) and myoglobin (early markers), troponin assays improve sensitivity to enable safe exclusion of acute myocardial infarction in the emergency department (Chiu *et al.*, 1999; Apple *et al.*, 1999; Hamilton *et al.*, 2008; Newby *et al.*, 2001). However, both CK-MB and myoglobin are not totally cardiospecific and does not differentiate between skeletal and cardiac origin of the damage (Apple *et al.*, 1999; Panteghini, 2004). Continuing with the hunt for early markers of myocardial ischemia even before irreversible myocyte injury induces, many promising, novel biomarkers have been identified. Heart type fatty acid binding protein (FABP3) is a stable, low molecular weight protein (14–15 kDa) abundantly found in the cytoplasm of myocardial cells (Wodzig *et al.*, 1997a; Storch and Thumser, 2000). Its

small size and water solubility facilitates rapid diffusion through the interstitial space, appearing as early as 90 min after symptom onset and peaking within 6 hrs (Alhadi and Fox, 2004; Glatz *et al*., 1998). These parameters of kinetic release make it an ideal candidate for both early assessment and exclusion of acute myocardial infarction (AMI) and the measurement of a recurrent infarction. Several investigations have revealed its potential as a sensitive biomarker for early detection of AMI as well as its prognostic utility in risk stratification of acute coronary syndrome (ACS) patients. Reviews pertaining to FABP3 detection have been published in the past with detailed elucidation of the processes involved (Chan *et al*., 2005).

1.1. Heart type fatty acid binding protein as early marker of acute myocardial infarction

According to the traditional WHO definition, the presence of two out of three characteristics namely characteristic chest pain (usually more than 20 min), diagnostic electrocardiographic changes and unequivocal elevation of cardiac enzymes in combination define a myocardial infarction (Keffer, 1996). However with the advent of new biochemical markers especially the cardiac troponins, this definition was redefined with increased importance on the use of biochemical markers of myocardial injury (Alpert *et al*., 2000). In recent times, the criteria for AMI have been changed by the ESC/ACCF/AHA/WHF task force to: the rise and fall of cardiac biomarkers (preferably troponin) with atleast one value above the 99th percentile of the upper reference limit (URL) together with evidence of myocardial ischemia with atleast one of the following symptoms of ischemia: ECG changes indicative of new ischemia; development of

pathological Q waves in the ECG; imaging evidence of new loss of viable myocardium or new regional wall motion abnormality (Thygesen *et al.*, 2007).

A number of biochemical serum markers are utilized at each of the three phases of plaque rupture and vascular occlusion, specifically cardiac troponins, myoglobin etc. A compilation of the characteristics of biomarkers of potential value is shown in Table 1.1. However, for the early diagnosis of AMI, the gold standard troponins are not helpful as they are released into the bloodstream only after 6 hrs, which itself defeats the mere purpose of early diagnosis. One of the promising new biomarker is FABP3 (Chan *et al.*, 2004; Ghani *et al.*, 2000; Glatz *et al.*, 1994; Kleine *et al.*, 1992; Kashtanova *et al.*, 2012; McMahon *et al.*, 2012; Viswanathan *et al.*, 2012; Lin *et al.*, 2012; Lippi *et al.*, 2013; Cappellini *et al.*, 2013; Otaki *et al.*, 2014; Hoffmann *et al.*, 2015; Willemsen *et al.*, 2015; Jacobs *et al.*, 2015; Gerede *et al.*, 2015).

Table 1.1 Characteristics and potential clinical values of different cardiac biomarkers in suspected acute myocardial infarction

Cardiac biomarker	Molecular weight (kDa)	Cardiac specificity	Elevation time (hrs)	Peak time (hrs)	Duration of elevation (days)
Troponin I	23.5	+++	4-10	16	4-7
Troponin T	37	+++	4-10	16	10-14
CK-MB	85	+++	3-4	16	2-3
Myoglobin	18	-	1-3	6	0.5-1
FABP3	15	++	<2	6	1-1.5

*+ extent of cardiac specificity.

FABP3 was first shown to be released from injured myocardium (Glatz *et al*., 1988), reaching peak levels at 5–6 hrs and returning to normal levels within 36 hrs (Glatz *et al*., 1994), which is similar to release characteristics for myoglobin. However, because of the higher content in cardiac cells and lower plasma value of FABP3, it is more sensitive than myoglobin for early AMI detection as well as early estimation of infarct size. Pelsers *et al*. (2005) reviewed several studies that investigated the potential of FABP3 as an early marker for myocardial injury. Table 1.2 lists the studies reported to date that compared the diagnostic performance of FABP3 with the established early marker myoglobin in patients admitted to hospital with chest pain. In each study, the area under the receiver operating characteristic (ROC) curve (AUC) was significantly larger for FABP3 compared to myoglobin, indicating an excellent performance of FABP3 within 6 hrs after symptom onset. The prognostic value of FABP3 for early prediction of adverse clinical outcomes in patients with suspected ACS has been supported by only a small number of studies.

However, the results suggested a high degree of correlation with increased cardiac event rates and cardiac mortality (Okamoto *et al*., 2000; McCann *et al*., 2008; Haastrup *et al*., 2000; Erlikh *et al*., 2005; Nizeki *et al*., 2008; Ishii *et al*., 2005; O'Donoghue *et al*., 2006; Kilcullen *et al*., 2007; Viswanathan *et al*., 2010; Huang *et al*., 2014; Shirakabe *et al*., 2014).

Table 1.2: Diagnostic performance of plasma FABP3 and Myoglobin (Mb) in detection of AMI: a comparison of several studies

Reference	Patient number	Patients with AMI (%)	Admission time (hr) [mean range]	Area under ROC[b] curve		Sensitivity (%)		Specificity (%)	
				FABP3	Mb	FABP3	Mb	FABP3	Mb
Abe *et al.* (1996)	123	100	<8	-	-	80	69*	-	-
Ishii *et al.* (1997)	165	60	3.5 (3-12)	0.898**	0.782	82	73	86	76
Glatz *et al.* (1997)	312	54	3.3 (2-8)	0.901***	0.824	-	-	-	-
Panteghini *et al.* (1997)	35	77	3.6 (2-5)	-	-	63	74	100	88
Glatz *et al.* (1998)	83	100	2.8 (1-4)	-	-	78**	53	-	-
Haastrup *et al.* (2000)	130	16	<6	0.890	0.840	90	81	81	89
Okamoto *et al.* (2000)	189	74	4 (0-12)	0.921*	0.843	93	89	67	57
Ghani *et al.* (2000)	460	21	3 (3-7)	0.800	0.730	39	38	95	95
Ohkaru *et al.* (2001)	88	65	3	-	-	95	53	83	83
Pagani *et al.* (2002)	41	83	2.6 (1-4)	0.798	0.771	91**	65	-	-
Nakata *et al.* (2003)	133	44	6 (0-48)	0.936***	0.862	86	77	100	100
Seino *et al.* (2003)	371	49	2-24	0.790*	0.760	95	62	49	58
	68[a]	100	<2	0.720**	0.610	89	22	52	94
Body *et al.* (2011)	705	18	24	0.86	0.79	75	59	89	82

[a] Subset of patients with admission time within 2hr. *P<0.5, ** P<0.01, ***P<0.001[b]ROC:Receiver operating characteristics.

The release of FABP3 can also be used to estimate myocardial infarct size taking into account the specific clearance rates from plasma (Glatz *et al*., 1994; de Groot *et al*., 1999; Wodzig *et al*., 1997a, 1997b; van der Laarse, 1999). Some studies also suggest the usefulness of FABP3 for early detection of post-operative myocardial tissue loss in patients undergoing coronary bypass surgery (Fransen *et al*., 1998; Hayashida *et al*., 2000; Suzuki *et al*., 1998; Petzold *et al*., 2001; Hasegawa *et al*., 2004). Inspite of demonstrating excellent performance as an early marker, FABP3 still has some drawbacks like its presence in both cardiac and skeletal muscles, a small diagnostic window and false high values due to renal inefficiency. However, these drawbacks can be eliminated or reduced by using a myoglobin/FABP3 ratio to differentiate between heart muscle and skeletal muscle injury, by using FABP3 in combination with cardiac troponin T (cTnT) to cover the entire diagnostic window of patients presenting with ACS. To avoid false FABP3 values the individual renal clearance rate can be estimated and applied.

1.2. Structure–function relationship of FABP3

The FABP3 belongs to a family of cytoplasmic fatty acid binding proteins (FABP) consisting of nine members with low molecular masses between 14 and 15 kDa (Ockner *et al*., 1972). The tissue specific fatty acid binding proteins are: FABP1 (liver), FABP2 (intestinal), FABP3 (heart), FABP4 (adipocyte), FABP5 (epidermal), FABP6 (Ileal), FABP7 (brain), FABP8 (myelin) and FABP9 (testis). The gene coding for human FABP3 has been mapped to chromosome 1 (p32–p33) extending upto 8 kb of genomic DNA. Consisting of four exons and three introns, the overall gene

organization, is similar to other members of the FABP family, the only difference being the variable lengths of their introns (Phelan *et al*., 1996). The gene is under the tight control of a 1.2 kb promoter region which dictates tissue specific expression of the FABP3 gene (Qian *et al*., 1999). The members of the FABP family show an amino acid sequence similarity of 22–73 % (Table 1.3) but, their three dimensional structures are highly conserved (Chmurzynska, 2006).

Table 1.3: Percentage identity of the amino acid sequence between different human FABPs

	FABP1	**FABP2**	**FABP3**	**FABP4**	**FABP5**	**FABP6**	**FABP7**
FABP2	23.6						
FABP3	18.9	31.8					
FABP4	18.9	31.8	64.4				
FABP5	18.1	25.0	48.9	52.3			
FABP6	36.2	27.3	21.1	27.3	20.3		
FABP7	27.6	34.1	66.7	56.8	44.7	18.0	
MP2/FABP8	19.7	28.0	62.9	66.7	56.1	17.2	59.1

They are composed of 10 antiparallel β strands which are arranged into two nearly orthogonal β-sheets forming an elliptical β-barrel. The β-barrel demonstrates high structural stability being unaffected by chemical modifications, presence of bulky fluorescent groups or targeted mutagenesis (Falomir-Lockhart *et al*., 2006; Liou *et al*., 2002; Ropson and Frieden, 1992). The fatty acid binding pocket is located inside the β -barrel with the two α-helices guarding the opening of the ligand binding cavity (Banaszak *et al*., 1994). X-ray diffraction studies were used to resolve the three dimensional structure of human FABP3 with bound fatty acid to 2.1 Å resolution (Zanotti *et al*., 1992) (Fig 1.3).

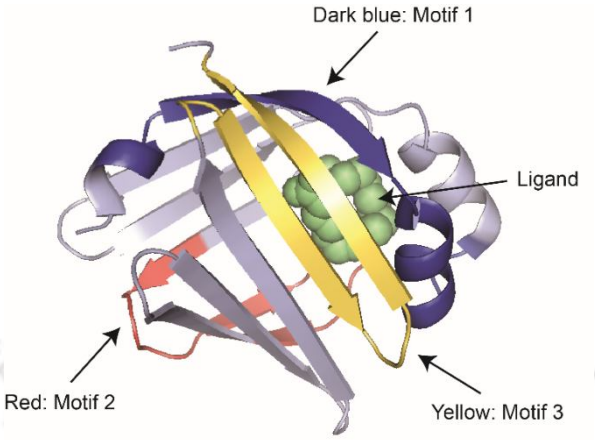

Figure 1.3: Crystal structure of human FABP3 (PDB Entry No: 4WBK).

The fatty acids appeared to be bound in a U-shaped conformation, the carboxylate group interacting with the side chains of Tyr 128 and Arg 126 and several internal water molecules. The helix-turn helix motif is thought to act as a putative fatty acid (FA) portal, the α-II helix being the key structural element (Hodsdon and Cistola, 1997; Sacchettini *et al*., 1989). Studies on the solution structure of human FABP3 have suggested that different FAs induce distinct conformational states of the protein backbone in this portal region indicating that the protein accommodates the ligand molecule by a 'selected fit' mechanism which is more prominent in FABP3 owing to a more rigid backbone structure compared to other FABPs (Lucke *et al*., 2001). All FABPs possess a conserved three element fingerprint: motif 1 includes the G–x–W triplet which forms part of the first β -strand (β A), motif 2 spans the C terminus of strand 4 (β D) and includes strand 5 (β E); and motif 3 encodes strands 9 (β I) and 10 (β J) (Flower *et al*., 1993). Site directed mutagenesis has been used to study the structure–function relationships of FABP3 in

detail. These studies exhibited the importance of amino acids present in the conserved regions in stability, ligand binding affinity and specificity. For instance mutation of Arg 106, Arg 126 or Tyr 128 affected ligand binding and stability of the FABP3, whereas Phe 16 plays a pivotal role in ligand binding (Zanotti *et al*., 1992; Prinsen and Veerkamp, 1996; Zimmerman *et al*., 1999). Binding affinities of FABP3 for different fatty acids revealed its greatest affinity for stearate with a dissociation constant of 6 ± 1 nM (Richieri *et al*., 1994).

1.3. Functions of FABP3

Fatty acids are the major source of energy for cardiac and skeletal muscles. Intracellularly FAs are bound by FABPs which increase their solubility and aid in their transport to different compartments of the cell for storage, oxidation, membrane synthesis, transcriptional regulation and even outside the cell for autocrine or paracrine signaling (Fig 1.4). FABP3 is highly expressed in cardiac as well as skeletal muscle including a lesser expression in other tissues like brain, lung and mammary gland. The function of FABP3 in muscle cells is predominantly FA transport and metabolism. However, reports indicating its role in cell proliferation and differentiation are also available. Studies in FABP3-deficient mice exhibited a steep decrease in the uptake of FAs in the heart and skeletal muscles (Binas *et al*., 1999). This decrease in FA oxidation was offset by an increase in glucose utilization resulting in reduced tolerance to exercise and cardiac hypertrophy in older animals (Schaap *et al*., 1999; Binas *et al*., 2003; Murphy *et al*., 2004). FABP3 may also interact with peroxisome proliferator-activated receptor alpha (PPARa), a nuclear receptor, to induce the expression of mitochondrial and peroxisomal β-oxidation pathways (Tan *et al*., 2002).

Findings also confirm the interaction of FABP3 with cytochrome P450 monooxygenase and lipoxygenase pathway products (Widstrom *et al*., 2001). Though FAs are not a primary substrate for ATP production, brain utilizes it for phospholipid synthesis. FABP3 knockouts compared with wild type mouse brain showed less arachidonic acid incorporation into total brain lipids. It may be specifically involved in transport/metabolism of *n*-6 FA in the brain and 20:4*n*-6 FA in the heart (Murphy *et al*., 2004, 2005). The growth regulator, mammary derived growth inhibitor (a mixture of FABP3 and adipose type FABP) present in mammary glands is thought to modulate cell growth and differentiation. Mammary derived growth inhibitor (MDGI)/FABP3 has been shown to inhibit proliferation of human breast cancer cells (Huynh *et al*., 1995).

Indirect evidence for its role in cell growth and differentiation comes from proteomic analysis which indicated an inverse correlation between FABP3/MDGI expression and proliferating cell nuclear antigen, a marker for proliferating cells (Tang *et al*., 2004). Differentiation promoting effects of MDGI/FABP3 were observed in mammary epithelial cells (Yang *et al*., 1994), pluripotent mouse embryonic stem cells (Wobus *et al*., 1990) and cardiac myocytes (Burton *et al*., 1994). Another study has demonstrated the interaction of FABP3 with a putative membrane FA transporter CD36 in mammary tissue, which was confirmed through co-immunoprecipitation (Spitsberg *et al*., 1995). Also the expression of the two proteins were found to co-vary in several animal and mouse models which indirectly supports the fact that they might act in a coordinated fashion inside the cell (van Nieuwenhoven *et al*., 1999). Reports have suggested that FABPs might have a protective function in the cell as well. FABP3 was suggested to bind FAs accumulating under pathophysiological circumstances (Vork *et al*., 1993). It could

also protect the heart by scavenging free radicals (Samanta *et al*., 1989) and by inhibiting a *β*-adrenergic response as observed in cultured neonatal rat heart cells (Wallukat *et al*., 1991).

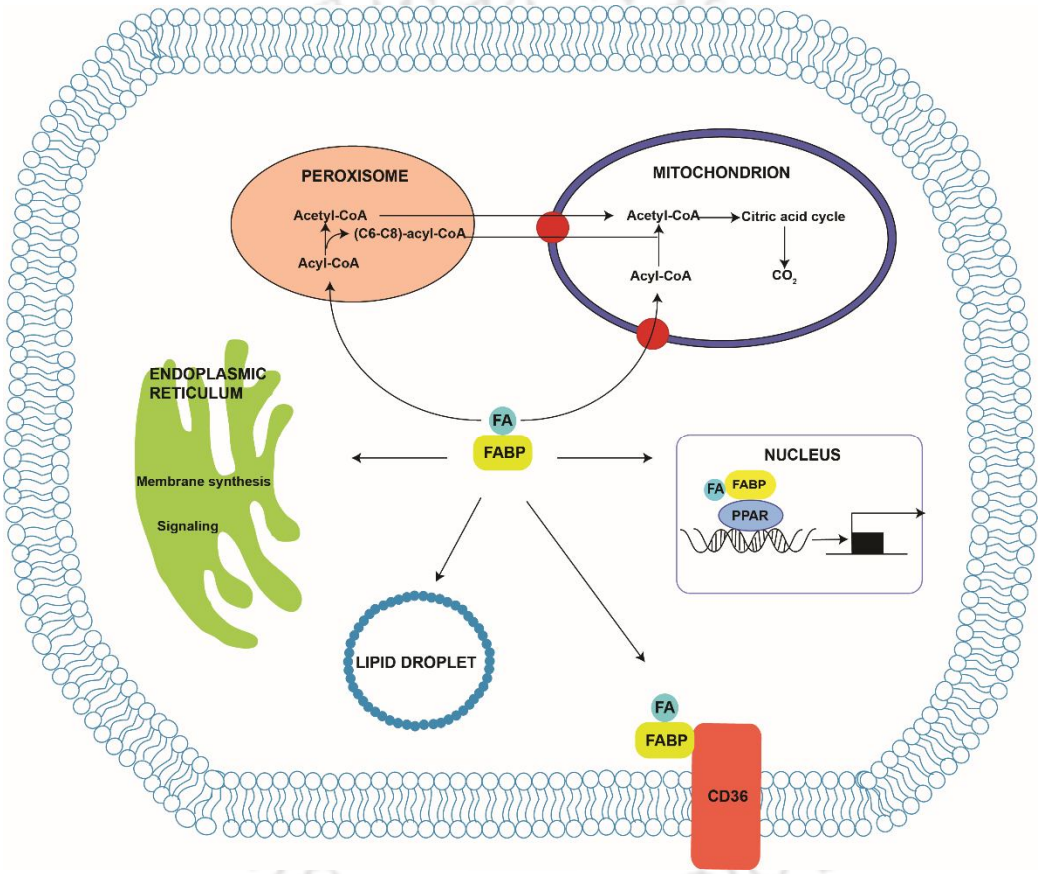

Fig 1.4: Potential functions of FABP in the cell. FABPs have been proposed to play an important role in the transport of fatty acids to specific compartments of the cell: to lipid droplets for storage; to the endoplasmic reticulum for membrane synthesis and signaling; to the mitochondria and peroxisomes for oxidation; to the nucleus for lipid mediated transcriptional programs or even outside the cell to signal in an autocrine or paracrine manner.

1.4. Detection techniques

1.4.1. Immunoassays

The majority of immunoassays employed in routine laboratory settings include mostly enzyme-linked immunosorbent assays (ELISAs). For these assays both monoclonal as well as polyclonal antibodies raised against human FABP3 has been used (Ohkaru *et al*., 1995; Pelsers *et al*., 1999; Roos *et al*., 1995; Wodzig *et al*., 1997a, 1997b; Zschiesche *et al*., 1995). However, monoclonal antibodies are preferred due to their stable production, epitope specificity and reduced or no cross-reactivity. Ohkaru *et al*. (1995) developed a sandwich ELISA for the determination of human FABP3 in plasma and urine using two different monoclonal antibodies specific for human FABP3. The assay had an assay range of 0–250 ng/ml, a minimum detection limit of 1.25 ng/ml and a total assay time of 2 hr which was much shorter than the competitive enzyme immunoassay (>16 hr) reported by Tanaka *et al*. (1991). This was followed by the successful development of a one-step ELISA for plasma FABP3 with a total performance time of 45 min. The use of monoclonal capture and detector antibodies recognizing different epitope groups, makes possible the simultaneous incubation of the FABP3 containing sample with the immobilized capture antibody and the conjugated detector antibody, thus making it a one-step assay. This assay had an assay range of 0.2–6 µg/L with a minimum detection limit of 0.2 µg/L. Although ELISA is the standard method of FABP3 detection, the long total assay time (45 min), requirement for dilution of sample prior to use, need for a skilled technician and elaborate testing and detection with sophisticated instruments contribute in its limitations.

On-line continuous monitoring of FABP3 in blood has been studied extensively by Kaptein *et al*. (1998a) through ultraslow microdialysis and ultrafiltration. Both the sampling techniques enable on-line *in vivo* measurements as well as sample collection to study time profiles of various compounds at flow rates of 100–300 nL/min. An on-line flow displacement immunoassay for FABP3 was developed by Kaptein *et al*. (1998b) based on an inverse setup: enzyme labeled antibodies associated with immobilized antigen are displaced by analyte present in the sample. This system allowed detection of both physiological (2–12 µg/L) and pathological concentrations (12–2000 µg/L) of FABP. van der Voort *et al*. (2003) developed a semicontinuous displacement assay which enables the measurement of FABP3 in human plasma. The continuous measurement was mimicked by repeated addition of FABP3 containing solutions followed by several washing steps. This study permits the measurement of even minor AMIs above 40 µg/L (when buffer is used as washing solution) and even above 20 µg/L (when plasma is used as washing solution). Although it presented with results in less than 30 min, this system needs to be optimized for real time analysis.

Robers *et al*. (1998) described a microparticle enhanced turbidimetric immunoassay that offers the advantages of being precise, easy to perform, rapid and fully automated. It demonstrated the use of a latex reagent prepared by physical adsorption of three monoclonal anti-human FABP3 antibodies onto carboxylated latex particles. Each of the three antibodies recognized distinct epitopes. The latex reagent was mixed with the reaction buffer at 37 ^{o}C for 75 s, and the resulting change in absorbance was measured at a wavelength of 550 nm from about 1 to 8 min after addition

of sample. FABP3 concentration of the sample could be interpolated automatically from the calibration curve. With a performance time of 10 min, detection limit of 1.1 µg/L and no requirement of predilution of sample, the present assay is comparatively superior to the standard ELISA (Wodzig *et al*., 1997a, 1997b). Also, no prozone phenomenon was observed up to 2400 µg/L FABP3 concentration implying a wide analytical range. However, it cannot be applied to whole blood samples and requires an expensive reading device.

Rapid and semiquantitative detection of FABP3 and myoglobin using magnetic microspheres modified with capture antibodies were reported by Wang *et al*. (2009a, 2009b, 2009c). In one approach, they used superparamagnetic (HSA)/γ-Fe_2O_3 microspheres as support for the immobilization of capture antibodies. The antibody carrying microspheres were used in a sequential sandwich fluoroimmunoassay along with FITC-labeled detector antibodies (Fig 1.5) (Wang *et al*., 2009b). The other assays embodied the use of carboxylated magnetic microbeads (Wang *et al*., 2009a) and superparamagnetic poly (styrene-divinylbenzene- acrylamide) microspheres (Wang *et al*., 2009c). All the three methods had a detection limit of 1 ng/ml and an analytical range of 1–25 ng/ml. Advantages of using magnetic microbeads includes a high surface to volume ratio for increased target binding, easy separation of bound antigens by application of an external magnetic field and homogeneous dispersion of microspheres in solution which reduces diffusional distances, facilitates analyte binding, thus reducing assay preparation and detection time. However, biodegradability and toxicity limits the use of these polymer microspheres for applications in biological analysis in online and point-of-care testing.

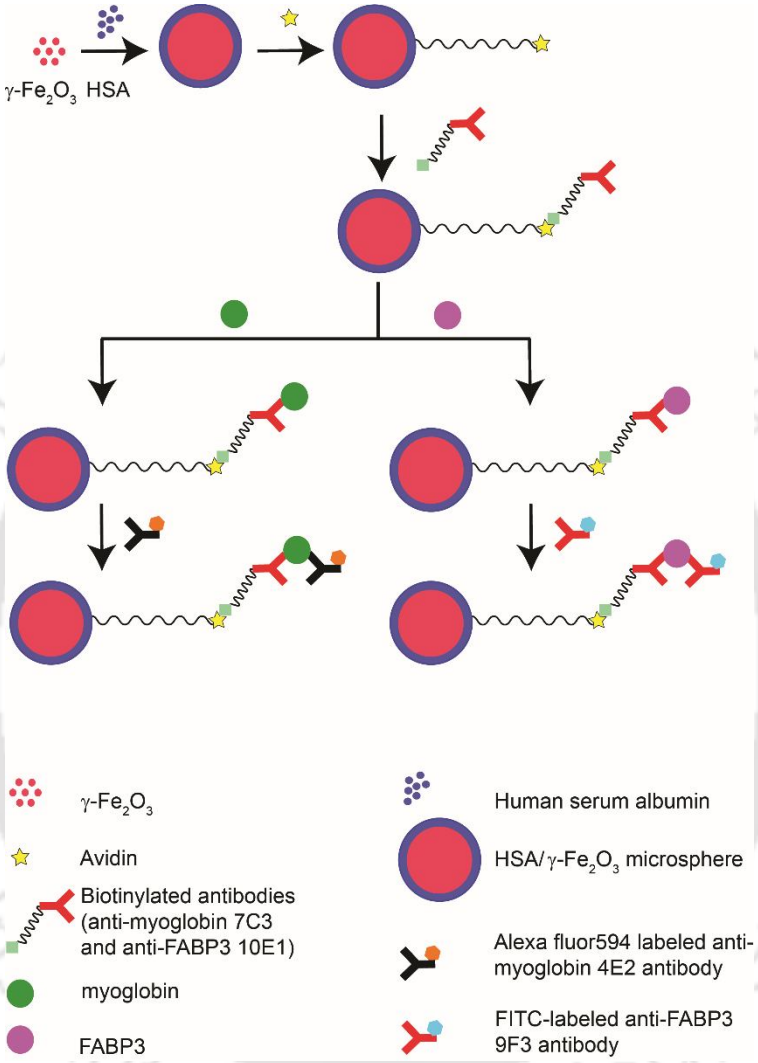

Figure 1.5: Schematic presentation of the process of analysis of AMI markers (myoglobin and FABP3) by superparamagnetic protein microsphere-aided fluoroimmunoassay (Wang *et al*., 2009b).

Ren *et al*. (2012) integrated the microbead assisted immunoassay with a microfluidic device consisting of pneumatic micro-valves and membrane mixer for detection of disease biomarkers. This on-chip platform enabled continuous immune microsphere trapping and reagent mixing both manually or automatically. However, use of whole blood samples and detection of trace amount of biomarkers are the main obstacles which needs further research for rapid and sensitive on-chip detection of actual blood samples.

1.4.2. Immunosensors

1.4.2.1. Electrochemical sensors

An amperometric enzyme immunosensor first reported by Siegmann-Thoss *et al*. (1996) was based on anti-FABP3 antibodies immobilized on nitrocellulose or activated nylon membranes covering a modified Clark-type oxygen electrode (Fig 1.6). Using bovine FABP3 as a model, two approaches were tested: first, a competitive immunoassay, where defined amounts of glucose oxidase (GOD)-labeled FABP3 competed with free FABP3 to bind the immobilized capture antibodies; second, a sandwich immunoassay, where free FABP bound to immobilized capture antibodies form a sandwich with secondary GOD-labeled antibodies. Both the approaches determined the resulting decrease in oxygen concentration after addition of glucose using the oxygen electrode at -600 mV versus Ag/AgCl. However, only the sandwich principle for determining human FABP3 was chosen for further studies owing to its superior results.

The immunosensor so developed had an assay range of 5–100 ng/ml and a much shorter assay time of 27 min as compared to ELISA measurements.

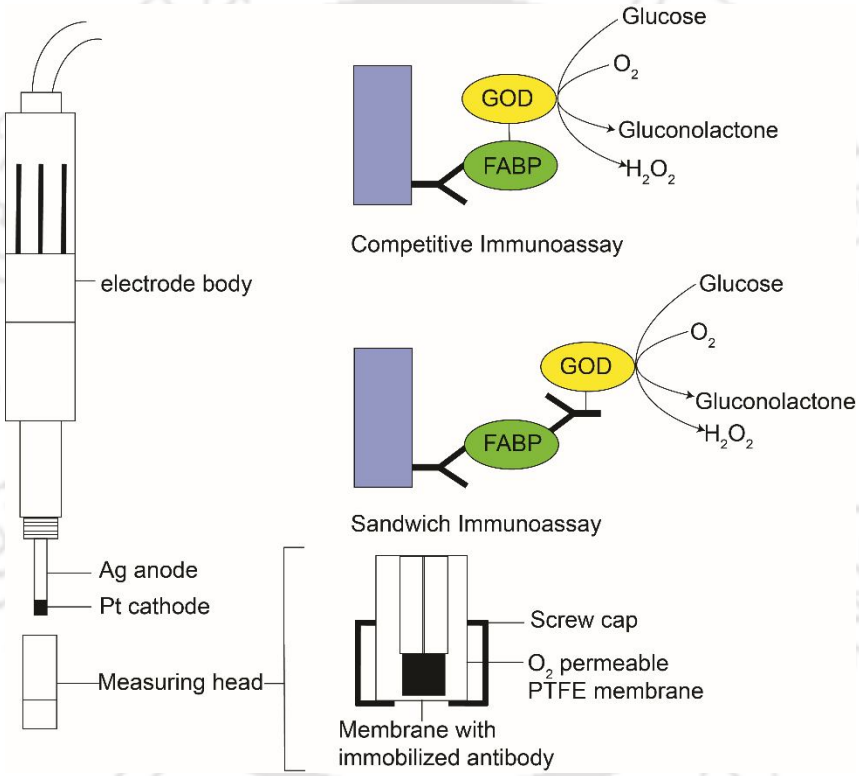

Figure 1.6: Setup of the first amperometric immunosensor for FABP3 using a modified Clark-type oxygen electrode (Siegmann-Thoss *et al*., 1996).

However, this biosensor had several shortcomings which included contamination risk as it is an open system, requirement of prior dilution of samples, interference due to other proteins present in real samples and limited number of use of the sensor for only 10 times as there is increased denaturation of the capture antibodies due to the regeneration step with glycine/HCl.

Schreiber *et al.* (1997) developed the first immunosensor for detection of FABP3 in plasma samples. Based on screen printed graphite working and Ag/AgCl reference electrodes and an immunosandwich procedure, the sensor surface was coated with capture antibodies which bind FABP3 in the sample, followed by the addition of a second monoclonal antibody conjugated with alkaline phosphatase (AP). This enzyme converts p-aminophenylphosphate to p-aminophenol, which is detected amperometrically at +350 mV. The immunosensor had an assay time of only 20 min and an analytical range of 10–350 ng/ml. Validation of the sensor was carried out by eight repeated measurements of normal human plasma spiked with eight different concentrations of FABP3 yielding recovery rates between 80–100 % and intra- and inter-assay coefficients of variation (CV) of 10–15 % and 9–16 %, respectively. The screen printing technique for preparation of electrodes can be easily scaled up and automated for cost-effective mass production. Also since the electrodes are stable for 3 months at 4 ^{o}C, they can be produced in large batches. Other advantages include short assay time and ability to measure FABP3 concentrations in the range of 10–350 ng/ml in undiluted plasma samples. However, the electrodes developed are for single use only. The first multicenter evaluation of this amperometric biosensor was carried out by Key *et al.* (1999) under the project ‘‘EUROCARDI’’ with four European hospitals contributing to this study by providing 20 patients per hospital. The results were compared with those obtained using ELISA

as described by Wodzig *et al*. (1997a, 1997b) and with the sensor used in Münster as the reference. The agreement between ELISA and sensor was excellent for FABP3 concentrations below 400 µg/L, but at lower concentrations (5–15 µg/L), it tended to overestimate. However, the detection limit of myocardial injury suggesting AMI has been set at about 6 µg/L, as a result the sensor appears unsuitable to detect minor infarctions, or distinguish minor AMIs from unstable angina. O'Regan *et al*. (2002) reported an immunosensor for the detection of FABP3 in whole blood using screen printed electrode. Based on a one-step direct sandwich assay involving the use of alkaline phosphatase labeled secondary antibody, the current produced by the oxidation of the reaction product p-aminophenol at +300 mV versus Ag/AgCl was measured. FABP3 concentrations in the range of 4–250 ng/ml could be measured in 50 min. Also, there was no cross-reactivity between myoglobin and FABP3 and bilirubin, human serum albumin and the anticoagulant citrate phosphate dextrose did not have any interfering effect. The coated screen printed electrodes retained 40 % of the original activity after 14 days at 37 ^{o}C. However, the longer assay time acts as a hurdle for its use in the emergency department for early diagnosis of AMI.

Gallardo *et al*. (2002) developed a quantitative immunosensor for diagnosis of AMI based on capacitance measurements of catalyzed polymer degradation. The sensor works by monitoring the capacitance changes in an electrode, which result from the partial or complete removal of an insulating film from its surface due to the occurrence of an enzymic reaction. The device consists of a lateral flow strip combined with an electrode coated with an enteric polymer Eudragit S100 which degrades rapidly above pH 7.4. Monoclonal anti-FABP3-antibody was deposited on a test zone and a detector antibody conjugated with urease acted as the mobile phase. FABP3 present in

the samples binds first to the detector antibody followed by the retention of the immunocomplex by the capture antibody bound to the membrane in the test zone. Addition of urea solution resulted in hydrolysis of urea to release carbon dioxide and ammonia increasing the local pH to values above 8. At alkaline pH, the polymer film starts degrading altering the insulating electrode coating causing a measurable change in capacitance. The change in capacitance was directly related to the analyte concentration in the sample, thus giving a quantifiable reading in less than 10 min. The preparation of the immunosensor is however, laborious and requires an expensive detection device.

Conducting glasses were used to construct a thin layer impedimetric biosensor by Miao *et al*, (2005). Antibodies against FABP3 were immobilized on the glass plates which acted as capture molecules. When sample was added, formation of the antigen–antibody complex on the glass plates changed the impedance signal which can be used for quantifying the amount of FABP3 present in the sample. This setup allowed detection of FABP3 in the range of 10 ng/ml to 1 µg/ml; however, the assay time was longer and the sensor needs to be characterized further for future optimizations.

1.4.2.2. Optical sensors

Kunz *et al*. (1996) developed a direct optical immunosensor for the label free detection of FABP3 based on surface plasmon resonance spectroscopy (SPRS). Two different SPRS devices were constructed: the widely used planar configuration and a new fiber-optical transducer. Instead of a direct immunoassay, competitive immunoassay was employed for detection of the antigen with immobilized antibodies. This is supported by the advantages it has over direct detection namely,

lower detection limit, shorter analysis time and lower amount of antibodies required. For the competitive assay, a silver layer of the sensor surface was covered with human recombinant FABP3 and remaining surface being blocked with BSA. A sample containing FABP3 was preincubated for 30 min with a fixed amount of polyclonal anti-FABP3 antibodies. In the measuring cell, sample FABP3 and surface bound FABP3 competed for binding with the antibodies. Any change in refractive index due to FABP3-antibody binding results in shifting of the SPR angle which is the basis of detection in this optical biosensor. Both the sensors were sensitive in the range of 0.2–2 µg/ml and had a long-term stability of 3 days for the planar and 4 days for the fiber-optical device. However, the real time optical immunosensor has several limitations for clinical use. It is prone to interference by lipids and proteins present in real samples; the sample requirement is also large (1 ml) combined with temperature dependence of the sensor. Moreover, its use is restricted to 20 subsequent measurements due to the regeneration steps involved which affected the recognition layer as well as the silver layer. In addition, detection limit of 200 ng/ml FABP3 is not suitable for the detection of micro-necrosis. Another report focuses on the use of colloidal gold based SPR system for the detection of FABP3 (Engelbienne, 1998). The SPR wavelength of colloidal gold particles coated with a monoclonal anti-FABP3-antibody was redshifted when the antibody interacted with FABP3 owing to the change in refractive index of the particles induced by ligand binding.

Use of grating coupler sensors for the development of a direct optical immunosensor for FABP3 was reported by Kroger *et al.* (1998) and Orban *et al*. (1998). Both the groups used the BIOS-1 system based on the input grating coupler principle. It is based on the detection of effective

refractive index of a thin planar waveguide due to the adsorption or desorption of proteins onto the waveguide surface. In general, one of the components of the antigen/antibody system is immobilized on the transducer surface, and the sample is brought in contact with the sensor surface. Due to the formation of immunocomplexes, the thickness of the protein layer increases which lead to an increase in the effective refractive index of the waveguide which in turn is detected by the different in coupling angles of the grating coupler. Kroger *et al.* (1998) investigated three types of immunoassays: direct, sandwich and competitive. Based on the individual preparation time and sensitivity of the different assays, the competitive assay gave the best results. The final response time was 7 min at a flow rate of 180 µL/min. In contrast to the rapid assay time, the detection limit of 330 ng/ml was relatively high which was not sensitive for detection of FABP3 in real samples. Another drawback was the nonspecific binding of plasma proteins to the sensor surface which would lead to false positive signals. Summarizing all the pros and cons, it can be inferred that this biosensor needs further improvement and optimization for real sample measurements. Orban *et al.* (1998) in their work described the application of grating coupling sensor for the kinetic analysis of immunointeractions with covalently immobilized FABP3 (Fig 1.7). The group elaborated on the calculation of surface coverage, measurement of apparent rate and affinity constants for the antibody–antigen system but did not reveal any studies determining the detection limit or assay time.

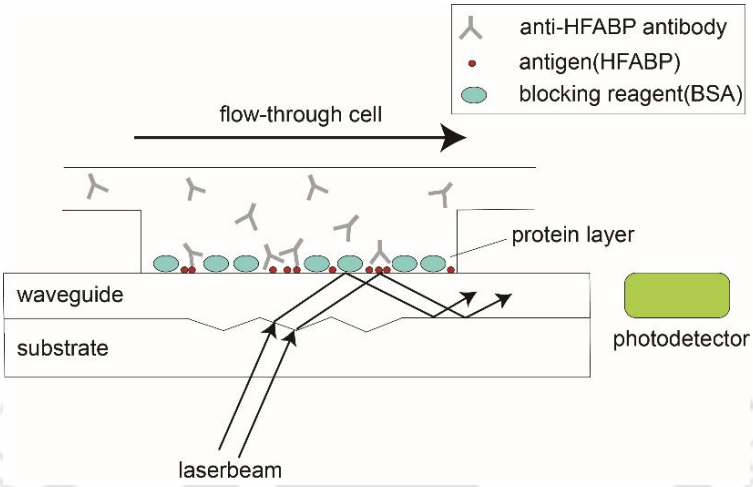

Figure 1.7: Schematic diagram of a grating coupler sensor with a flow through cell (Orban *et al.*, 1998).

1.4.3 Point of care immunotests

1.4.3.1. Immuno-affinity filtration chromatography

Immuno-affinity filtration chromatography uses colloidal gold as a label which gives rapid signal instead of a time dependent reaction with an enzyme label (Chan *et al.*, 2003a). The configuration of the assay was vertically designed to speed up antigen–antibody binding kinetics. The assay was based on a sandwich principle, in which a mixture of goat polyclonal and mouse monoclonal capture antibodies are immobilized on the nitrocellulose membrane and a colloidal gold-labeled monoclonal antibody was used as detector. After addition of sample, colloidal gold labeled antibodies were added followed by a washing step to remove all unbound or nonspecifically bound colloidal gold labeled antibodies. Samples containing an FABP3 concentration below 10 µg/L did

not result in any red spot. However, a red spot can be observed if the FABP3 concentration in the sample is over the physiological range. The results can be qualified either as a straightforward ‘‘Yes/No’’ format or by measuring the intensity of the red spot with a digital image analyzer. The test was validated against sandwich FABP3 ELISA by studying 242 serial blood samples obtained from 83 patients admitted to hospital with chest pain. Using an upper reference level of 12 µg/L, the specificity and sensitivity of the rapid test were 96 % and 86 %, respectively. The immunotest is easy to use and offers results in 15 min; however, it requires sample pretreatment and involves several working steps.

1.4.3.2. One-step FABP immunotest

A rapid and quantitative immunotest for the detection of FABP3 in whole blood was developed by Chan *et al.* (2003b) in collaboration with 8 sens.biognostic AG and rennesens GmbH. It is commercially available as CardioDetects med and self-tests. The immunotest comprises of four main elements: the sample pad, the conjugate release pad, the analytical membrane and the absorbent pad. A specific capture antibody for FABP3 is immobilized as a test line on the nitrocellulose membrane, whereas antimouse IgG is immobilized as a control line on the same membrane. Another specific detector monoclonal antibody labeled with colloidal gold is impregnated on the conjugate pad. When sample is added, FABP3 present in the sample binds to the detector antibody and the immunocomplex is trapped on the test zone. The excess detector reagent is trapped by the control zone. Two bands appear at the test and control zones if FABP3 is present in levels above the detection limit however, one band at the test zone is visible if FABP3

concentration in the sample is below the detection limit. No bands develop at both the zones if the test is invalid. The intensity of the test line is proportional to the amount of FABP3 present in the sample. The estimation of the results can be performed visually with naked eyes or by measuring the absorption of the red band with a Personal Analyzer for Rapid Tests (PART) which is a portable reflection meter with a selected wavelength developed by LRE Technology Partner GmbH. With a performance time of 15 min, storage stability of 1 year (4 ^{o}C or room temperature), no sample dilution step and upper reference limit of 7 µg/L, this test allowed more accurate targeting of therapy and considerable cost savings. Watanabe *et al*. (2001) and Seino *et al*. (2003, 2004) described a whole blood panel test (Rapichecks, Dainippon Pharmaceutical Co Ltd., Osaka, Japan) for rapid detection of human FABP3. Based on the same principle as CardioDetects, this test detects FABP concentrations above 6.2 µg/L in whole blood samples in 15 min. No interference was observed in the presence of hemoglobin, bilirubin, ascorbic acid, human serum albumin (HSA) and human immunoglobulin and no cross-reactivity was observed with troponins, myosin light chain I and myoglobin, which are commonly released during myocardial infarction. These immunotests provide a practical and handy method for detecting FABP3 in near patient and bed side settings.

1.4.4. Microarray systems

Antibody microarrays are useful tools for measuring multiple proteins in complex mixtures using a small amount of samples. They use immobilized antibody molecules onto a chemically modified solid support in an array format and used to quantify proteins in biological samples. Generally two

types of antibody microarrays are used: direct labeling and sandwich immunoassays. In direct labeling, all proteins in a complex mixture are labeled, providing a means for the detection of bound proteins post hybridization, while in sandwich immunoassays, unlabeled proteins are captured onto antibody array and then labeled specific detection antibodies are used to detect bound proteins. Both these approaches employ fluorophore conjugated streptavidin molecules which bind to biotin labeled detection antibodies or biotinylated proteins.

In a study carried out by Gul *et al*. (2007), using a sandwich type antibody array multiple CVD risk markers (C-reactive protein, TNF-a, serum amyloid-A and FABP) were detected and quantified. The results have been compared with commercially available ELISA kits which presented with several advantages including the ability to detect and quantify multiple markers at one time and better dynamic ranges over some of the commercially available ELISA kits. However, the anti-FABP antibodies utilized cross-reacted with all the other detector antibodies resulting in noise, interference in detection and quantification of markers. This problem could however be eradicated with proper study of the antibody pairs used with the other antibodies used on the same format. Based on the same principle, RANDOX Laboratories Ltd., United Kingdom developed a fully automated protein biochip microarray system for simultaneous determination of 6 markers: CK-MB, myoglobin, glycogen phosphorylase BB (GPBB), FABP3, carbonic anhydrase III and cardiac troponin I. Analytical and clinical performance of this panel was evaluated by Mion *et al*. (2007), concluding that FABP3 showed the highest accuracy in patients with AMI while cTnI + FABP3 was the most effective two marker strategy with sensitivity and specificity of 83.3 % and 92.2 % respectively.

A comparison of some prominent detection techniques developed is covered in Table 1.4.

Table 1.4: A critical comparison of performance of various analytical and sensor techniques used to detect FABP3

Reference	Assay type	Assay time (mins)	Detection limit (ng/ml)	Analytical range (ng/ml)
Ohkaru *et al.* (1995)	Sandwich ELISA	120	1.25	0-250
Kunz *et al.* (1996)	Direct optical immunosensor	25	200	$0.2\text{-}2x10^3$
Siegmann-Thoss *et al.* (1996)	Amperometric enzyme immunosensor	27	5	5-100
Schreiber *et al.* (1997)	Amperometric immunosensor	20	10	10-350
Wodzig *et al.* (1997)	One-step sandwich ELISA	45	0.2	0.2-6
Kroger *et al.* (1998)	Grating coupler sensor	7	330	-
Kaptein *et al.* (1998)	Displacement immunoassay	20-60	2	0-2000
Robers *et al.* (1998)	Microparticle –enhanced turbidimetric immunoassay	10	1.1	0-2400
Key *et al.* (1999)	Amperometric immunosensor	20	10	10-350
Cheng *et al.* (2000)	Immuno-affinity filtration chromatography	10-15	10	-
Watanabe *et al.* (2001)	One-step FABP immunotest Rapicheck®	15	6.2	-
O'Regan *et al.* (2002)	Amperometric immunosensor	50	4	4-250

Continued…

Gallardo *et al.* (2002)	AC impedance immunosensor	10	-	-
Chan *et al*. (2003)	One- step FABP immunotest CardioDetect®	15	7	-
van der Voort *et al.* (2004)	Displacement immunoassay	30	250	250-650
Mion *et al*. (2007)	Evidence® Cardiac Panel	>60	0.3	0-100
Wang *et al*. (2009a)	Magnetic microbead-assisted fluoroimmunoassay			1-25
Wang *et al*. (2009b)	Magnetic microsphere-aided sandwich fluoroimmunoassay	30	1	1-25
Wang *et al*. (2009c)	Supermagnetic microsphere-assisted fluoroimmunoassay for rapid assessment of acute myocardial infarction		1	-
Ren *et al*. (2012)	Magnetic microsphere-based enzymatic immunoassay	60	1	1-25

*Values are normalized for maintaining uniformity in units for better comparison.

With the advent of enhanced automated immunoassays and less time consuming immunotests, such as the one-step FABP test and the microparticle enhanced turbidimetric assay, the field of point of care testing for early monitoring of AMI has witnessed a significant boost. However, the feasibility for their permanent incorporation into the standard diagnostic format has not yet been met due to cost issues and reusability. Furthermore, as reported by WHO, over three quarters of CVD deaths take place in low- and middle-income countries. Therefore, for affordable early detection of CVD in these countries, low cost detection systems are a prerequisite for detection and management of the disease. Additionally, antibody based detection mechanism suffer from various factors like thermal instability, laborious and limited methods for chemical modification, batch to batch variations and high production cost. In this respect aptamers are considered as excellent alternatives to supplement or replace antibody based methodologies.

1.5. Nucleic acid aptamers as biorecognition elements

Nucleic acid aptamers are a group of oligonucleotide ligands comprising of single stranded DNA or RNA sequences with abilities to bind to their targets with great specificity and affinity often rivalling those of antibodies. The word "aptamer" was derived from the Latin words "aptus" meaning "to fit", and Greek "meros" meaning "region". Since its independent inception by Ellington *et al*., Tuerk *et al.* and Robertson et al. in the year 1990, aptamers have caught the attention of researchers as an emerging molecular recognition probe in diagnosis and therapeutics. An extensive array of targets starting from small molecules to cells have been investigated for developing aptamers [Yang *et al.,* 1998; Stoltenburg *et al*., 2012; Marangoni *et al*., 2015; Radom *et al*., 2013]. Aptamers are generated by an *in vitro* selection process called SELEX (systematic evolution of ligands by exponential enrichment) which involves the screening of large combinatorial libraries of oligonucleotides by an iterative process of *in vitro* selection and amplification. The aptamers so developed possess the ability to fold into distinct three-dimensional (3D) structures and bind to their targets in a manner similar to antibody-antigen interactions, rendering dissociation constants usually in the pico- to nano-molar range [Kimoto *et al*., 2013; Kraemer *et al*, 2011; Parekh *et al*., 2013]. Aptamer-target recognition is dominated by intermolecular interactions such as aromatic rings, π-π system stacking, van der Waals and electrostatic interactions between charged groups and hydrogen bonding. Aptamers are also known to undergo adaptive conformational changes translated as unique 3D structural binding conformation for its target. Among other features, aptamers are known to discriminate targets even on the basis of subtle structural differences [Xiong *et al*., 2014; Cho *et al*., 2009; Ng *et al*., 2006;

Jenison *et al*., 1994; Geiger *et al*., 1996]. For example, the theophylline binding aptamer shows a 10,000 fold higher affinity for its ligand than caffeine, which differs from theophylline by only a single methyl group at nitrogen atom N7. Another example is the aptamer that shows 12,000 fold stronger affinity for L-arginine than D-arginine. Aptamers are nonimmunogenic and nontoxic [G Eyetech Study., 2002; Ireson *et al*., 2006], can penetrate more efficiently through tissues, exhibit fast renal filtration and short circulating halftime [Martinez *et al*., 2014; Melancon *et al*., 2014]. Aptamers additionally addresses the practical issues of its commercial viability with promising characteristics like thermal stability, low cost production, rapid mass scale synthesis and chemical modification capability [Sun *et al*., 2015; Potyrailo *et al*., 2015]. Due to their thermal stability, the activity and functionality of aptamers can be restored after a simple reversible heat denaturation step. They can be easily and reproducibly produced in large scale by chemical synthesis or simple polymerase chain reaction. In addition, aptamers can be easily modified by reporter molecules, linkers, and different functional groups on both the phosphate/ribose backbone and the nucleobases to improve resistance to enzymatic degradation, reduce off-target events [Kool *et al*., 1997; Ramzaeva *et al*., 2000; Tung *et al*., 2000; Williams *et al*., 2001; Niemeyer *et al*., 2002; Ito *et al*., 2003; Schoetzau *et al*., 2003; Tennilä *et al*., 2008; Kricka *et al*., 2009], and to immobilize on solid-phase substrates or beads for various applications [Schena *et al*., 1995; Pirrung *et al*., 2002; Sassolas *et al*., 2008; Zhao *et al*., 2011]. Moreover, aptamers can also be expressed *in vivo* when the cells contain plasmids that encode an aptamer sequence [Famulok *et al*., 2001; Burke *et al*., 2002; Famulok *et al*., 2002; Choi *et al*., 2006; Kwak *et al*., 2009]. Lastly, one of the most important advantages of using an aptamer as a probe is that the technique requires no animals or *in vivo*

immunization, thus minimizing batch-to-batch variations [Zhang *et al*., 2012; Qin *et al*., 2014]. Over the last few years, aptamers based therapeutics and sensing are gaining momentum, with potential therapeutic aptamers in various stages of clinical trials [Sun *et al*., 2014] and aptamer-based diagnostic arrays being introduced in the market [Penner., 2012; Webber *et al*., 2014; Lollo *et al*., 2014; Vance *et al*., 2014; Bruno *et al*., 2014].

1.5.1. General process of SELEX

The process of SELEX starts with the generation of a randomized nucleic acid (DNA or RNA) sequence library, normally consisting of ~10^{15} different aptamers sequences. The diversity of the library is determined by the length of random sequence regions at the center flanked by designed primer binding sites at the 5′ and 3′ ends. Generally, each sequence in the library has a central randomized sequence (20–90 nucleotides) flanked by fixed primer binding sites for PCR amplification. The basic steps involved in SELEX include binding, partition, elution, and amplification. Once the library is created, the library pool is incubated with the target molecule. During the incubation stage, the target molecules interact with the aptamer library either in free form or in a form that is immobilized on a solid support substrate surface. The aptamer-target complex formation is followed by partitioning from unbound and weakly bound oligonucleotides, which are removed through several washing steps. The target bound oligonucleotides are eluted and followed by PCR or RT-PCR amplification. The enriched selected oligonucleotide pool so generated is then used for the next SELEX selection cycle. Typically 6-20 selection cycles are carried out including counter SELEX cycles to select specific and high affinity aptamers. The

enriched aptamer pool obtained at the last step of SELEX is cloned and sequenced for further analysis. Fig 1.8 depicts a typical SELEX process.

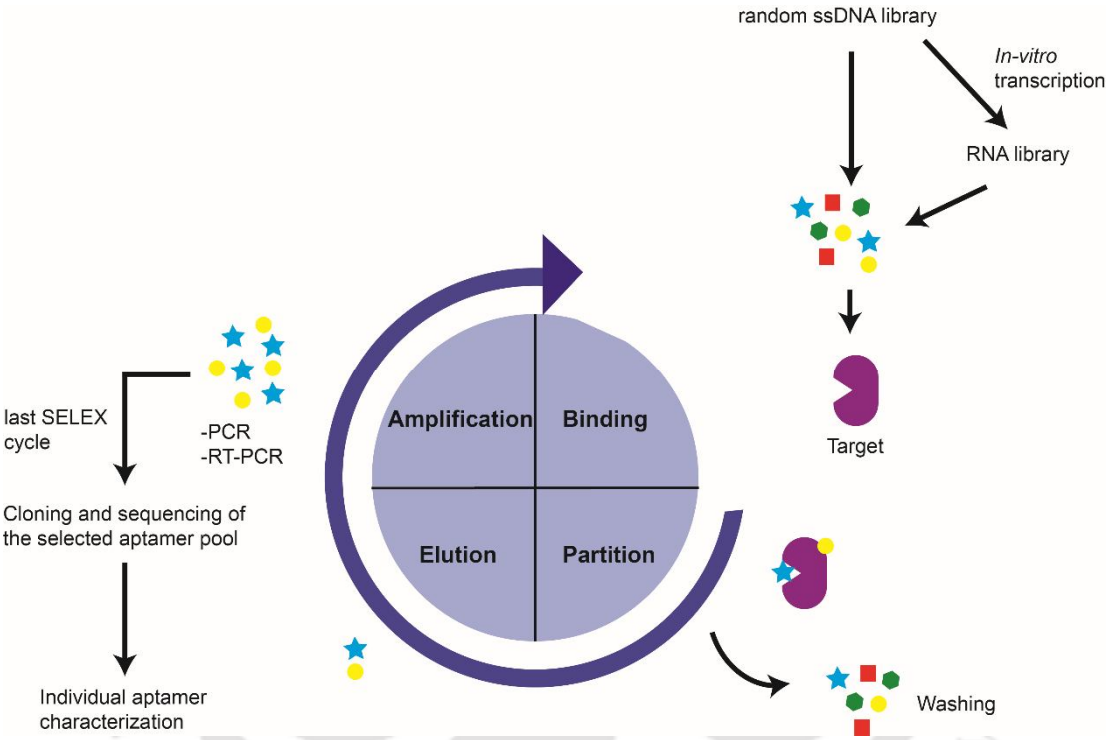

Fig 1.8: Development of target specific aptamer through SELEX process.

1.5.2. Aptamer-target interaction studies

With the ever expanding reports on potential aptamers for both analytical and therapeutic purpose, understanding aptamer-target interactions has become ever more important. Aptamer-target interactions are generally governed by the nature of the target, sequence of the aptamer and the resulting 3D structure adopted by the aptamer. While there is a plethora of information on the

generation of new aptamers, characterization of their specific interaction with target is largely limited to binding affinity determination. Detailed information on aptamer-target interactions is provided mainly by X-ray crystallography, electron crystallography, and nuclear magnetic resonance (NMR) studies. However, obtaining co-crystals of aptamer-target complexes have proven to be difficult with only a few reported structures as reviewed in Table 1.5 [Ruigrok *et al*., 2012; Jarvis *et al*., 2015; Yatime *et al*., 2015; Hansen *et al*., 2016].

In addition, screening of conditions to yield well-diffracting crystals is a trial and error method and often requires significant time and effort. Though the chance of obtaining well-ordered 2D crystals for electron crystallography is higher, yet, structure determination and data processing from 2D crystals is still a labor intensive and time consuming process. Similarly determination of high-resolution structures by NMR is mainly limited to relatively small molecules (<30-40 kDa), due to complexity of data [Snyder *et al*., 2005; Yee *et al*., 2005; Chayen *et al*., 2008]. Besides the methods described above, other techniques like surface plasmon resonance (SPR), isothermal titration calorimetry (ITC), circular dichroism (CD), small angle X-ray scattering (SAXS), quartz crystal microbalance (QCM) , foot-printing assays etc. [Ruigrok *et al*., 2005; Garbett *et al*., 2007; Chang *et al*., 2012; Lin *et al*., 2011; Sun *et al*., 2014] have been used to study aptamer-target interactions. Furthermore, computational methods like molecular dynamics simulations and online structure prediction and docking software are increasingly being used to predict binding models [Joubert *et al*., 2010; Schneider *et al*., 1999; Sund *et al*., 2015; Reshetnikov *et al*., 2010; Tatarinova *et al*., 2014; Albada *et al*., 2015; Sharma *et al*., 2009; Rhinehardt *et al*., 2015; Lin *et al*., 2012; Liberman *et al*., 2015].

Table 1.5: Available structures of aptamer-target complexes in Protein Data Bank (PDB)

Target	DNA/RNA	PDB entry code
		Aptamer-protein complexes
von Willebrand Factor Domain A1	DNA	3HXO 3HXQ
Alpha-thrombin (human)	DNA	1HUT 1HAO 1HAP 3QLP 4DII 4DIH 4LZ1 4LZ4 4I7Y 5CMX
Alpha-thrombin (human)	RNA	3DD2
NF-κB (p50)2	RNA	1OOA
NF-κB P50-RelB	DNA	2V2T
YmaH (Hfq)	RNA	3HSB 3AHU
A human IgG	RNA	3AGV
Enterobacterio phage MS2 coat protein complex	RNA	6MSF
Enterobacterio phage MS2	RNA	5MSF 7MSF
Enterobacterio phage MS2	RNA	1U1Y
G Protein-Coupled Receptor Kinase 2	RNA	3UZT
G Protein-Coupled Receptor Kinase 2-Heterotrimeric G Protein Beta 1 and Gamma 2 Subunit Complex	RNA	3UZS
human interleukin 6	Modified DNA	4NI7 4NI9
Lysozyme	RNA	4M4O 4M6D
Plasmodium falciparum lactate dehydrogenase	DNA	3ZH2
prion protein	RNA	2RSK 2RU7
human PDGF-BB	Modified DNA	4HQU 4HQX
HIV-1 reverse transcriptase	DNA	5HLF 5D3G
C5a complement anaphylatoxin	L-RNA/L-DNA	4WB2 4WB3
Chemokine CCL2	RNA	4R8I
Bacillus anthracis ribosomal protein S8	RNA	4PDB
Fab	RNA	4KZE 4Q9Q 4Q9R

Continued…		**Aptamer-small molecule complexes**
Malachite green	RNA	1F1T
Vitamin B12	RNA	1ET4 1DDY
Streptomycin	RNA	1NTB 1NTA
Biotin	RNA	1F27
GFP-like fluorophore	RNA	4KZD

When used individually, these methods do not provide a much detailed information as a crystal structure, however, using a combination of complementary techniques may provide very detailed information on the interactions involved. A complementation of these techniques can be considered as an alternative to X-ray crystallography when crystallization trials fail to produce well diffracting crystals or when there is no adequate equipment or expertise to conduct crystallization trials. Moreover, some of these techniques may provide information on the dynamics of complex formation, as compared to crystallography which provides a time and position averaged image.

1.6. Paper based microfluidic device as a sensing platform

The next step in realizing a low cost effective detection mechanism, is the construction of a biosensing platform to render affordable detection in low income regions. Improved global health in the current scenario is greatly influenced by the accessibility of standard diagnostic tests. Current laboratory-based diagnostic tests involve the use of sophisticated techniques, instruments and also depend on the availability of highly skilled operators. However, implementation of these

standard procedures remains inconceivable in developing and under developed countries especially in the countryside/remote locations under emergency conditions owing to lack of regular power resource, cost effectiveness and trained professionals [Chin *et al*., 2007; Sia *et al*., 2004; Daar *et al*., 2002; Yager *et al*., 2006; Mabey *et al*., 2004]. Alternative detection assays are available but with their own set of limitations. For example the lateral flow immunoassays readily available over-the-counter are less cost effective and involve larger sample volumes which is of concern for sample analysis in infants. Also these immunoassays use nitrocellulose as the substrate which has certain disadvantages: shelf life issues, low tensile strength, protein incompatibility with surfactants used during pretreatment, inconsistencies in flow characteristics due to desiccation, protein inability to bind covalently or directionally to nitrocellulose and involvement of elevated drying temperatures [Yetisen *et al*., 2013]. Similarly, conventional microfluidic devices require external pumps and detectors for sample movement and detection. Circumventing these drawbacks, paper based microfluidic devices has emerged as an effective alternative to high end costly bioassays and thus qualifying for the ASSURED (affordable, sensitive, specific, user-friendly, rapid and robust, equipment free and deliverable to end-users) criteria suggested by the World Health Organization (WHO) [Peeling *et al*., 2006]. Paper as a substrate has the following advantages: (i) inexpensive, portable, easily accessible [Macek *et al*., 1971], (ii) compatible with biological samples [Pelton *et al*., 2009], (iii) can be easily modified to immobilize different biomolecules like protein, DNA, small molecules, etc. [Zhao *et al*., 2008; Giddings *et al*., 1965], (iv) ease of storage, transport and disposal [Martinez *et al*., 2010], (v) paper absorbs liquids through capillary motion and evaporation, which eliminates the need for external pumps to drive

fluid movement [Martinez *et al*., 2010], (vi) it serves as a good medium for colorimetric tests, providing a strong white contrast against the colored substrate [Martinez *et al*., 2010]. Paper as a substrate has been extensively used in analytical and clinical chemistry; most common examples include paper chromatographic techniques used for the separation of different biomolecules, litmus paper and paper based diagnostic tests [Chin *et al*., 2007; Yetisen *et al*., 2013; Feigel *et al*., 1946; Clegg *et al*., 1950; Jungreis *et al*., 1997; Hossain *et al*., 2009; Oberhofer *et al*., 1982; Zocher *et al*., 1999; Wong *et al*., 2006; Allen *et al*., 1995; Hardman *et al*., 2003; Gussenhoven *et al*., 1997; Wang *et al*., 2006; Deborggraeve *et al*., 2006; Liu *et al*., 2006; Zlateva *et al*., 2005]. It also finds use as a substrate for the storage of biological samples like blood, saliva, etc. [Mwaba *et al*., 2003; Bourdoux *et al*., 1991; Civallero *et al*., 2006; Chamoles *et al*., 2001; Martinez *et al*., 2007]. With the advent of advanced fabricating and patterning techniques, paper based microfluidic devices were introduced for multiplex analyte detection [Martinez *et al*., 2010; Martinez *et al*., 2008; Wang *et al*., 2010]. Majority of these fabrication techniques employs the use of hydrophobic patterning reagent to define hydrophilic flow channels to direct the movement of sample from an inlet to a specified location for subsequent analysis (Fig 1.9). A few of the fabrication techniques are described in Table 1.6.

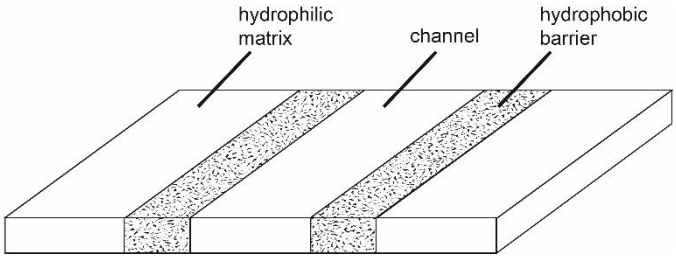

Figure 1.9: Hydrophilic channels bounded by hydrophobic barriers on paper.

Table 1.6: Comparison of techniques for patterning hydrophilic-hydrophobic contrast on paper

Fabrication method	Patterning agents	Patterning principles
Photolithography	Photoresist (e.g., SU-8) (Martinez *et al.*, 2007, 2008; Klasner *et al*., 2010)	Physical blocking of pores in paper with hydrophobic polymers.
Wax printing	Wax (Lu *et al.*, 2009; Carrilho *et al.*, 2009; Leung *et al.*, 2010)	Physical deposition of reagent on fibre surface.
Inkjet printing	AKD (Li *et al.*, 2010; Delaney *et al.*, 2011)	Chemical modification of fibre surface.
Flexographic printing	Polystyrene (Olkkonen *et al*., 2010)	Physical deposition of reagent on fibre surface.
Plotting	PDMS (Bruzewicz *et al*., 2008)	Physical blocking of pores in paper.
Ink jet etching	Polystyrene (Abe *et al*., 2008, 2010)	Physical deposition of reagent on fibre surface.
Plasma treatment	AKD (Li *et al*., 2008, 2010)	Chemical modification of fibre surface.
Laser treatment	Depend on paper types (Chitnis *et al*., 2011)	Physical blocking of pores in paper.
Screen printing	Wax (Dungchai *et al*., 2011)	Physical deposition of reagent on fibre surface.
Paper cutting and shaping	---	Cutting and/or paper removal to create microfluidic devices.
Indelible ink stamping, screen printed PDMS, lacquer spraying, vapor phase polymer deposition	PMS ink, acrylic lacquer, hydrophobic parylene (Curto *et al*., 2013; Nurak *et al.*, 2013; Demirel *et al*., 2014; Ma *et al*., 2014)	Require masks or stamps to pattern the hydrophobic regions and protect the remaining hydrophilic regions in paper.

*AKD- alkyl ketene dimer, PDMS- Polydimethylsiloxane, Parylene- dichloro-[2,2]-paracyclophane, fluoropolymer.

Quantitative analysis of analyte detection on paper based microfluidic devices so patterned are carried out by various transduction mechanisms. Among them colorimetric, chemiluminescence, electrochemiluminescence and electrochemical methods are the most widely used. While colorimetric approaches are more suitable for semi-quantitative tests, the other three techniques specifically electrochemical method offers highly sensitive detection of analytes. In the context of disease biomarkers, paper based microfluidic devices as detection platform has been utilized for the detection of various disease markers like carcinoembryonic antigen, alpha fetoprotein, prostate specific antigen etc. for cancer (Wu *et al*., 2014, Li *et al.*, 2013); glucose for diabetes (Ornatska *et al*., 2011); food borne pathogens (Li *et al*., 2010); and various other specific disease biomarkers.

2

Cloning, expression and purification of human fatty acid binding proteins

CHAPTER 2

Cloning, expression and purification of human fatty acid binding proteins

2.1. Overview

The human heart type fatty acid binding protein (FABP3) is a member of the nine cytoplasmic fatty acid binding proteins. Its isolation was first reported by Unterberg *et al* in 1986 from the human heart. Since then stable isolation of the protein has been performed by various groups, later followed by the expression of the recombinant protein in bacterial systems. The protein consists of 132 amino acids, a molecular weight of 14768 Da and an isoelectric point of 5.25. The crystal structure of the recombinant protein unveiled a secondary structure consisting of 10 antiparallel β-strands and two short α-helices, which are arranged into two orthogonal β-sheets (Zanotti *et al*., 1992). All the members of the FABP family show an amino acid sequence similarity of 22–73 % but, their three dimensional structures are highly conserved (Chmurzynska *et al*, 2006). Based on sequence similarity they are categorized into three groups-(1) FABP1 and FABP6, (2) FABP3, FABP7, FABP5, FABP8, FABP4 and FABP9, (3) FABP2. All proteins of group 1 are capable of binding fatty acids (FAs) and bulky ligands, such as bile salts, cholesterol

and haem. Members of group 2 bind FAs and additionally retinoids and eicosanoids (Schaap *et al*. 1999). FABP2 binds solely FAs, but in a different conformation than other FABPs (bent instead of U-shaped) (Sacchettini *et al*. 1989).

Since our aim is to develop nucleic acid aptamer against human FABP3, recombinant GST tagged FABP3 has been considered as the analyte. In order to achieve high specificity of the aptamer developed, recombinant GST tagged FABP1, FABP4 and FABP7 were used as controls. Henceforth, the GST tagged FABP3, 1, 4 and 7 proteins will be referred to as FABP3, FABP1, FABP4 and FABP7 respectively, for ease of expression. Two proteins (FABP4 and FABP7) with maximum and one (FABP1) with minimum sequence similarity with FABP3 were considered as controls. Clones were obtained from the DNASU Plasmid Repository. However considering the absence of suitable restriction sites and tag in the received clones, we subcloned the coding sequences of the genes into a suitable vector for our purpose. In this section we discuss the cloning, expression and purification of FABP3 along with the aforementioned control proteins.

2.2. Experimental Approaches

2.2.1. Materials

pANT-cGST clones of human *fabp3* and *fabp7*; and pMCSG7 clone of human *fabp1* and *fabp4* were purchased from the DNASU Plasmid Repository (USA). Primers were synthesized from Bioserve Biotechnologies India Pvt. Ltd. BioMix™ Red PCR kit was obtained from Bioline (UK). Quick ligation kit was obtained from Promega (USA). Gel extraction kit was purchased

from Sigma (USA). All other chemicals were of analytical or molecular biology grade and are cited in the methodology section, wherever necessary.

2.2.2. Bacterial cell culture

E.coli strains and clones were stored at -80 ºC as glycerol stocks and were cultured in LB medium containing suitable antibiotics. The *E.coli* strains used in this work and the composition of culture media are given in Table A1 and A2, respectively in the appendix.

2.2.3. Quantification of DNA

DNA was quantified spectrophotometrically. Samples were diluted in water and the optical densities (O.D.) were measured at 260 nm and at 280 nm. One O.D. at 260 nm represented 50 µg of double stranded DNA. Concentrations of DNA samples were calculated from the optical densities using suitable dilution factors.

2.2.4. Protein estimation

Protein concentrations were determined spectrophotometrically at 595 nm using Coomassie Brilliant Blue (CBB) G-250 with BSA as a standard following the method of Bradford (Bradford., 1976).

2.2.5. Plasmid DNA isolation

Plasmid DNA was isolated from 5 ml of over-night grown cultures by alkaline lysis method (Green and Sambrook., 2012). Reagents used in this method are enlisted in appendix Table A3. A single *E.coli* colony carrying a recombinant plasmid was grown for 14-18 hrs in LB medium containing specific antibiotic, at 37 ^{o}C with shaking at 180 rpm. The culture was harvested and the cells were resuspended in 100 µl of solution I. The cells were lysed with 200 µl of freshly prepared solution II. Thorough mixing of the contents was done by gently inverting the tube. Bacterial genomic DNA and bacterial cell debris were differentially precipitated by adding 150 µl of ice cold solution III and incubated on ice for 5 mins followed by centrifugation at 12,000 x g for 10 min at 4 ^{o}C. The supernatant was transferred to a fresh tube and equal volume of phenol/chloroform/isoamyl alcohol (25:24:1 v/v) was added. The resulting mixture was mixed gently by inversion and the phases were separated by centrifugation at 12,000 x g for 10 mins at 4 ^{o}C. The aqueous phase was aspirated out into a fresh tube and 2 volumes of ethanol were added to precipitate the plasmid DNA. After incubation at room temperature for 10 mins, precipitated plasmid DNA was separated by centrifugation at 12,000 x g for 10 mins at 4 ^{o}C. The DNA pellet was washed with 70 % ethanol, air-dried and resuspended in the required amount of nuclease-free water.

2.2.6. Agarose gel electrophoresis

DNA samples were resolved by agarose gel electrophoresis using agarose gel (0.8-2 %, containing 0.5 µg/ml of ethidium bromide) in 1 X TAE at 75 V until the desired resolution was achieved. The DNA fragments were visualized on a UV-Trans-illuminator and imaged using a gel documentation system (ChemiDoc XRS+ Imaging System, BIO RAD).

2.2.7. Gel elution of DNA

PCR amplified products, digested plasmids and inserts were eluted out of agarose gels using GenElute Gel Extraction kit (Sigma Aldrich, USA) following the manufacturer's protocol. DNA fragment of interest was excised out of the agarose gel and stored at -20 ^{o}C for further use. Gel solubilizing solution was added in a ratio of 100 mg agarose gel: 300 µl gel solubilization solution and then allowed to incubate for 10 min at 50-60 ^{o}C, until the gel slice is completely dissolved. The mixture was vortexed briefly during incubation to help dissolve the gel, completely. A GenElute binding column was placed in a 2 ml sterile collection tube, equilibrated with 500 µl of column preparation solution and centrifuged for 1 min at 12,000 x g. The flow through was discarded. One gel volume of 100 % iso-propanol was added to the sample and mixed. The sample DNA solution was then loaded onto the pre-equilibrated binding column in a maximum volume not exceeding 700 µl at one time and centrifuged for 1 min at 12,000 x g. After discarding the flow through liquid, the column was washed again with 700 µl of wash solution at 12,000 x g. Another centrifugation step was performed for 1 min to remove residual traces of ethanol. The DNA was

eluted by adding 50 µl of preheated nuclease free water to the binding column. After an incubation time of 1-2 mins at room temperature, DNA was eluted out by centrifugation at maximum speed for 1 min. Eluted DNA was stored at -20 ^{o}C for further use.

2.2.8. Polymerase chain reaction

BioMix™ Red PCR kit was used for all PCR reactions. A total of 25-50 ng of DNA sample was used in 25 µl reaction mixture. The composition of the reaction mix was as follows:

2 X Biomix Red	12.5 µl
5’ primer (20 pmole/µl)	1 µl
3’ primer (20 pmole/ µl)	1 µl
DNA	25 ng
Nuclease free water to final volume	25 µl

PCR amplification was performed by thermal cycling (Palm Cycler, Genetix Biotech. Asia Pvt. Ltd.). A typical thermal cycling involved initial denaturation for 5 mins at 95 ^{o}C, followed by 30 cycles each of which is as follows: 30 s at 95 ^{o}C, 45 s at 62.1 ^{o}C or 63.6 ^{o}C, 45 s at 72 ^{o}C and the final extension was performed for 10 mins at 72 ^{o}C. Sequence of primers and reaction conditions used are given in appendix (Table A5).

2.2.9. Digestion of DNA by Restriction Enzyme

Plasmids or PCR amplified DNA fragments were subjected to digestion using restriction endonucleases. An aliquot of plasmid DNA (~1µg) was digested overnight with the required amount of restriction endonuclease according to the conditions specified by the manufacturer. An aliquot was loaded on a 0.8 % agarose gel for analysis after electrophoresis. The composition of the digestion mix is as follows:

10 X Buffer 4	5 µl
Bam H I-HF (NEB, 20 U/µl)	1 µl
Xho I (NEB, 20 U/µl)	1 µl
BSA (100X)	0.5 µl
DNA	1 µg
Nuclease free water to final volume	50 µl

2.2.10. Ligation reaction

The restriction enzyme digested vector and insert were resolved by agarose gel electrophoresis and eluted using GenElute Gel Extraction kit. The gel eluted products were ligated using T4 DNA ligase. For ligation, linearized vector and insert fragment were mixed in a 1:3 molar ratio, followed by incubation with 2 X Quick ligation reaction buffer and 1 µl of Quick T4 DNA ligase. The ligation reaction was carried at room temperature (25 ^{o}C) for 5 mins, chilled on ice and then used for transformation/or stored at -20 ^{o}C. The composition of the ligation mix is as follows:

Insert DNA	150 ng
pGEX-4T2 vector (GE)	50 ng
2 X Quick Ligation Reaction Buffer	12.5 µl
Quick T4 DNA Ligase	1 µl
Nuclease free water to final volume	25 µl

The ligated mixture was transformed into *E.coli* DH5α cells by standard heat shock method described in section 2.2.12. Transformed cells were then plated in LB agar/ampicillin plates.

2.2.11. Preparation of competent cells

A one-step competent *E.coli* DH5α/BL21 (DE3) cell preparation protocol was adopted in this work for transformation and storage of competent bacterial cells as described by Chung *et al*. (1989). Briefly, a single colony of bacterial cell was inoculated aseptically in 5 ml of LB media as a primary culture and allowed to incubate overnight at 37 ^{o}C under constant shaking at 180 rpm. A 1 % primary culture was charged aseptically in a 25 ml LB broth and grown till early exponential phase until the optical density (O.D) at 660 nm wavelength read 0.4-0.5. The culture was then centrifuged at 3000 x g for 10 min at 4 ^{o}C. The sedimented bacterial pellet was isolated and resuspended aseptically in 2.5 ml of sterile ice-cold transformation and storage solution (TSS solution) (Appendix Table A3). Aliquots in an appropriate volume were prepared and frozen immediately at -80 ^{o}C for long term storage.

2.2.12. Transformation in bacterial cells

For transformation 10 µl of the ligation mixture was added to 100 µl aliquot of competent bacterial cells, mixed and then incubated on ice for 30 min. The competent cells were subjected to heat shock at 40 ^{o}C in a circulating water bath for 90 s and chilled on ice immediately. A total of 800 µl of pre-warmed sterile LB broth at ~37 ^{o}C was added to the cells and incubated for 1 hr at 37 ^{o}C with constant shaking at ~180 rpm. The cells were harvested by centrifugation at 3000 x g for 10 min at 4 ^{o}C and resuspended in 100 µl of LB media. Resuspended cells were plated on LB agar plates containing the appropriate antibiotic followed by incubation at 37 ^{o}C for 12-16 hr. Subsequently, the colonies were picked, gridded on a LB agar plate containing appropriate antibiotic and screened by restriction digestion.

2.2.13. Sequencing of clones

Insert in various clones were sequenced by dideoxy method using universal T7 forward and reverse primers. Sequencing was performed by Xcelris Genomics (Ahmedabad).

2.2.14. Cloning of *fabp3, fabp1, fabp4* and *fabp7* in pGEX-4T2 expression vector

The plasmid DNA containing *fabp3, fabp1, fabp4* and *fabp7* cloned in pANT-cGST/pMCSG7 vectors were procured from DNASU Plasmid Repository with the following corresponding IDs HsCD00732739, HsCD00674470, HsCD00343151 and HsCD00732847 which were used as the template for amplifying using specific primers (Appendix Table A5). The primer

sets used contain the restriction enzyme sites for *BamH I* and *Xho I* at 5' and 3' end, respectively. The PCR products as well as the plasmid pGEX-4T2 were double digested separately with *BamH I* and *Xho I* and the double digested PCR products were ligated to double digested pGEX-4T2 using the Quick ligation kit (Promega). An aliquot of the ligated product was subsequently used to transform competent *E.coli* DH5α using standard heat shock method mentioned earlier. Transformed cells were plated on LB/ampicillin plate. After 16 hrs of incubation at 37 ^{o}C, bacterial colonies were picked and plasmid DNA isolated from the cells by alkaline lysis method. The recombinant clones were screened by restriction enzyme digestion and the selected clones were stored at -80 ^{o}C. One of the selected clones for each gene was confirmed through sequencing and the recombinant plasmids were further transformed to *E.coli* BL21 (DE3) for protein expression.

2.2.15. Expression of GST-tagged FABP3, FABP1, FABP4 and FABP7 in *E.coli* BL21 (DE3)

A fresh colony of *E.coli* BL21 (DE3) with pGEX-4T2 *fabp3* or *fabp1* or *fabp1* or *fabp7* each were inoculated in 5 ml of LB media containing ampicillin (100 mg/L) and incubated at 37 ^{o}C overnight. This was further subcultured in 100 ml of LB media with the same amount of antibiotic till the O.D. reached 0.6-0.8. Expression of the recombinant proteins were induced with Isopropyl *β*-D-thiogalactopyranoside (IPTG) (0.1 mM for *fabp3*, *fabp1* and *fabp4*; and 0.05 mM for *fabp7*) for 12 hrs at 37 ^{o}C for *fabp3*, *1* and *4* and 30 ^{o}C for *fabp7*, respectively with shaking (180 rpm). Cells were harvested by centrifugation at 8000 x g and resuspended in 50 mM PBS, pH 8. The cells were then subjected to sonication using a ultrasonic processor (Hielscher) at 25 % amplitude with 0.5 cycle at 4 ^{o}C till the lysate appeared clearer. The homogenate was clarified by

centrifugation at 12,000 x g for 20 mins at 4 ^{o}C. The supernatant was collected and stored at 4 ^{o}C or -20 ^{o}C for further processing.

2.2.16. Purification of GST tagged FABP3, FABP1, FABP4 and FABP7

The pGEX-4T2 vector carries a GST tag upstream to the multiple cloning site. The recombinant GST tagged proteins (FABP3, 1, 4 and 7) were purified by glutathione agarose affinity chromatography using glutathione agarose beads from Sigma (USA). The purification was conducted as per the manufacturer's protocol. Briefly, the clarified protein sample was loaded on to the column under gravity flow and allowed to incubate at 4 ^{o}C for 1 hr. The resin was then washed with 50 mM PBS (300 mM NaCl, pH 8) for 4-5 times to remove unbound sample, followed by elution of the bound proteins using elution buffer (50 mM Tris-HCl, pH 9) supplemented with 10 mM glutathione. The residual glutathione was removed by dialysis against an appropriate buffer. The Bradford assay was used to determine the concentration of the purified proteins. Henceforth, the GST tagged FABP3, 1, 4 and 7 proteins will be referred to as FABP3, FABP1, FABP4 and FABP7 respectively, for ease of understanding.

2.2.17. Sodium dodecyl sulfate polyacrylamide gel electrophoresis (SDS-PAGE) of protein

SDS-PAGE was performed to analyze the expression of the recombinant proteins and for western blot. Required amount of purified protein or cell lysates were mixed with 4 x SDS-PAGE gel loading buffer with reducing agent (2-mercaptoethanol) and heated in a boiling water bath for 5 mins. Standard SDS-PAGE protein marker for regular SDS-PAGE and pre-stained protein

marker for western blots were procured from New England Biolabs (USA) and processed simultaneously as per the manufacturer's instructions. Denatured protein samples along with standard SDS-PAGE protein markers were subjected to SDS-PAGE following the method of Laemmli, (1970). Electrophoresis was carried out using 5 % stacking and 12 % separating gels of thickness 0.75 mm at a constant voltage of 120 V for both stacking and resolving gel, respectively in MiniVE vertical electrophoresis unit (GE Healthcare). After the electrophoresis, the gels were stained with "Blue silver staining" protocol of Candiano *et al*, (2004), using colloidal Coomassie G-250 (Sigma Aldrich, USA) (Appendix Table A3).

2.2.18. Western Blot

Western blot was performed to analyze the expression of the recombinant proteins in bacterial system. Protein samples were resolved by SDS-PAGE using 12 % gel in the MiniVE vertical electrophoresis unit at 120 V. The electrophoresed protein gels were transferred to PVDF membrane at a fixed voltage of 25 V, 300 mA for 3-4 h at 4 ^{o}C in Blot module (GE Healthcare). The membrane was carefully taken out from the electro-blotting module and transfer of proteins on membrane was confirmed by Ponceau S staining (Sigma). Membranes were washed with PBS, pH 7.4 with 0.1 % Tween 20 (PBS-T) for 10 mins to remove the Ponceau S stain. The buffer was discarded and the membrane was washed again with PBS on a shaker. The membrane was then blocked with blocking buffer supplemented with 5 % BSA overnight to prevent non-specific adsorption. The blot was then washed with an excess of PBS-T three times for 10 mins each. The wash buffer was discarded and the membranes were then incubated with monoclonal anti-GST

antibody as the primary antibody (Sigma) using an optimized concentration in PBS containing 1 % BSA for 2 hr at room temperature. The membrane was washed three times with PBS-T for 10 mins each. This was followed by incubation with secondary antibody (HRP modified anti-rat IgG) from R&D systems (USA) appropriately diluted in PBS (1 % BSA) for 1 hr at room temperature with slow shaking. Thereafter the membrane was thoroughly washed with PBS for three times. Finally, the blot was developed using 3, 3'-Diaminobenzidine (DAB) tetrahydrochloride hydrate (Amresco, USA) at a concentration of 4 mg per 10 ml of PBS and charged with 10 µl 30 % hydrogen peroxide (Sigma Aldrich, USA) followed by imaging with a gel documentation system (ChemiDoc XRS+ Imaging System, BIO RAD). Details of reagents used are given in Table A3.

2.2.19. Circular dichroism

Circular dichroism (CD) spectra of the proteins were recorded using a spectropolarimeter (J-815, Jasco, Japan.) calibrated with 0.06 % (w/v) aqueous solution of (±)–10– camphorsulfonic acid. The spectrum was recorded in the wavelength range of 190-240 nm, in 0.1 cm path length suprasil quartz cuvette at 25 ^{o}C, at a scan rate of 100 nm/min, 1 nm bandwidth, with a time constant of 2 s, and an average of 4 scans. The spectrum was corrected for baseline and smoothed by Savitsky–Golay filter using Jasco spectral analysis software. The secondary structure analysis was performed using the Jasco SSE-protein secondary structure estimation program supplied with the instrument.

2.3. Results and Discussion

2.3.1. Cloning of *fabp3, fabp1, fabp4* and *fabp7*

The clones for *fabp3, fabp1, fabp4* and *fabp7* were obtained from DNASU Plasmid Repository. However, due to the absence of suitable tags and restriction enzyme sites, the gene fragments were subcloned into pGEX-4T2 expression vector and expressed in *E.coli*. Our cloning strategy is shown in Figure 2.1. The DNA fragments corresponding to FABP3, FABP1, FABP4 and FABP7 were amplified by PCR using specific primers for the fragments (Figure 2.2). The amplified fragments were cloned into the *BamH I – Xho I* sites of pGEX-4T2 expression vector and then transformed into competent *E.coli* DH5α by standard heat shock method. The recombinant clones were checked by restriction digestion. Four representative clones are shown in Figure 2.3. Subsequently, sequence of insert in one of the selected clone was confirmed by DNA sequencing by dideoxy method and compared with the repository sequence as well as the complete coding sequence of the respective *Homo sapiens* fatty acid binding protein through multiple sequence alignment (GenBank: BC007021.1 for FABP3; GenBank: BC032801.1 for FABP1; GenBank: BC003672.1 for FABP4 and GenBank: BC012299.1 for FABP7). The FABP3 insert showed complete sequence alignment (100 %) with the repository sequence and 99 % similarity with the complete coding sequence obtained from NCBI with a single base mismatch (C - T) which results in coding for arginine in place of stop. The FABP4 and FABP7 inserts displayed 99 % similarity with both the repository and complete coding sequence, respectively. Both the inserts had a single base mismatch (T-C). For FABP4 insert the single mismatch did not result in change

in the protein sequence with both coding for the tyrosine, however, for FABP7 insert the single mismatch resulted in a change in protein sequence from isoleucine to threonine. The FABP1 insert showed complete sequence alignment with both the repository and complete coding sequence.

2.3.2. Expression and purification of recombinant FABP3, FABP1, FABP4 and FABP7 in *E.coli*

The individual inserts were used for the expression of the respective GST tagged proteins in *E.coli* BL21 (DE3) cells. The transformed cells were induced at an optical density of 0.6 with an optimized IPTG concentration of 100 µM at 37 ^{o}C for FABP3, 1 and 4, and 50 µM for FABP7 at 30 ^{o}C for 12 hrs. Subsequently, the cells were harvested by centrifugation and whole cell lysate was prepared by sonication and checked by SDS-PAGE (Figure 2.4). The recombinant proteins were purified from clarified cell lysate using glutathione agarose affinity columns. Elution buffer containing glutathione was used for elution of the recombinant proteins. The residual glutathione in the eluant containing the recombinant protein was removed by dialysis. The purified proteins were analyzed by SDS-PAGE (Figure 2.5) and further characterized by Western Blot analysis with rat anti-GST antibody followed by anti-rat HRP antibody (Figure 2.6). The yield of the purified recombinant proteins expressed in *E.coli* BL21 (DE3) varied from 3.5-4 mg/ 100 ml of culture as estimated by Bradford assay.

2.3.3. Characterization of recombinant FABP3, FABP1, FABP4 and FABP7

To ascertain the correct secondary structures of the recombinant proteins, CD studies were performed. CD spectra of all the recombinant proteins were recorded at 25 ^{o}C in the range of 190-240 nm. The spectra of GST was subtracted from the combined spectra to obtain spectra for the recombinant protein only. CD spectra for all the proteins represented a spectra dominated by β-sheet conformation which conforms to the reported data obtained from X-ray crystallography (Figure 2.7, Table 2.1).

Table 2.1: Secondary structure composition of FABP 3, 1, 4 and 7.

Protein	α-helix (%)	β-sheet (%)	random coil (%)
FABP3	18.0	61.9	20.0
FABP1	15.0	72.1	12.9
FABP4	10.2	60.9	28.9
FABP7	17.4	61.8	20.8

2.4. Conclusion

As an initial step for the development of aptamers specific for FABP3, the coding sequence for FABP3 and three control proteins belonging to the family of intracellular fatty acid binding proteins (FABP1, FABP4 and FABP7) were cloned into pGEX-4T2 expression vector and finally transformed into BL21 (DE3) cells. The GST tagged recombinant proteins were purified by

glutathione agarose affinity chromatography, observed on SDS PAGE gels and identified on Western blots using anti-GST antibodies. The CD spectra of all the proteins were recorded to reveal major β-sheet composition, which were comparable to already reported data.

Figures

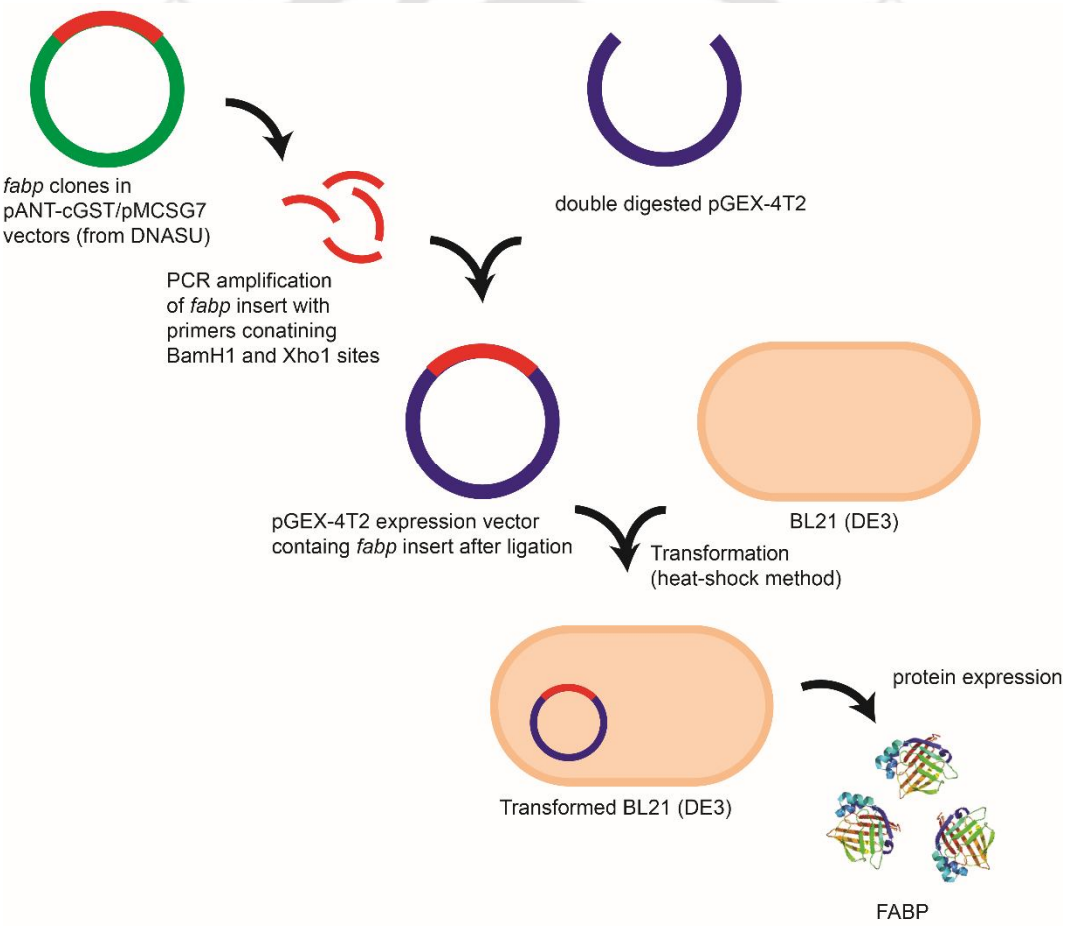

Figure 2.1: Scheme representing the cloning strategy used in the present work.

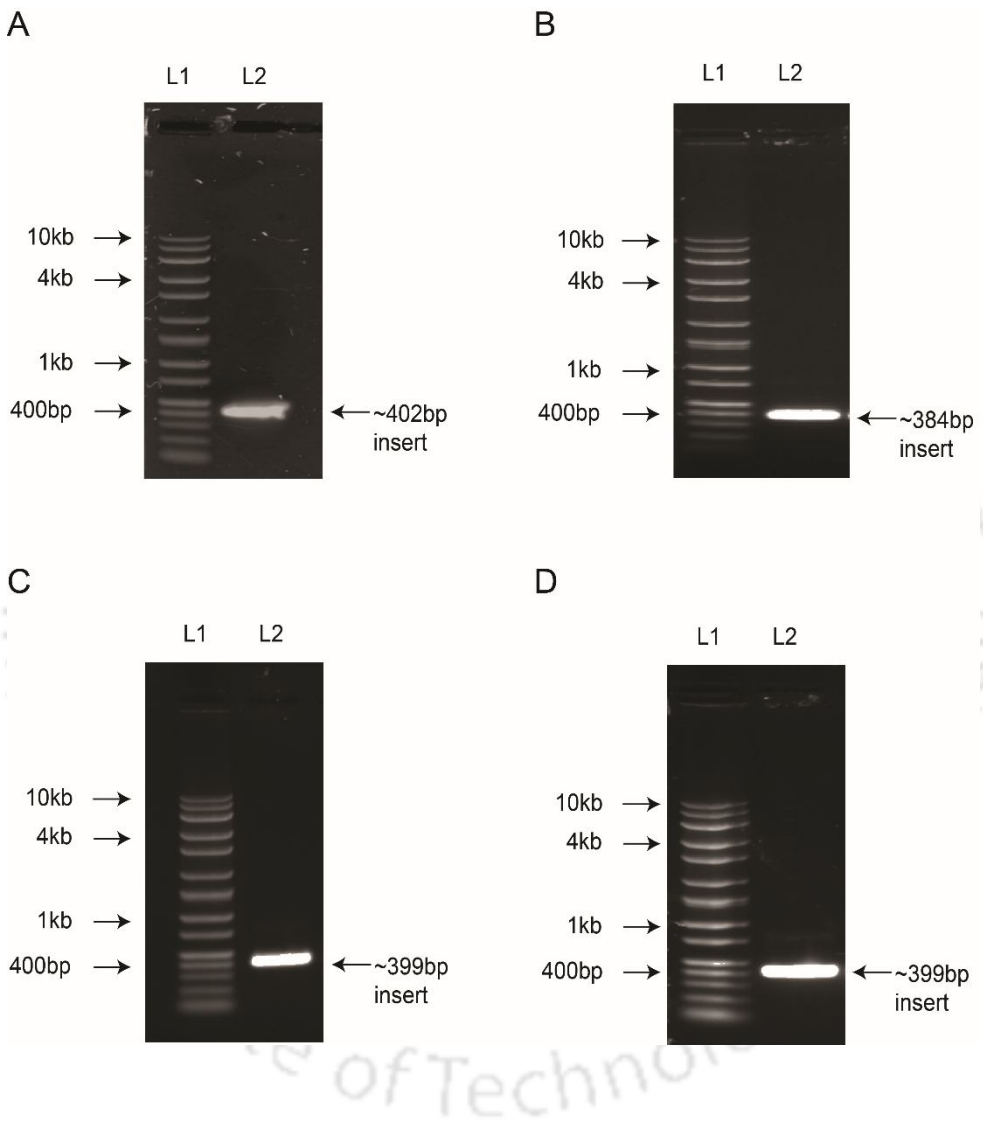

Figure 2.2: PCR product analysis of (A) *fabp3*, (B) *fabp1*, (C) *fabp4* and (D) *fabp7* in 0.8% agarose gels. Lane L1: wide range DNA marker, L2: *fabp* PCR amplicon.

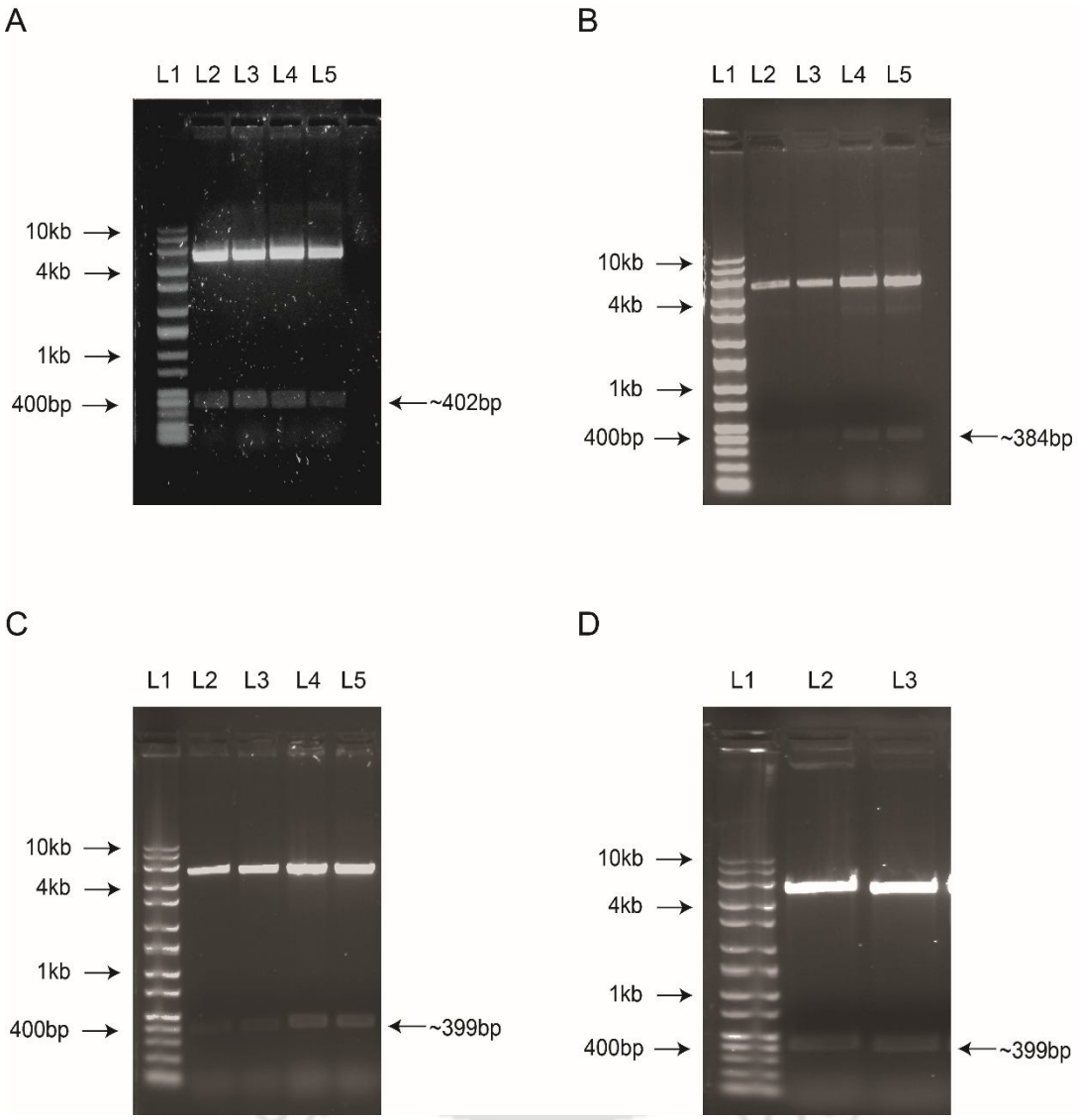

Figure 2.3: Restriction enzyme digestion of PCR product cloned in pGEX-4T2 vector. Lane L1: DNA marker, L2-L5: *BamHI* and *XhoI* digested pGEX-4T2 (A) *fabp3*, (B) *fabp1*, (C) *fabp4* and (D) *fabp7* clones.

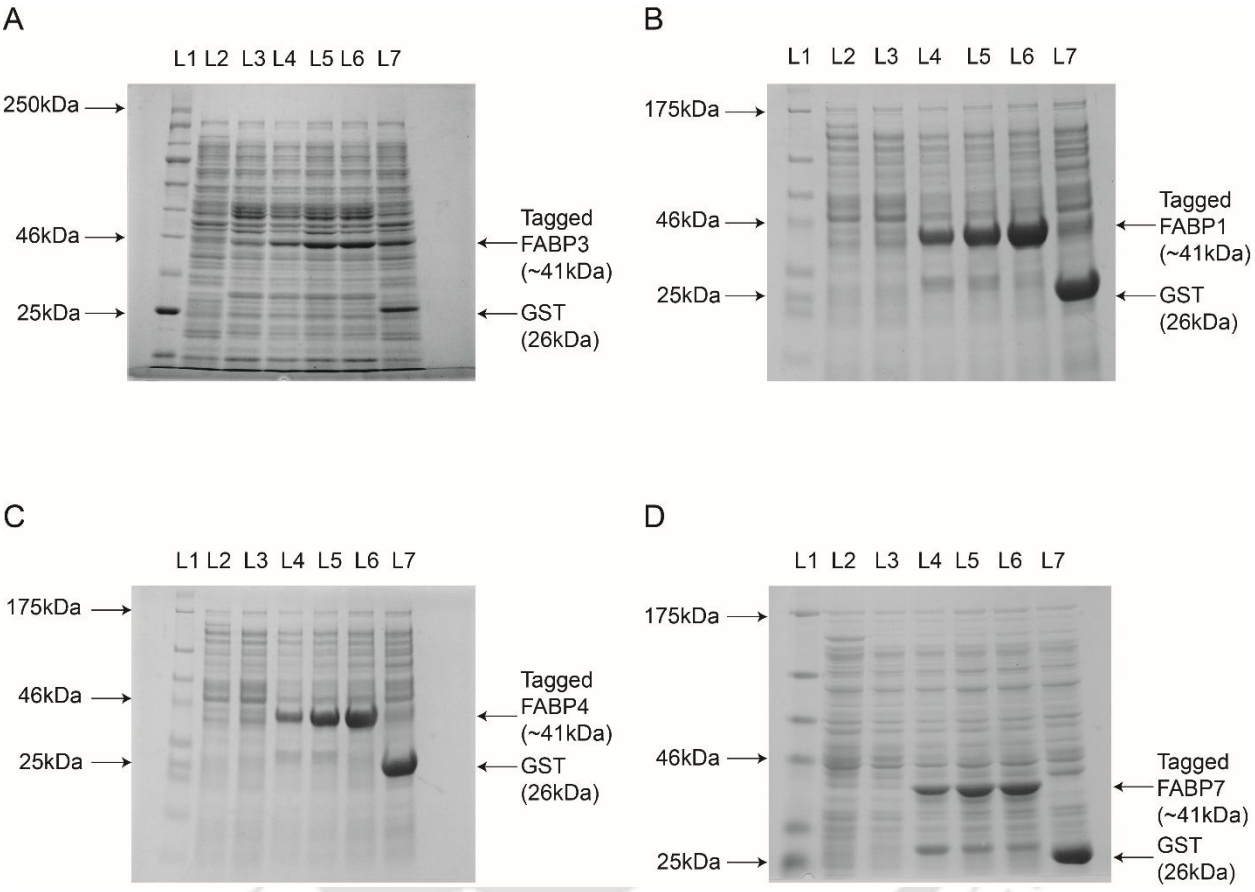

Figure 2.4: SDS PAGE (12 % gel) analysis of expressed GST tagged (A) FABP3, (B) FABP1, (C) FABP4 and (D) FABP7. FABP1, 4 and 3 were induced at an IPTG concentration of 100 µM for 4, 8 and 12 hrs at 37 ^{0}C while FABP7 was induced at 50 µM IPTG for 4, 8 and 12 hrs at 30 ^{0}C. Lane L1: protein molecular weight marker, L2: BL21 (DE3) induced, L3: clone uninduced, L4: clone induced for 4 hrs, L5: clone induced for 8 hrs, L6: clone induced for 12 hrs and L7: GST clone induced for 4 hrs.

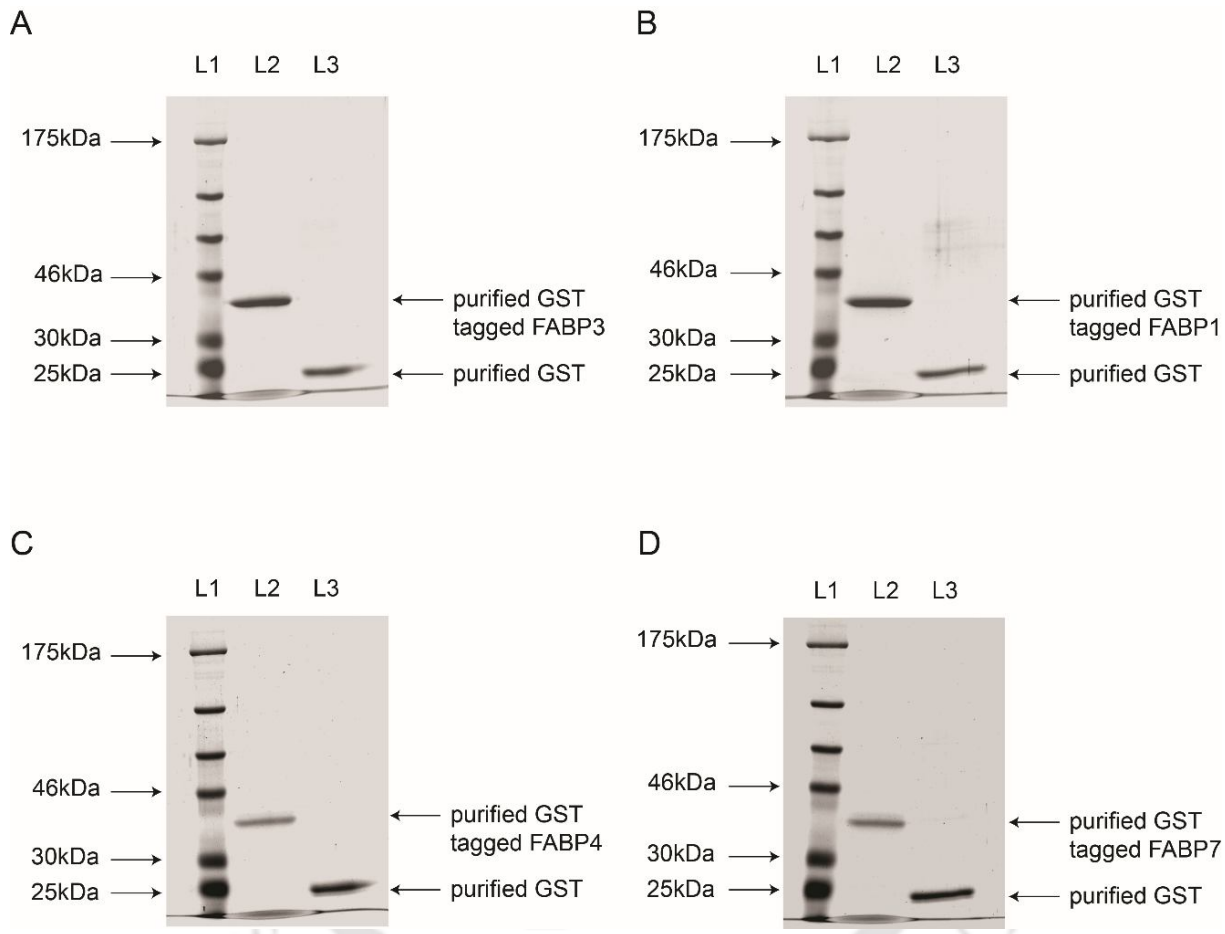

Figure 2.5: SDS PAGE of purified GST tagged (A) FABP3, (B) FABP1, (C) FABP4 and (D) FABP7. Lane L1: protein molecular weight marker, L2: purified GST tagged protein and L3: purified GST.

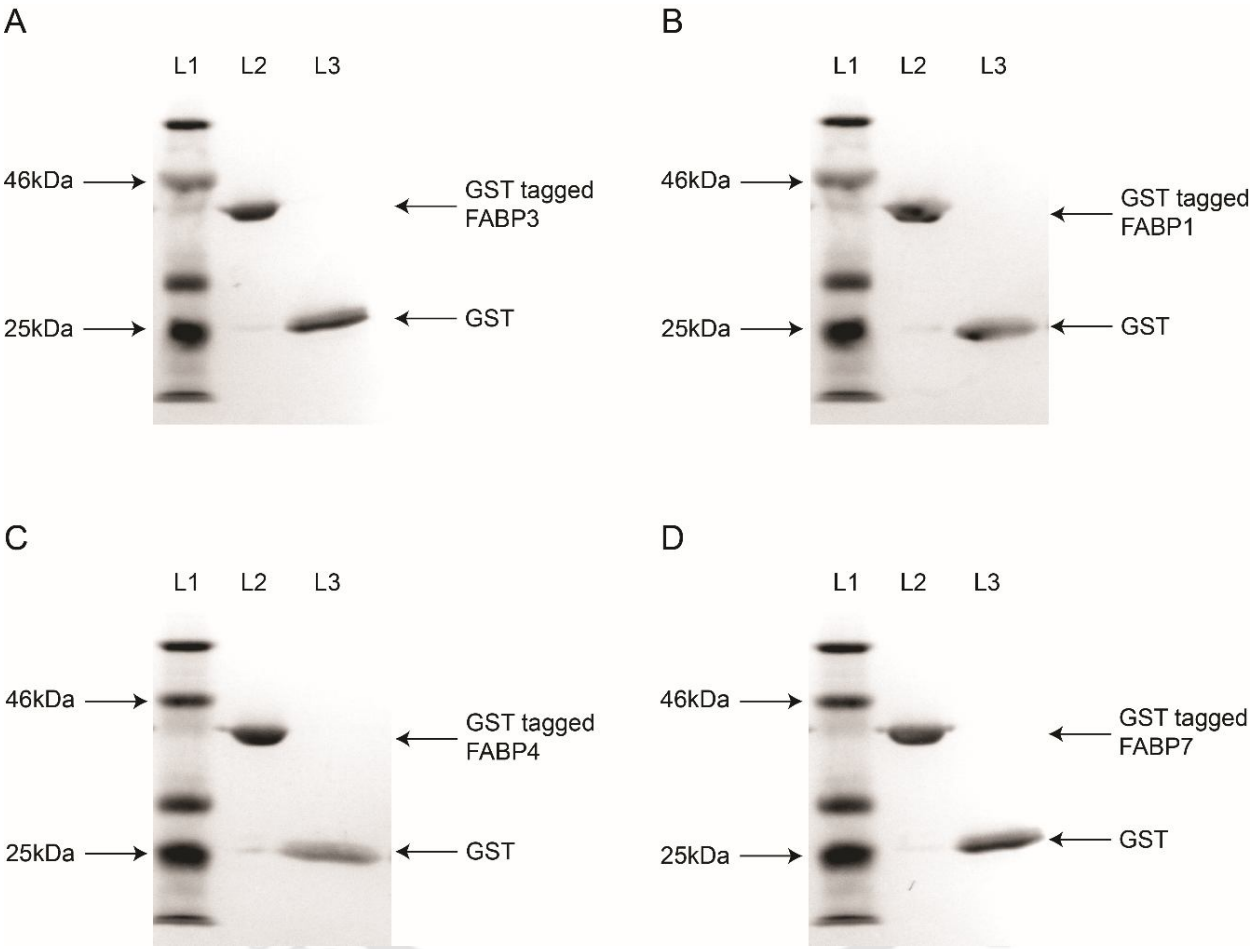

Figure 2.6: Western blot of GST tagged (A) FABP3, (B) FABP1, (C) FABP4 and (D) FABP7. Lane L1: protein molecular weight marker, L2: GST tagged protein and L3: GST.

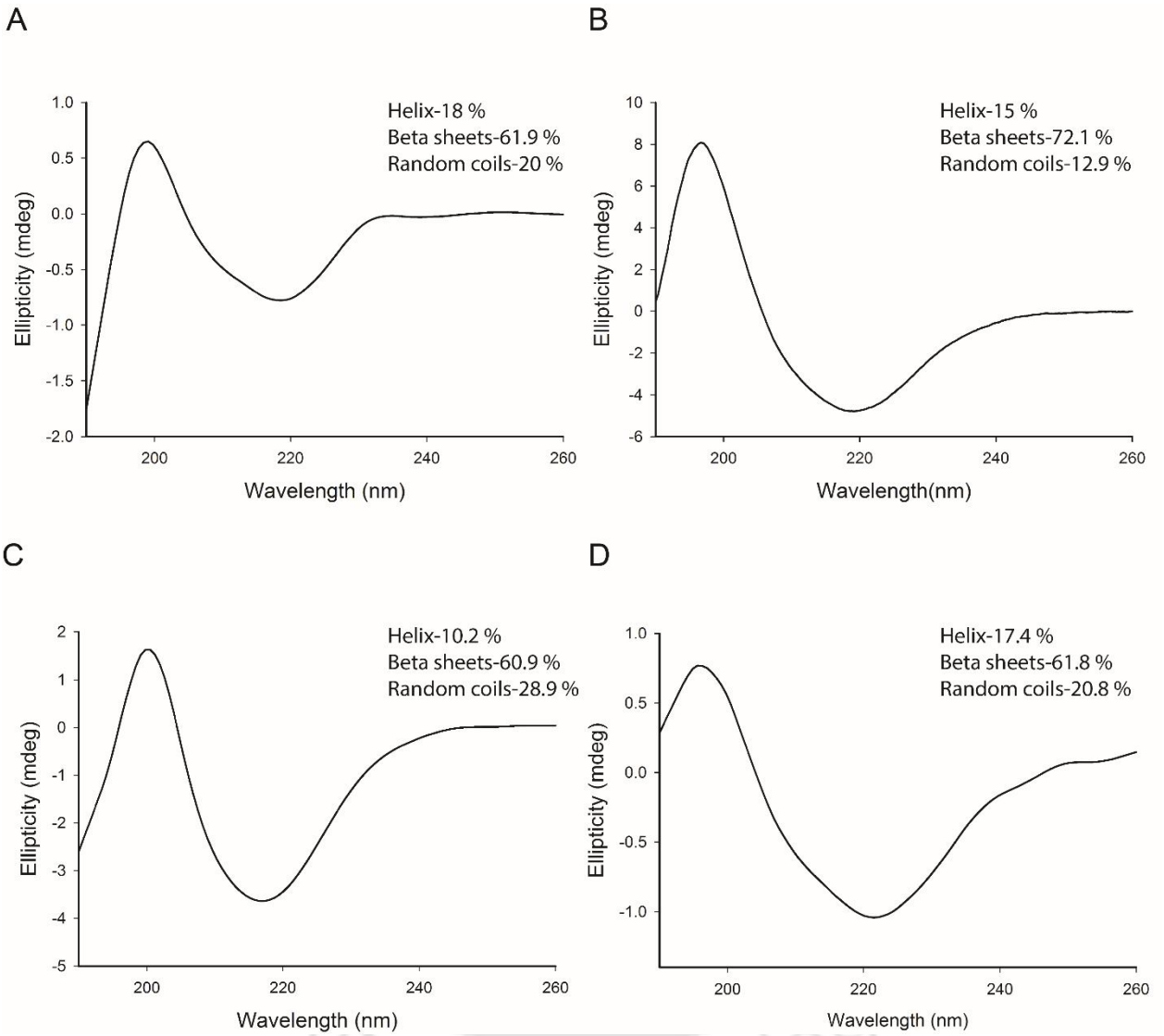

Figure 2.7: CD spectra of recombinant (A) FABP3, (B) FABP1, (C) FABP4 and (D) FABP7.

3

Development of aptamers specific for human FABP3 and their characterization

CHAPTER 3

Development of aptamers specific for human FABP3 and their characterization

3.1. Overview

Detection of FABP3 has been mainly achieved through antibody based assays or biosensors. However, the inherent instability of antibodies at high temperatures, high cost of production and batch to batch variations makes the whole process of testing expensive and less available to the common man. As a means of circumventing the disadvantages of antibodies, various types of alternative bio-recognition systems have been developed like nucleic acid and peptide aptamers. Nucleic acid aptamers are a group of oligonucleotide ligands comprising of single stranded DNA or RNA sequences with abilities to bind to their targets with great specificity and affinity often rivalling those of antibodies. Since its independent inception by Ellington *et al*., Tuerk *et al* and Robertson *et al* in the year 1990, aptamers have caught the attention of researchers as an emerging molecular recognition probe in diagnosis and therapeutics. Aptamers generated by the *in vitro* selection process of SELEX have several advantages over antibodies such as, comparable binding strength, discriminational binding to targets on the basis of subtle structural differences, high thermal stability, regeneration and chemical modification capability,

nonimmunogenic and nontoxic, fast renal filtration and short circulating halftime, low cost production and rapid large scale synthesis and chemical modification capability. As a replacement of antibodies in diagnostics and therapeutics, aptamers demonstrate great potential as an evolving versatile tool in biomedical research.

In this chapter, we describe selection of ssDNA aptamers against FABP3 (15 kDa), an early biomarker of acute myocardial infarction, for the first time. The FABP3 protein expressed and purified in Chapter 1 was used as target for SELEX whereas FABP1, 4 and 7 were used for counter SELEX. Through the selection process two aptamers that specifically bind to the target were isolated and subsequently characterized to yield interesting results pertaining to their converging sequences yet diverging structures. Furthermore, stability studies were conducted to assess the behavior of both the aptamers under variable conditions.

3.2. Experimental Approaches

3.2.1. Materials

Primers, ssDNA library, and aptamers were synthesized from Bioserve Biotechnologies India Pvt. Ltd. Restriction enzymes and streptavidin coated magnetic beads were obtained from New England Biolabs (USA). SYBR Gold was purchased from Invitrogen (USA), glutathione agarose magnetic beads from Thermo Fisher Scientific (USA) and pGEM-T easy vector from Promega (USA). X-Gal (5-bromo-4-chloro-3-indolyl-β-d-galactopyranoside) and IPTG (Isopropyl β-D-thiogalactopyranoside) were purchased from Himedia (India). All other chemicals

were of analytical grade.

3.2.2. Initial library design

A ssDNA library containing 40 randomized nucleotides flanked by two primer binding sites was designed as follows:

5'-CACCTAATACGACTCACTATAGCGGATCCGA-N40-CTGGCTCGAACAAGCTTGC-3'

3.2.3. Immobilization of protein on glutathione agarose magnetic beads

A total of 50 µl glutathione magnetic beads were washed twice with binding buffer (50 mM sodium phosphate buffer (SPB), pH 7.4, 50 mM NaCl, 5 mM KCl, 2.5 mM $MgCl_2$) containing 0.05 % Tween 20 for 10 mins each at room temperature. The beads were incubated with an excess of protein in a hybridization chamber for 1 hr at 25 ^oC. The beads were then washed twice to remove any unbound protein and were used for the subsequent SELEX cycles.

3.2.4. SELEX

A total of 2.5 nmole ssDNA pool (5'-CACCTAATACGACTCACTATAGCGGA-N40-GCAAGCTTGTTCGAGCCAG-3') dissolved in binding buffer was denatured by heating at 90 ^oC for 10 mins, then cooled to room temperature before binding. The ssDNA pool was incubated with FABP3 immobilized on glutathione agarose magnetic beads for 1 hr. The unbound ssDNA sequences were removed through washing and the sequences bound to FABP3 were amplified by

PCR using the following primers and conditions: Forward primer: 5'-CAC CTA ATA CGA CTC ACT ATA GCG GA-3', Reverse primer: 5'-biotin-GCA AGC TTG TTC GAG CCA G-3', initial denaturation at 95 ^{o}C for 10 mins, followed by 18 cycles of 95 ^{o}C, 15 s, 68 ^{o}C, 15 s, 72 ^{o}C, 3 s, and final extension at 72 ^{o}C for 10 mins was carried out. To separate ssDNA from the amplified dsDNA, the PCR product was incubated with 30 µl of streptavidin coated magnetic beads in a coupling buffer (20 mM Tris-HCl, pH 7.5, 0.5 M NaCl, 1 mM EDTA) at room temperature for 1 hr. The beads were then washed with coupling buffer and ssDNA strands were separated from biotinylated strands using 100 µl of 100 mM NaOH. The pH of the solution was then adjusted to 7.5. The separated ssDNA strands were used for the next round of SELEX. A total of 20 SELEX cycles were carried out, out of which 8 were counter cycles. To increase the stringency of SELEX cycles, the incubation time for binding of aptamers were varied as follows: 60 mins for 1-6 cycles, 40 mins for 7-9 cycles and 20 mins for 10-12 cycles. Individual counter SELEX against FABP4, FABP1 and FABP7 were carried out after cycle 6, 11 and 16, respectively, whereas counter SELEX against GST was carried out four times one at the beginning and the other three after cycle 5, 10 and 15, respectively. One counter SELEX was also incorporated for the glutathione magnetic beads at the beginning. Buffer compositions are mentioned in Appendix Table A3.

3.2.5. Cloning and sequencing of enriched aptamers

The screened aptamer candidates after the 20th round of SELEX were cloned into a pGEM-T easy vector and used to transform competent DH5α cells. The transformed cells were selected on the basis of blue-white screening and restriction enzyme digestion. The positive clones were

then sequenced and aligned using ClustalX2 software to compare the sequences.

3.2.6. Electrophoretic mobility shift assay (EMSA)

An amount of 0.2 pmole aptamer was heated at 90 ^{o}C for 10 mins, cooled to room temperature for 10 mins followed by addition of 30 µM of each protein. The mix was incubated for 1 hr at room temperature and then separated in a 6 % native (29:1) TBE gel for 2 hrs at 100 V and 4 ^{o}C. The gels were subsequently stained with SYBR Gold dye and visualized. EMSA were also performed to study the formation of the aptamer-protein complex with an increasing concentration of FABP3 (0, 0.1, 0.5, 1, 10, 25, 50, 75, 100 µM) at a fixed concentration of aptamer. Control experiments were also performed in the presence of an unrelated 90 bp ss DNA.

3.2.7. Circular dichroism (CD) studies

A total of 4 µM aptamer was heated for 10 mins at 90 ^{o}C, cooled to room temperature, followed by addition of 4 µM of the individual proteins. The mixture was incubated for 30 mins at room temperature followed by recording of the CD spectra at 25 ^{0}C using a Jasco J-815 spectropolarimeter. Far UV scans were obtained in continuous mode, collecting measurements every 1nm between 200-340 nm. Spectra were collected with an average of 4 accumulations, scan rate of 100 nm/min, bandwidth of 1nm and response of 2 s. Buffer contributions were subtracted from spectra and smoothed by Savitsky-Golay algorithm. To determine the dissociation constants of the selected aptamers, the increase in CD signal on binding to increasing concentrations of FABP3 were recorded. The differences in intensities at the peak wavelength were plotted against

concentrations of FABP3 added to obtain a graph which was fitted to a single site ligand binding model to obtain the K_d of the individual aptamers (Garbett *et al*., 2007). Effect of K^+, Na^+ and Mg^{2+} ions on aptamer secondary structures were studied at concentrations of 100 mM in SELEX binding buffer. Similarly, influence of pH on aptamer structure was studied in the range of pH 4-9, while the effect of aptamer strand concentration on melting temperature was studied at an aptamer concentration range of 2-20 µM and temperature range of 4-90 ^oC.

3.2.8. Secondary structure and G-quadruplex mapping

Secondary structure prediction of the screened aptamers was carried out using the Mfold web server (Zuker *et al*., 2003). The ionic conditions were chosen as 50 mM NaCl and 2.5 mM $MgCl_2$ and temperature was fixed at 25 ^oC. G-quadruplex prediction software QGRS (**Q**uadruplex forming **G**-**R**ich **S**equences) mapper was used to predict the possibility of the sequences to fold into a quadruplex structure (Kikin *et al*., 2006). The default parameters were set with maximum QGRS length of 30, minimum G-group of 2 and loop size between 0-36 nucleotides.

3.2.9. Multidimensional melting data acquisition and analysis

Multidimensional 3D melting curves were obtained by recording the whole CD spectra (200-340 nm) as a function of temperature. The singular value decomposition (SVD) method was used for characterization of 3D melting sets and the results obtained were fit to equilibrium models to obtain mechanistic and thermodynamic information (Gray *et al*., 2011). Briefly, using the CD

spectrophotometer, the ellipticity versus wavelength of the selected aptamers were recorded in the 200-340 nm wavelength range at different temperatures (4-90 ^{o}C). A reference blank spectrum was also collected for the buffer alone at the same wavelength and temperature range. A D matrix was prepared with the normalized data, imported to MATLAB for SVD analysis and calculation of the S, U, V and U x S matrices were done. The dataset was then fit to a two-state process using the GlobalWorks software package to obtain the optimized parameters (Matheson *et al*., 1987).

3.3. Results and Discussion

3.3.1. SELEX and screening of positive clones

A total of 20 SELEX cycles were carried out against the target protein FABP3, out of which 8 were counter cycles incorporating three intracellular fatty acid binding proteins, more specifically liver (FABP1), adipocyte (FABP4) and brain (FABP7), followed by cloning of the enriched pool in TA vectors (Figure 3.1). A total of 57 clones were picked and screened (Figure 3.2) and finally 50 positive clones were sequenced and analyzed with Clustal X2. The analysis showed 7 sequences were enriched at levels more than the others (Table 3.1). Alignment studies of these sequences did not display any significant conservation in the random regions of these sequences (Figure 3.3).

Table 3.1: Enriched aptamer candidates obtained after 20 rounds of SELEX.

Aptamer name	Sequence
N13	5'CACCTAATACGACTCACTATAGCGGATCCGAAGGGGGCGCGAGGTGTAAGGGTGTGGGGTGGTGGGTGGGCCTGGCTCGAACAAGCTTGC3'
N34	5'CACCTAATACGACTCACTATAGCGGATCCGACACCCACACCCCCCTGCACCTCCCCTACACCACCCCCCGCCTGGCTCGAACAAGCTTGC3'
N35	5'CACCTAATACGACTCACTATAGCGGATCCGACCACTTCCCCCGCCCCCGCCCCATGCCCTCCCTCTCCCGCCTGGCTCGAACAAGCTTGC3'
N36	5'CACCTAATACGACTCACTATAGCGGATCCGAGGAGTAAGGCGGGCGTGGGAATCGGGGTTAGCGGGGGGGCCTGGCTCGAACAAGCTTGC3'
N41	5'CACCTAATACGACTCACTATAGCGGATCCGAACTACACACACCCGTCCCAACACACCCATCCTCCATGTGCCTGGCTCGAACAAGCTTGC3'
N52	5'CACCTAATACGACTCACTATAGCGGATCCGAAAGAGGTGAGGAGATGGTAGTACGGGAAAGATGGAGGGGCCTGGCTCGAACAAGCTTGC3'
N53	5'CACCTAATACGACTCACTATAGCGGATCCGAGGGGGTAGCGGGTGGGCCGGTGGATGCGGGGCGCCGGCGCCTGGCTCGAACAAGCTTGC3'

3.3.2. Specificity and affinity studies of aptamers

To ascertain the specificity of the 7 enriched aptamers EMSA were conducted in the presence of the target protein FABP3 and each of the control proteins FABP1, FABP4, FABP7,

and GST. The EMSA results suggest specific binding in the event of two aptamers N13 and N53 while the rest of 5 aptamers bound to one or more of the control proteins (Figure 3.4 A, B). The increase in intensity of the aptamer-protein complex band with increase of protein concentration in the mixture was observed for both N13 and N53 suggesting increased interacting population between the aptamer and FABP3 (Figure 3.4 C, D). Control studies were also performed in the presence of an unrelated ssDNA of 90 bp. The results displayed no binding of the protein to the unrelated DNA (not included in figures). On the basis of EMSA results N13 and N53 were considered for further study. The EMSA outcome was supported by the CD studies, wherein the aptamer candidates demonstrated binding to FABP3 resulting in change in the CD spectra of the aptamers. N13 did not show any spectral changes on addition of the control proteins whereas N53 displayed a negligible change. However, the spectral change of N53 on binding to FABP3 was far more pronounced than the change on binding to FABP1, FABP4, FABP7 and GST (Figure 3.4 E, F). Increase in CD peak intensity of aptamers (Figure 3.4 G, H) on binding to increased concentrations of FABP3 was utilized to determine the dissociation constants of the aptamers. The dissociation constants (K_d) so determined were 0.0743 ± 0.0142 µM and 0.3337 ± 0.1485 µM for N13 and N53, respectively (Figure 3.5).

3.3.3. Structure prediction of aptamers

Based on the sequence alignment of their random regions, both N13 and N53 were found to have regions of 100 % identity depicted in blue while regions in green depict 70 % similarity. Overall, both the sequences including their primer regions share a sequence identity of 75 %.

However, these similarities in sequences do not reflect in their secondary structures as predicted by Mfold (Figure 3.6). N13 has one circular structure with two small and one bent long arm while N53 has one big circular structure with four small arms. Analysis of the sequences of both N13 and N53 uncovers the presence of G-rich regions which might contribute to the formation of complex G-quadruplex structures. The G quadruplex prediction software QGRS Mapper predicted a total of 2 QGRS sequences for N13 and 1 QGRS sequence for N53 (Table 3.2).

Table 3.2: The QGRS sequences as predicted by the QGRS Mapper software for N13 and N53.

Aptamer	Position	Length	QGRS	G-Score
N13	24	21	**GG**ATCCGAA**GG**G**GG**CGCGA**GG**	15
	50	21	**GGG**TGTG**GGG**TGGT**GGG**T**GGG**	39
N53	32	30	**GGG**GGTAGC**GGG**T**GGG**CCGGTGGATGC**GGG**	32

To confirm the structure of the aptamers as predicted by the QGRS Mapper, the CD spectra of both the aptamers were studied under the same conditions as SELEX. The signature peaks corresponding to a G-quadruplex structure were not found but the aptamers demonstrated peaks corresponding to duplex B DNA i.e. a positive peak at 260-280 nm and a negative peak at 245 nm, which suggests that the aptamers hybridize to form double stranded regions (Figure 3.7 A, B).

3.3.4. Effect of ionic strength, pH and temperature on aptamer structure

Salt ions play a major role in maintaining the structure of DNA. Therefore the effect of different salt ions on the native structure of the aptamers was investigated in presence of the

binding buffer used for SELEX (Figure 3.8). For both N13 and N53 there was no significant change in the peak intensity at 283 nm in the CD spectrum (Fig 3.8 A and B), which enforces the fact that in the settings of the binding buffer, even in the presence of high salt concentrations, both the aptamers maintained their structure intact. This study confirms the stability of the aptamers at high salt concentrations.

A similar study was performed to evaluate the effect of different pH conditions on the conformation of the aptamers. For both the aptamers the CD spectra at acidic conditions displayed reduced peak intensity at 281 nm and 245 nm and a peak shift from around 195 nm to 205-210 nm. For N13 the peak intensity at 281 nm was observed to be increased in the following sequence pH 4 < pH 5 < pH 9 < pH 7 < pH 8 < pH 6 with the peak shape being slightly broad shaped at pH 6. Similarly for N53 the peak intensities at 280 nm and 245 nm were similar for pH 6, 7 and 9 whereas at pH 8 the aptamer showed maximum peak intensities at both these wavelengths. At pH 4 and pH 5, the peak intensities at both 245 nm and 280 nm were reduced (Figure 3.9).This study suggests that the aptamers were comparatively stable at neutral and slightly alkaline conditions as compared to acidic conditions.

To determine the thermal stability as well as the thermodynamics of its folding-unfolding process, thermal denaturation experiments were carried out. Firstly, the effect of the aptamer strand concentration on the melting temperature (T_m) in the range of 2-20 µM in the absence of ligands was studied. The results indicated that for both N13 and N53, the T_m varied in the range of 47-58 ^oC and 52-56 ^oC, respectively (Figure 3.10). Therefore, to ascertain the correct model dependent thermodynamic parameters, multidimensional 3D melting curves were obtained by recording the

whole CD spectra (200-340 nm) as a function of temperature. For aptamer N13, both the singular value and Scree plot analysis suggests that 2 components are required to reproduce the CD data matrices within the level of noise. From the basis spectra, it can be suggested that 2 species contribute to the CD matrix. The first spectra being the most prominent and the second spectra the least, supported by its smaller singular value and low contribution to the variance. The autocorrelation coefficients of the U matrix elements were high, however, the V matrix elements showed a cutoff value after the third component, with the first three values being significant with coefficients greater than 0.8 (Figure 3.11). The dataset was then fit to a two state process using the GlobalWorks software package to obtain the optimized parameters. The least squares optimized parameters T_m and ΔH along with the standard error of the fits are summarized in Table 3.3.

Table 3.3: Summary of thermodynamic parameters for melting of N13 and N53 in SELEX buffer.

Aptamer	SD of fit	T_m (^{0}C)	ΔH (kcal/mol)
N13	0.0478	60.7 ± 0.9	14.9 ± 1.9
N53	0.0536	53 ± 8.0	12 ± 7.0

*SD – standard deviation

The SVD analysis of the N53 dataset suggested a three state melting process based on the singular values and Scree plot. However, the plot for the temperature dependence of V matrix elements as well as the autocorrelation coefficients strongly suggested a two component melting profile (Figure 3.12). Fitting the dataset to a two state process yielded T_m and ΔH parameters as in Table 3.3. The 3D melting study reinforced the finding that both N13 and N53 exists in a simple two

state form independent of strand concentrations and do not take part in the formation of higher ordered DNA structures with complex interactions. The melting temperatures so determined justifies the greater extent of hybridization observed in Mfold predicted structure of N13 as compared to N53. Furthermore, the autocorrelation coefficient for N13 (Figure 3.11 E) indicates at the formation of an intermediate species during the melting experiments, which can be highly possible considering the structure predicted by Mfold. However, the intermediate species do not have a significant effect on the overall thermal denaturation process as observed in the combined studies.

3.4. Conclusion

We report here the selective evolution of aptamers against human FABP3 for the first time. This study entails the generation of two concurrently evolved anti-FABP3 aptamers with significant sequence variance from the same ssDNA pool. These bulky aptamers (90 bp) though confer equally specific interactions with the target protein their binding affinities significantly vary. Both the aptamers displayed stable behavior at certain ionic, pH and temperature conditions. Furthermore, both computational and experimental methods confirmed the formation of simple stem-loop structures by the aptamers, which served as a basis for the prediction of 3D structures for further interaction studies in the next chapter.

Figures

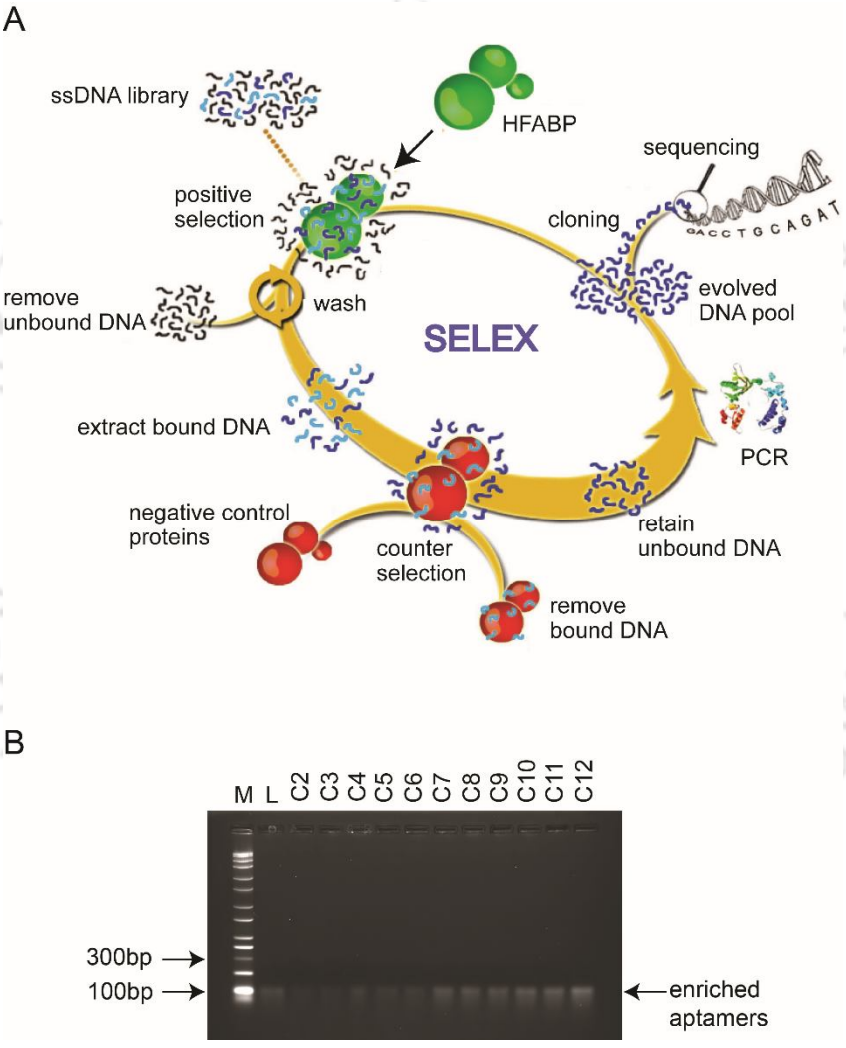

Figure 3.1: (A) SELEX cycles. (B) PCR amplification at the end of every cycle of positive SELEX. Lane M: Wide range DNA marker, L: aptamer library, C2-C12: PCR amplification at the end of SELEX cycle 2-12, respectively.

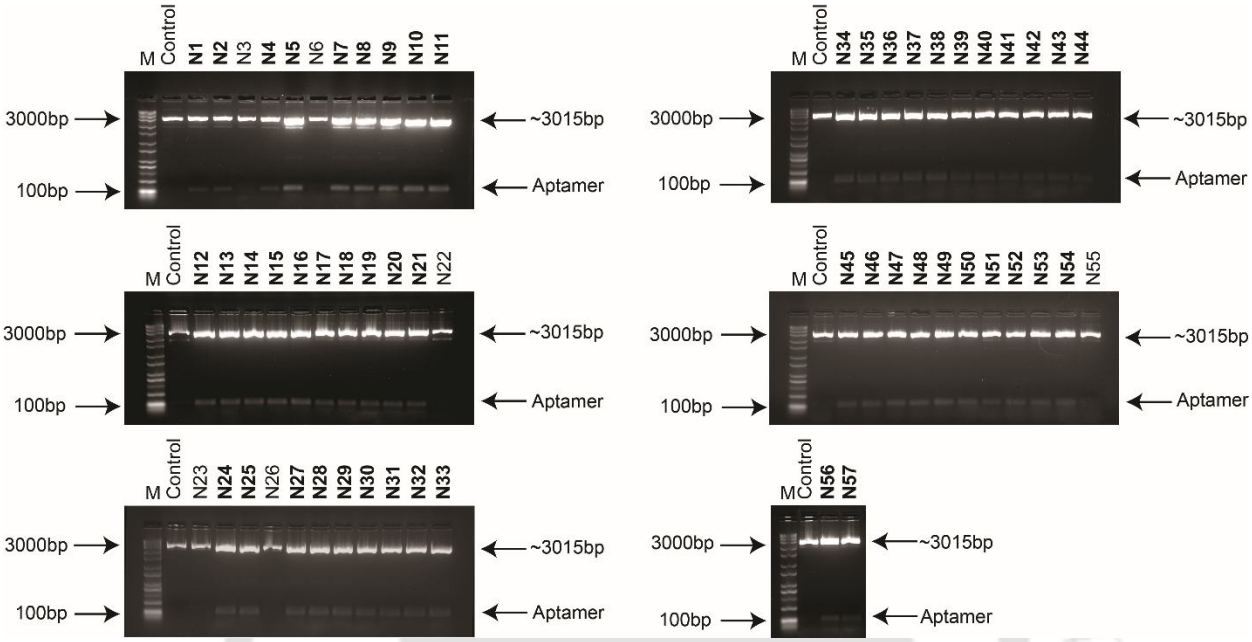

Figure 3.2: Screening of 57 TA clones (N1-N57) through restriction enzyme digestion. Lane M: Wide range DNA marker, Control: digestion product of plasmid from a blue colony. Positive clones are labeled in bold.

Figure 3.3: Sequence alignment of the random region of N13, N53, N36, N52, N41, N34 and N35. Blue regions depict 100 % similarity while green and yellow regions depict 70 % and 50 % similarity, respectively.

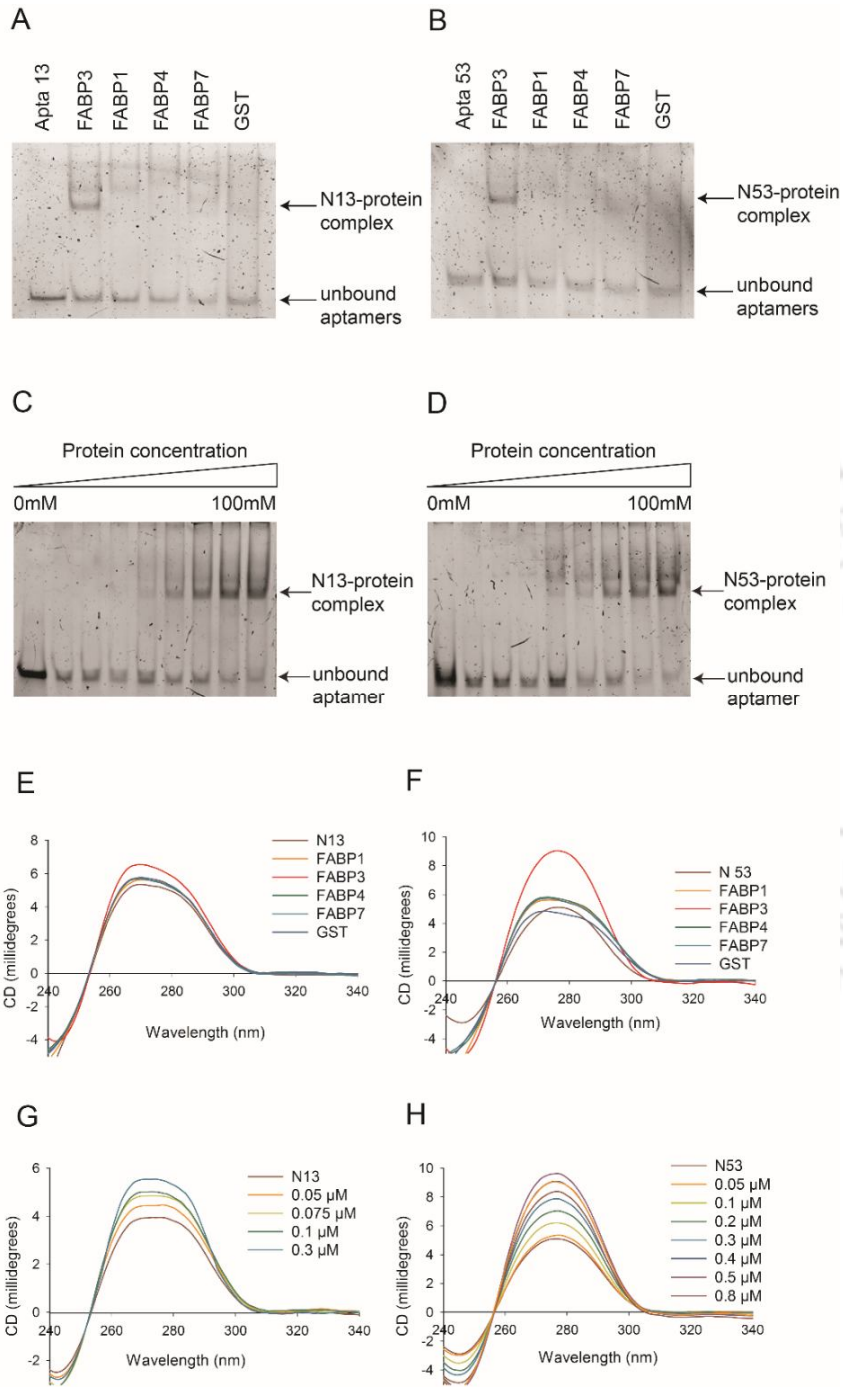

Figure 3.4: EMSA and CD for specificity study of aptamer in respective order N13: (A) and (E); N53: (B) and (F). EMSA band intensity as a function of FABP3 concentration: (C) for N13 and (D) for N53. Spectral intensity as a function of FABP3 concentration: (G) for N13 and (H) for N53.

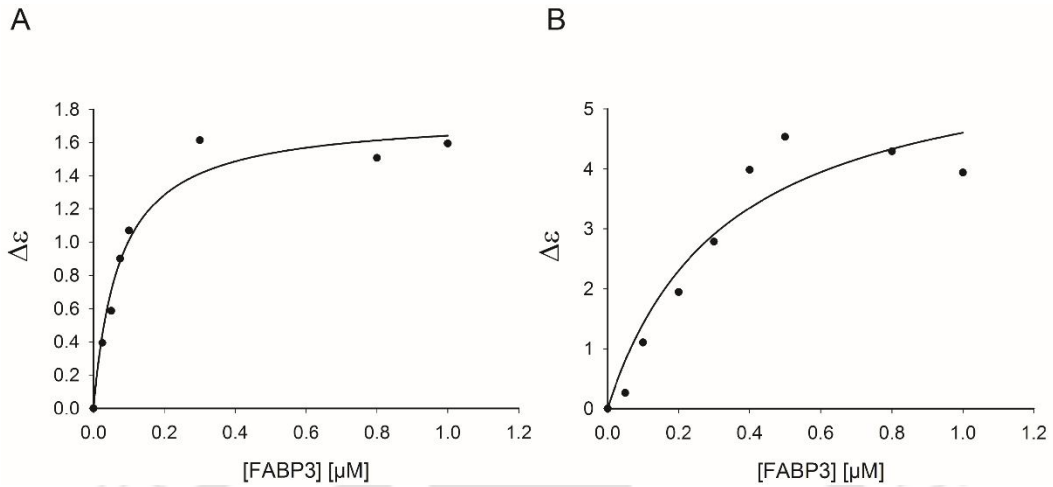

Figure 3.5: Plot of Δε (change in CD peak intensity) vs FABP3 concentration for determining the dissociation constants of (A) N13 and (B) N53.

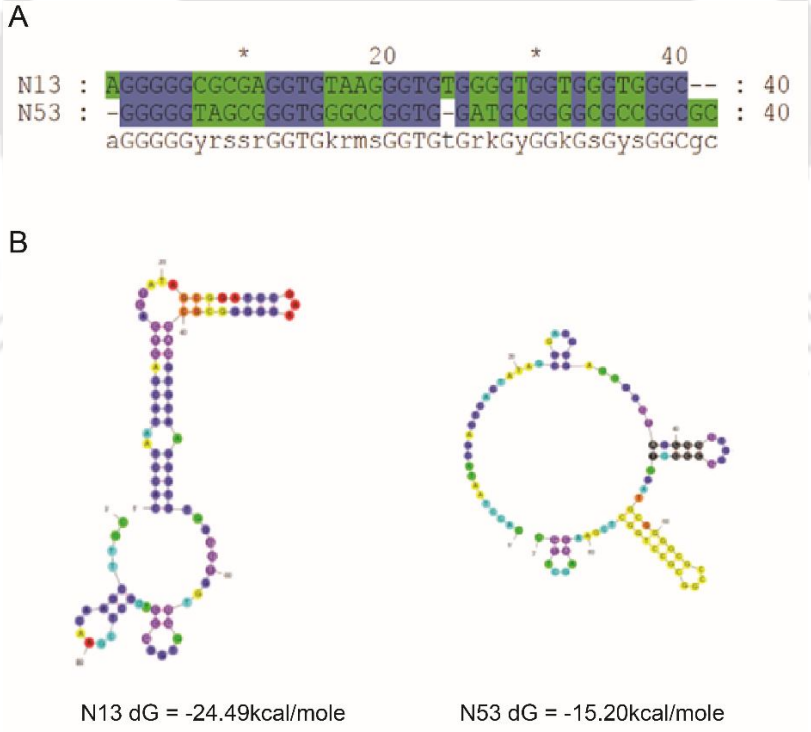

Figure 3.6: (A) Sequence alignment of the random region of N13 and N53. Blue regions depict 100% similarity while green regions 70 % similarity. (B) Secondary structures of selected aptamers as predicted by Mfold.

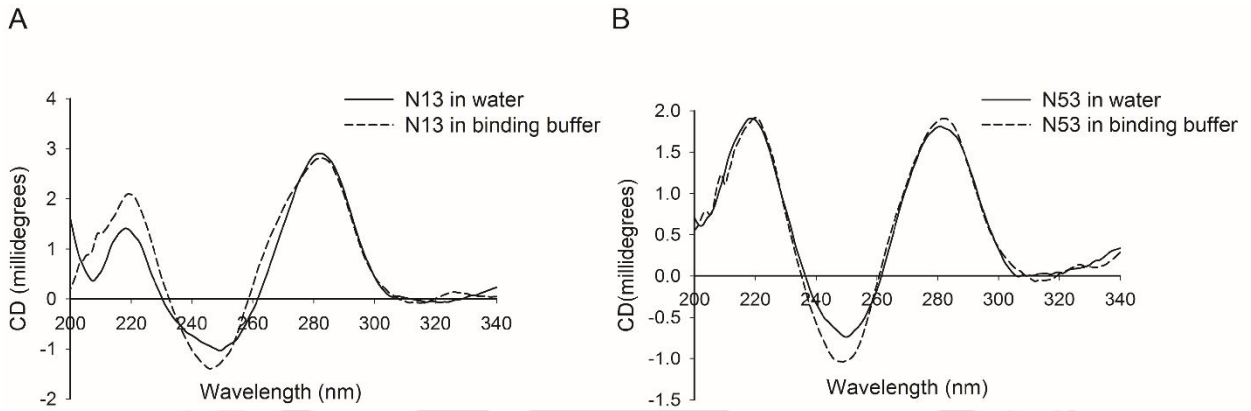

Figure 3.7: CD spectra of N13 (A) and N53 (B) in presence of water and binding buffer.

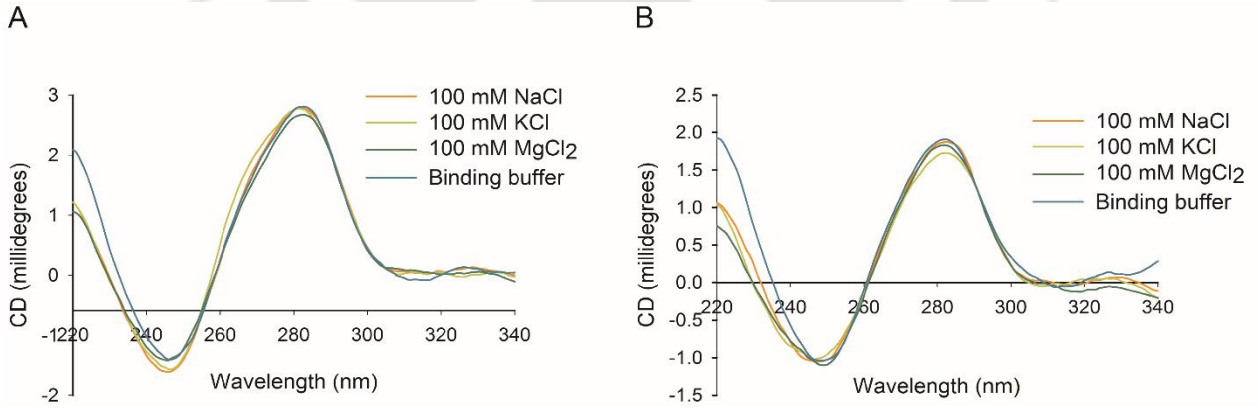

Figure 3.8: Effect of salt ions on the structure of (A) N13 and (B) N53 in SELEX binding buffer.

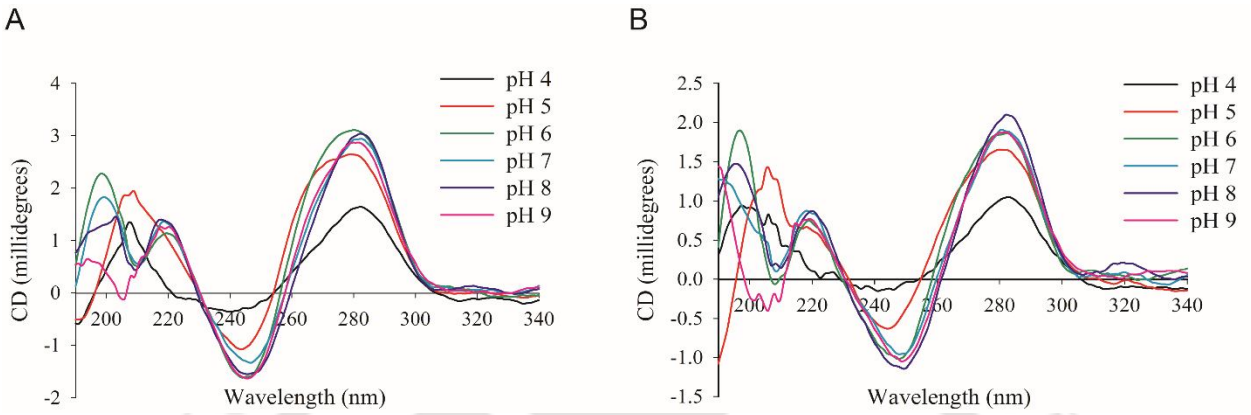

Figure 3.9: Effect of pH on the structure of N13 (A) and N53 (B) in SELEX binding buffer.

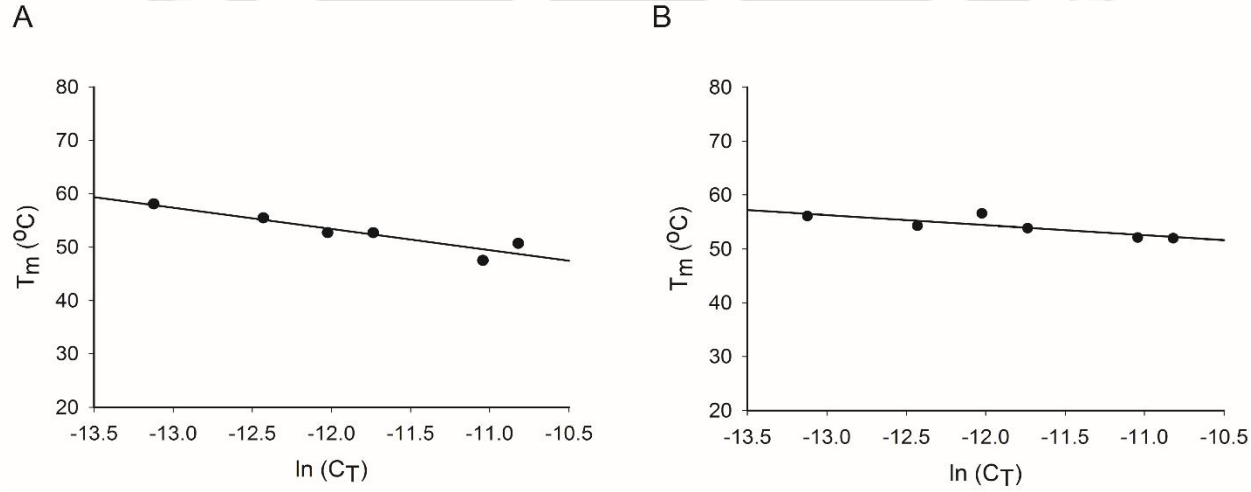

Figure 3.10: Effect of strand concentration on the thermal denaturation (A) N13 and (B) N53.

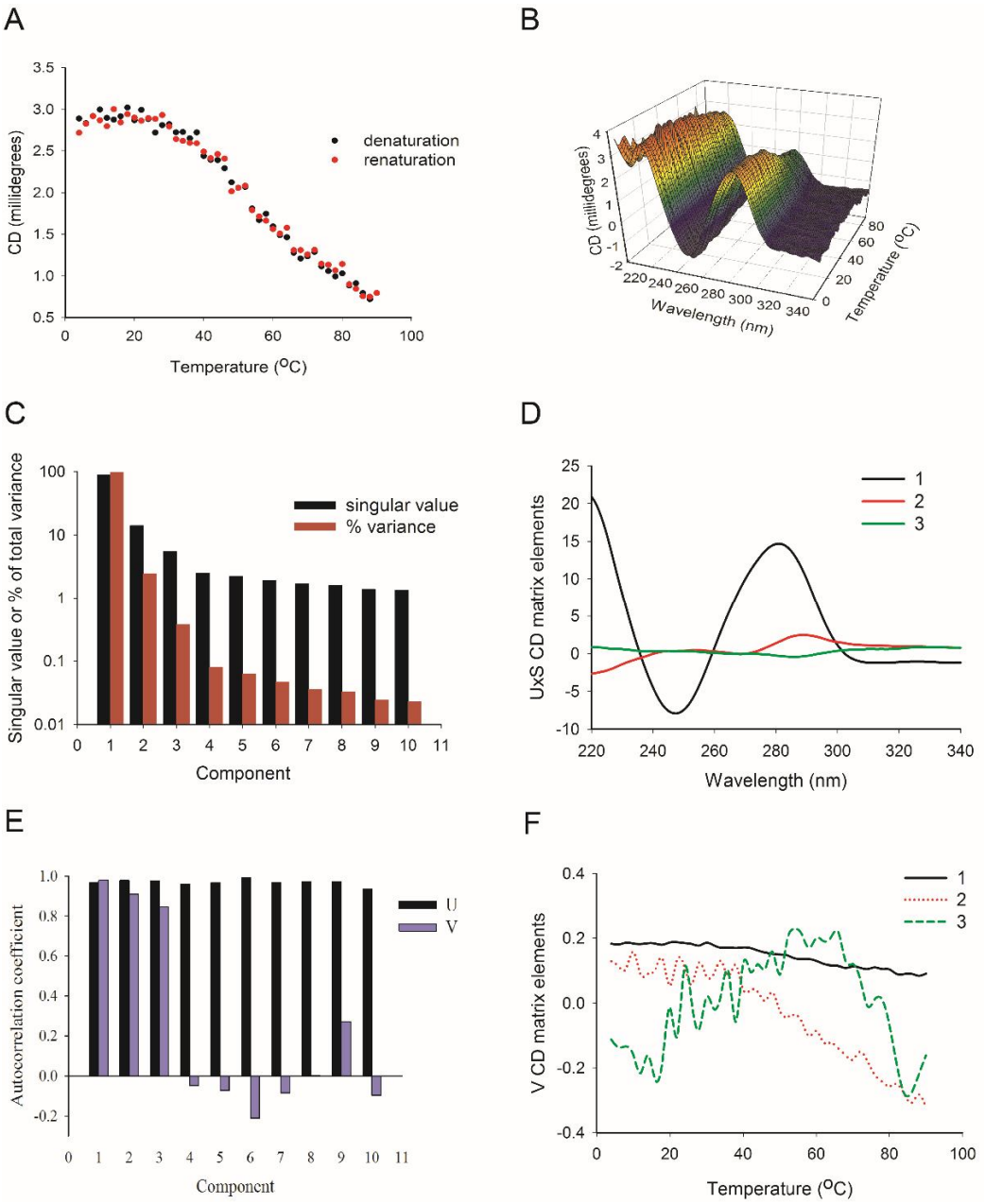

Figure 3.11: (A) 2D melting curve and (B) 3D melting curve of N13.(C) Singular values and their relative variance for the first ten significant components of the CD data. (D) Basis spectra determined using SVD analysis of the CD data sets by MATLAB. The numbers in the plot legends correspond to the rank order of the significant spectroscopic species. (E) Autocorrelation coefficients estimated for the first ten significant components of the U and V matrices. (F) Plot of three most significant elements of the V matrices corresponding to the dataset in (B).

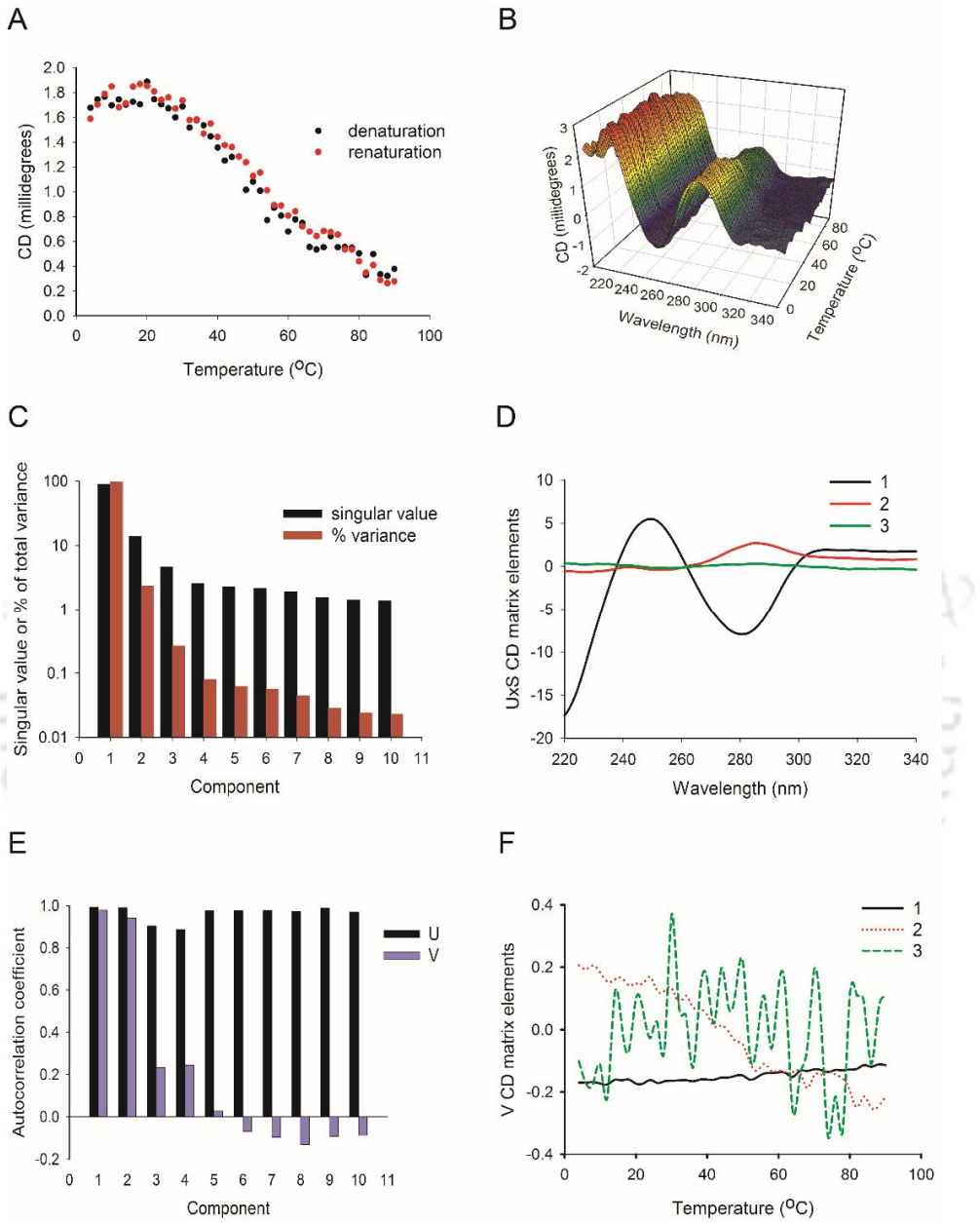

Figure 3.12: (A) 2D melting curve and (B) 3D melting curve of N53.(C) Singular values and their relative variance for the first ten significant components of the CD data. (D) Basis spectra determined using SVD analysis of the CD data sets by MATLAB. The numbers in the plot legends correspond to the rank order of the significant spectroscopic species. (E) Autocorrelation coefficients estimated for the first ten significant components of the U and V matrices. (F) Plot of three most significant elements of the V matrices corresponding to the dataset in (B).

4

Aptamer-FABP3 interaction studies

CHAPTER 4

Aptamer-FABP3 interaction studies

4.1. Overview

The subsequent step after aptamer generation and characterization is the investigation of aptamer-target interaction pattern in order to understand the bio recognition function of the aptamer with respect to its strength and specificity of binding. Various techniques are used to elucidate the mechanism of aptamer-target interaction, among which X-ray crystallography, electron crystallography and NMR are considered as core techniques. However, these methods are labor-intensive, time-consuming and require special skills to correctly analyze the generated complex data set. Besides the methods described above, other techniques like surface plasmon resonance (SPR), isothermal titration calorimetry (ITC), circular dichroism (CD), small angle X-ray scattering (SAXS), quartz crystal microbalance (QCM), foot printing assays, computational approaches etc. have been used to study aptamer-target interactions which however are non-exclusive techniques and thus do not provide detailed information . Another missing link is the unavailability of suitable 3D structure determination tools for ssDNA, which hinders the further characterization of interaction studies. Nevertheless, researchers now use RNA 3D structure determination tools to predict ssDNA 3D structures for docking studies (Dong *et al*., 2015; Wang

et al., 2015; Lao *et al*., 2014), based on the assumption that ssDNA folds in a similar way as RNA. These multiple techniques when used in conjunction, detailed information about the interactions involved in maintaining aptamer-target binding can be obtained.

In this chapter, we study the interaction patterns involved in maintaining aptamer-target binding using a combinatorial approach. Based on computationally obtained aptamer-protein complex models, the interacting residues in aptamer and protein were predicted and validated by limited proteolysis coupled mass spectrometry experiments.

4.2. Experimental Approaches

4.2.1. Materials

Aptamers were synthesized from Bioserve Biotechnologies India Pvt. Ltd. Trypsin and α-cyano-4-hydroxycinnamic acid were purchased from Sigma (USA), whereas trifluoroacetic acid (TFA) was obtained from Merck (Germany). FABP3 was expressed and purified as mentioned in Chapter 2. All other chemicals were of analytical grade and used as received.

4.2.2. 3D structure and binding mode predictions

The 3D structures of aptamers were predicted using the RNAComposer software (http://rnacomposer.cs.put.poznan.pl/) (Popenda *et al*., 2012) using the Mfold dot-bracket notation of the aptamers as input. Since the aptamers were single stranded like RNA, they were first converted into their corresponding RNA sequences. Aptamer-FABP3 (PDB: 4WBK) docking

studies were conducted using NPDock (http://genesilico.pl/NPDock) (Tuszynska *et al*., 2015) and analyzed using PyMOL.

4.2.3. Electrostatic potential calculations and bond prediction

Electrostatic surface potential map of FABP3 at pH 7.4 was generated using the Adaptive Poisson-Boltzmann Solver (APBS) online web server (http://nbcr-222.ucsd.edu/pdb2pqr_2.0.0/) (Dolinsky *et al*., 2004) based on Poisson-Boltzmann model. Color code units are in ±5 kT/e with red and blue being most electropositive and electronegative, respectively. Bond formation at the aptamer-protein interface was predicted using the PLIP (protein-ligand interaction profiler) software (https://projects.biotec.tu-dresden.de/plip-web/plip/index) (Salentin *et al*., 2015).

4.2.4. Limited Proteolysis

Limited trypsin digestions were performed in 100 mM ammonium bicarbonate buffer (pH 8) at a protein: enzyme ratio of 100:1 (w/w) whereas the aptamer: protein molar ratio was maintained at 4:1. A total of 5 µl aliquots of each digest were extracted every 10 mins up to 120 mins. Trypsin activity was terminated by adding 5 µl of 0.1 % TFA (pH 1.9). One µl of a saturated solution of α-cyano-4-hydroxycinnamic acid in 50 % acetonitrile in 0.05 % trifluoroacetic acid solution was mixed with 1 µl of the tryptic digest and deposited on the MALDI (Matrix-assisted laser desorption/ionization) sample plate.

4.2.5. MALDI MS analysis

MALDI mass spectra were acquired using a Bruker Ultraflex speed mass spectrometer (USA) equipped with a smartbeam 2 laser. All mass spectra were obtained in positive ion and reflectron mode with a global attenuator offset of 32 %, detector gain voltage of 1800 V for reflector base and averaged over 150 laser shots. For each time point in the time-resolved limited proteolysis, 8 total mass spectra were obtained, 2 each for N13: FABP3, N53: FABP3, FABP3 and GST digests. To avoid inherent inconsistencies in ionization and ion yield, the data were represented as normalized relative ion intensity.

4.2.6. Statistical analysis

All quantitative variables were expressed as mean ± standard deviation and analyzed by Student's t-test. Results were considered statistically significant at $p < 0.05$.

4.2.7. CD studies

Four µM aptamer was heated for 10 mins at 90 ^{o}C, cooled to room temperature, followed by addition of 4 µM of FABP3. The mixture was incubated for 30 mins at room temperature followed by recording of the CD spectra at 25 ^{o}C using a Jasco J-815 spectropolarimeter (Japan). Far UV scans were obtained in continuous mode, collecting measurements every 1nm between wavelength 200-340 nm. Spectra were collected with an accumulation number of 4, scan rate of

100 nm/min, bandwidth of 1nm and response of 2 s. Buffer contributions were subtracted from spectra and smoothed by Savitsky-Golay algorithm.

4.3. Results and discussion

4.3.1. Limited proteolysis studies

Mapping the regions involved in protein-ligand interactions is considered as an important step for characterizing the interactions, the information of which may eventually help to develop efficient ligands to be utilized in detection assays, as drugs in therapy or as purification agents, etc. The aptamer binding domain of FABP3 both in the presence of aptamer and alone was investigated by limited proteolysis with trypsin. The incubation time for proteolytic digestion was extended up to 120 mins. However, the time point of 10 mins was finally selected for analysis, as it offered more stark comparisons among the peptide peaks. Additionally, at early stages of proteolysis at elevated temperatures the combined effect of weak interactions and protein deformation is expected to be low. MALDI-MS analyses of the time-resolved limited proteolysis experiments representing the peptide maps generated at 10 mins of FABP3-GST, N13-FABP3-GST, and N53-FABP3-GST, respectively are represented in Figure 4.1.

For N13 significant differences were observed for m/z values of 907 and 2693 (p values of 0.0305 and 0.0369, respectively) (Figure 4.2). The m/z 907 peptide fragment (amino acids: 22 Lys-31 Arg) displayed an increased relative ion intensity in comparison to ligand-free protein ion

intensity, which might be interpreted as an outcome of an apparent change in conformation of the protein on N13 binding, resulting in an increased accessibility of trypsin to the specific amino acids 22 Lys and 31 Arg. Similarly, the observed decrease in intensity for the tryptic peptide m/z 2693 can be interpreted in two ways: one interpretation pertains to the physical obstruction presented by N13 to trypsin from accessing the sites 66 Lys and 91 Lys. Another possible explanation is that upon binding, N13 induces a conformational change that alters the tertiary structure of the protein to reduce the rate of proteolysis at the given site. The exposition of a viable conformational change of protein structure on N13 binding is further supported by the CD study of FABP3 in the presence of N13 displaying a prominent reduction of the negative CD peak at around 216 nm and the positive peak at 196 nm (Figure 4.3A). As FABP3 is a major β sheet protein any changes in its secondary structure CD spectra eventually indicates towards a perturbation in its β sheet composition. There was a reduction in both helix and β sheet composition upon binding to N13: helix percentage completely disappeared whereas β sheet percentage reduced to 58.9 % from 61.9 % and random coil increased to 41.1 % from 20 %. The effect of limited proteolysis on the GST tag was also monitored revealing a prominent effect on the intensity of two GST tryptic peptide fragments: m/z 1011 and m/z 1517 with p values of 0.0206 and 0.0005, respectively (Figure 4.4A). The increased ion intensity of the fragment m/z 1011 can be attributed to the increased accessibility of the protease to the sites 9 Lys and 18 Arg owing to possible conformational change on N13 binding. Similarly, the reduction in ion intensity of m/z 1517 can be explained in two ways: either N13 induces a conformational change in the protein, altering the accessibility of trypsin to the 89 Arg-103 Arg sites or N13 might physically block these sites.

However as evidenced in the EMSA and CD studies, N13 do not interact with GST, therefore physically obstructing trypsin from accessing the sites arises as a less plausible explanation.

In a similar study for the N53 aptamer-FABP3 interaction, indicative differences were observed for 7 tryptic peptide fragments: m/z 1474, 907, 1546, 1540, 1823, 2693 and 1204 with p values 0.0002, 0.0481, 0.0001, 0.0001, 0.0006, 0.0360 and 0.0001, respectively (Figure 4.2, 4.5). The increased ion intensity of the peptide fragments m/z 907, 1474, 1546, 1540, 1823 and 1204 suggests increased exposure of the trypsin cleavage sites 10 Lys, 22 Lys, 31 Arg, 53 Lys, 66 Lys, 82 Lys, 97 Lys and 107 Arg resulting from a possible protein conformational change on N53 binding. For the peptide m/z 2693, a decreased ion intensity was observed implying physical obstruction to trypsin action at site 91 Lys or a possible conformational change in FABP3 affecting trypsin action at 91 Lys. Evidence of protein conformation change on N53 binding is displayed in the CD study where on N53 binding the negative CD peak at 216 nm increases accompanied by a simultaneous decrease in peak intensity at 196 nm (Figure 4.3B). There was a decrease in helix (from 18 % to 0 %) and β sheet composition (from 61.9 % to 54.7 %), whereas random coils increased from 20 % to 45.3 %. Since the GST tag was present during SELEX and limited proteolysis experiments, the effect on its fragmentation pattern during limited proteolysis was studied. Significant differences were observed for 6 GST tryptic peptide fragments: m/z 1011, 603, 1032, 1831, 1517 and 500 with p values 0.0048, 0.0026, 0.0067, 0.0281, 0.0005 and 0.0018, respectively (Figure 4.4B, 4.6). The increased ion intensities of the peptide fragments m/z 1011, 603, 1032, 1831 and 500 indicates towards a heightened receptiveness of the following trypsin digestion sites: 9 Lys, 18 Arg, 40 Lys, 44 Lys, 64 Lys, 73 Arg, 89 Arg, 135 Arg and 139 Lys,

while decreased ion intensity was observed for m/z 1517 owing to decreased trypsin digestion at site 103 Arg. This change in pattern is suggestive towards a protein conformational change leading to altered accessibility to the aforementioned sites or physical obstruction posed by N53 to the affected sites. This appears to be plausible as CD studies have indicated towards limited interactions of N53 with the GST tag (Figure 3.4F).

4.3.2. Comparison of molecular docking, surface electrostatic potential mapping and limited proteolysis data to predict binding sites of the aptamers

In silico docking of the aptamers and target FABP3 were undertaken to explore protein and aptamer domains involved in interactions. For prediction of the minimal aptamer binding region, PyMOL was utilized to scan any protein residues within a 4Å distance of the aptamer nucleotide residues (Table 4.1).

Table 4.1: NPDock predicted models with amino acids and aptamer nucleotides within binding range

Aptamer	Predicted models	Predicted amino acid residues involved in binding	Predicted nucleotide residues involved in binding
N13	1	1Met, 15Lys, 16Asn, 48Asp, 66Lys, 67Leu, 68Gly, 69Val, 70Glu, 84Ile, 85Val, 86Thr, 87Leu, 88Asp, 91Lys, 95Leu, 102Glu, 104Thr, 106Val, 117Thr, 119Thr, 121Gly, 122Thr, 124Val	8T, 9A, 10C, 11G, 24G, 25G, 26A, 27T, 35G, 36G, 37G, 38C, 39G, 46G, 47T, 48A

Continued…

	2	10Lys, 17Phe, 20Tyr, 21Met, 26Val, 27Gly, 29Ala, 30Thr, 31Arg, 32Gln, 33Val, 34Ala, 35Ser, 37Thr, 38Lys, 39Pro, 41Thr, 54Thr, 56Ser, 57Thr, 58Phe, 59Lys, 60Asn, 61Thr, 62Glu, 74Thr, 75Thr, 76Ala, 77Asp, 78Asp, 79Arg, 105Leu, 107Arg, 116Leu, 118Leu, 127Arg, 129Tyr, 130Glu, 131Lys, 132Glu	69G, 71C, 72C, 73T, 78C, 79G, 80A, 81A, 82C, 83A, 84A
	3	12Val, 13Asp, 14Ser, 15Lys, 16Asn, 18Asp, 19Asp, 31Arg, 32Gln, 33Val, 35Ser, 36Met, 88Asp, 91Lys, 95Leu, 97Lys, 100Gly, 102Glu, 103Thr, 104Thr, 106Val, 108Glu, 117Thr, 118Leu, 119Thr, 120His, 121Gly, 122Thr, 123Ala, 124Val, 126Thr, 127Arg, 128hr	7A, 8T, 9A, 10C, 11G, 24G, 25G, 26A, 27T, 37G, 38C, 39G, 47T, 48A, 49A, 50G
	4	10Lys, 11Leu, 12Val, 13Asp, 14Ser, 15Lys, 16Asn, 19Asp, 34Ala, 35Ser, 36Met, 37Thr, 38Lys, 57Thr, 102Glu, 104Thr, 106Val, 113Lys, 117Thr, 119Thr, 120His, 121Gly, 122Thr, 123Ala, 124Val, 127Arg, 130Glu, 132Glu	7A, 8T, 9A, 24G, 25G, 26A, 27T, 36G, 37G, 38C, 39G, 41G, 47T, 48A, 49A, 50G, 51G, 52G
	5	24Leu, 25Gly, 26Val, 30Thr, 40Thr, 42Ile, 53Lys, 55His, 56Ser, 57Thr, 58Phe, 59Lys, 60Asn, 61Thr, 62Glu, 64Ser, 65Phe, 66Lys, 69Val, 70Glu, 71Phe, 72Asp, 74Thr, 75Thr, 76Ala, 77Asp, 78Asp, 79Arg, 80Lys, 81Val, 96Gln, 97Lys, 98Trp, 99Asp, 101Gln, 102Glu, 120His	59G, 60T, 62G, 64G, 71C, 72C, 73T, 74G, 75G, 82C, 83A, 84A, 85G, 86C, 87T, 88T, 89G, 90C
N53	1	13Asp, 14Ser, 15Lys, 16Asn, 18Asp, 19Asp, 20Tyr, 22Lys, 23Ser, 24Leu, 35Ser, 91Lys, 94His, 98Trp, 101Gln, 102Glu, 103Thr, 104Thr, 105Leu, 106Val, 107Arg, 108Glu, 110Ile, 113Lys, 114Leu, 115Ile, 116Leu, 117Thr, 118Leu, 119Thr, 120His, 121Gly, 122Thr, 123Ala, 125Cys, 126Thr, 127Arg, 128Thr	53G, 54G, 55A, 56T, 57G, 58C, 59G, 60G, 61G, 62G, 63C, 64G, 65C, 68G, 69C, 70G, 71C, 75G, 77T

Continued…

N53	2	8Thr, 10Lys, 14Ser, 18Asp, 21Met, 28Phe, 31Arg, 32Gln, 35Ser, 36Met, 38Lys, 40Thr, 42Ile, 44Glu, 45Lys, 46Asn, 49le, 50Leu, 51Thr, 53Lys, 55His, 56Ser, 57Thr, 62Glu, 64Ser, 132Glu, 133Ala	6A, 7A, 8T, 9A, 10C, 11G, 12A, 13C, 14T, 15C, 16A, 17C, 18T, 31A, 32G, 33G
	3	5Phe, 6Leu, 7Gly, 8Thr, 9Trp, 10Lys, 11Leu, 12Val, 13Asp, 14Ser, 15Lys, 16Asn, 18Asp, 22Lys, 26Val, 27Gly, 28Phe, 29Ala, 31Arg, 35Ser, 36Met, 38Lys, 40Thr, 41Thr, 42Ile, 43Ile, 44Glu, 55His, 130Glu, 131Lys, 132Glu, 133Ala	5T, 6A, 7A, 8T, 9A, 10C, 11G, 12A, 13C, 14T, 15C, 16A, 32G, 33G
	4	1Met, 3Asp, 4Ala, 5Phe, 6Leu, 44Glu, 45Lys, 46Asn, 48Asp, 49Ile, 50Leu, 51Thr, 62Glu, 63Ile, 64Ser, 65Phe, 66Lys, 68Gly, 69Val, 70Glu, 71Phe, 72Asp, 84Ile, 86Thr, 87Leu, 88Asp, 93Val, 94His, 95Leu, 104Thr, 131Lys, 132Glu, 133Ala	12A, 13C, 14T, 15C, 16A, 18T, 19A, 20T, 21A, 22G, 23C, 43G, 44T, 45G, 46G, 48C, 49C
	5	8Thr, 10Lys, 24Leu, 38Lys, 39Pro, 40Thr, 42Ile, 53Lys, 55His, 56Ser, 57Thr, 58Phe, 59Lys, 60Asn, 61Thr, 62Glu, 72Asp, 78Asp, 79Arg, 80Lys, 81Val, 82Lys, 97Lys, 98Trp, 99Asp, 100Gly	25G, 26A, 39G, 40C, 41G, 42G, 50G, 51G, 62G, 63C, 64G, 65C, 67G, 68G, 69C, 70G, 71C, 72C, 73T

A radius of 4Å was employed as most weak interactions occur at that range. This helped to ascertain as to which protein residues are physically blocked by the aptamer binding or which affects the action of trypsin on FABP3. A total of 5 best-scored solution structures were evaluated for both N13- and N53- FABP3 complexes and compared with the limited proteolysis data. Briefly, the data obtained from the limited proteolysis experiment indicated towards the increased and decreased accessibility of trypsin cleavage sites of FABP3 in the presence of aptamer which

was then compared to the docking data for each complex, to reach a consensus as to which docking model best fit the limited proteolysis data. In the context of N13, model 1 best fit the limited proteolysis data, where 91 Lys and 66 Lys are totally masked by the aptamer while the sites 22 Lys and 31 Arg are exposed for trypsin action (Figure 4.7A). A total of 16 nucleotide residues in the double-stranded regions of N13 were within interacting range of 24 protein amino acid residues. Among the 16 nucleotides within interacting range, both the forward primer and random region equally contributed to the figure with 8 residues each. Figure 4.7A and C highlights the trypsin digestion sites being affected and the various domains involved or affected by N13 binding.

Based on the prerequisites obtained from the limited proteolysis data, model 1 best fit the data with 10 Lys, 31 Arg, 53 Lys, 66 Lys, 82 Lys, 97 Lys accessible for trypsin action while 91Lys remains sheltered from trypsin digestion. A total of 19 nucleotide residues of N53 fall within the interacting range of 38 protein amino acid residues (Figure 4.7B). 17 of the nucleotide residues are part of the random region while only 2 residues belong to the reverse primer. The various domains are represented in Figure 4.7B and D.

Furthermore, qualitative examination of the electrostatic potential of FABP3 at the surface of its interaction with N13 and N53 shows that the proposed binding sites as analyzed following docking studies on FABP3 involve mostly electropositive regions. In the context of N13 a total of 10 amino acid (1 Met, 15 Lys, 16 Asn, 66 Lys, 67 Leu, 70 Glu, 85 Val, 87 Leu, 91 Lys and 119 Thr) and 6 amino acids (15 Lys, 16 Asn, 22 Lys, 91 Lys, 113 Lys and 119 Thr) in the case of N53 juxtaposed with the electropositive regions of the protein at pH 7.4 (Figure 4.8). Since protein-

DNA interactions are mainly governed by electrostatic and van der Waals forces, the probability of the amino acid residues in the electropositive regions, in contributing towards aptamer-protein binding is significant. Based on the result output of PLIP, a total of 11 hydrogen bonds and 3 salt bridges involving 11 amino acid residues was the basis of N13-FABP3 interaction. This range was further narrowed down to 5 amino acids based on the surface electrostatic potential of FABP3 at pH 7.4, the hydrogen bond (hydrogen-acceptor) H-A distance < 2.7Å and (donor-acceptor) D-A distance < 3.35Å (Table 4.2, Figure 4.7E). Similarly, N53-FABP3 interaction interface involved a total of 25 hydrogen bonds, 4 salt bridges, and 7 hydrophobic bonds. However, on further analysis on the premises as mentioned above it was narrowed down to 17 amino acids (Table 4.2, Figure 4.7F).

Table 4.2: Amino acids and nucleotides involved in bond formation at aptamer-protein interface

Aptamer	Salt bridges	Hydrogen bond	Hydrophobic bond
N13	45Lys: 27T 91Lys: 9A 97Lys: 39G	16Asn: 48A 87Leu: 24G, 37G	----
N53	38Lys: 68G 120His: 58C	16Asn: 71C, 20Tyr: 59G, 22Lys: 54G, 117Thr: 60G, 122Thr: 56T, 23Ser: 56T, 123Ala: 56T, 126Thr: 71C	103Thr: 58C, 104Thr: 58C, 105Leu: 59G, 106Val: 59G, 107Arg: 60G, 118Leu: 59G, 119Thr: 58C

Comparison of both the interaction patterns of N13 and N53 with FABP3 reveals that N53-FABP3 interaction is based on more amount of hydrogen and hydrophobic bonds as compared to salt bridges, which is in contrast to N13-FABP3 interaction with more salt bridges. Furthermore,

a glance at the results focusses on the fact that N53 has 3 times more interacting sites as compared to N13, which indicates towards more strong binding to FABP3. However, interaction studies have confirmed a prominent change in N53 as well as FABP3 conformation on binding (Figure 3.4H and 4.3). This simultaneous change of conformation for both N53 and FABP3 might ultimately affect the bonding pattern in the interacting interface which might explain the greater dissociation constant. Explanation on the same foundation for N13-FABP3 interaction yields a stronger bonding owing to the 3 salt bridges, supported by the findings that the magnitude of N13 and FABP3 conformation change on binding is lesser as compared to N53-FABP3 interaction (Figure 3.4C,3.4D and 4.3).

Studies in detail of the amino acids predicted to be involved in securing aptamer-target interaction, for N13, a single amino acid 45 Lys was found to be exclusively present in FABP3, while all the other control proteins share the remaining 4 amino acids. This residue thus might play an important role in determining the specificity of N13 towards FABP3 alone. Similarly in case of N53, 5 amino acids are exclusive to FABP3 while 12 amino acids are shared by one or more of the control proteins. This result enlightens the fact that in N53-FABP3 interaction, all or few of the 12 shared amino acids among the control and target proteins might have an effect on the specificity of N53 binding, accompanied by a negligible presence of interaction between N53 and the control proteins (Figure 3.4F). This negligible change could be attributed to the very weak interactions at N53-control proteins interface since the interaction patterns are not visible for N53-FABP3 in the EMSA gels (Figure 3.4B).

4.4. Conclusion

This study elucidates the interaction patterns of the aptamers with FABP3 using a combinatorial approach, combining the strength of limited proteolysis information and *in-silico* docking. In our investigation, the docking studies were experimentally supported by SVD analysis of aptamer 3D melting curves, which indicated the validity of Mfold derived secondary structures. This was followed by the comparison of the predicted docked structures with limited proteolysis experiments to arrive at the best model.

The limited proteolysis data analysis identified specific FABP3 trypsin digestion sites that were protected or overexposed on aptamer binding, which acted as a prerequisite for selecting among the docking models obtained. Based on this criteria the best fit models were selected after extensive position visualization of the respective amino acids in the complexed state. Comparative study of the pH-dependent surface electrostatic potential and profiling of the non-covalent interactions at the protein aptamer binding interface suggested a mixed type of interaction for both the aptamers. The nucleotide residues involved in binding are contributed from the primers as well as random regions, which reinforces the fact that primer regions might be directly implicated in binding or might secure the 3D aptamer structure for optimal interactions and hence are important to aptamer-target binding studies. However, interactions in the context of ssDNA should be carefully examined to avoid misprediction of bonds involving the –OH group at C2'of sugar and the absence of $–CH_3$ group at the 5C position of the T residues. The results support that N53 has a comparatively larger footprint on FABP3 surface compared to N13. Another strong observation has been the binding-induced conformation change in both the aptamers as well as the target. Since

a change in conformation has a cumulative effect on the bonding pattern at the aptamer-protein interface, the strength of binding ultimately is influenced by the extent of conformation change as observed in the context of N53. Though having a predisposition for forming a greater number of stable interactions with FABP3 compared to N13, N53 has a greater dissociation constant owing to a greater conformational change induced loss of binding contacts. This is strongly supported by the CD studies, which in turn explains the greater dissociation constant of N53. This study also suggests the basis of specificity of N13 towards FABP3, a single amino acid 45 Lys which is conserved in FABP3. Similarly, the minor binding exhibited by N53 towards the control proteins could be due to one or more of the 12 amino acids conserved in FABP3 and one or more of the control proteins, more specifically 16 Asn, 22 Lys and 38 Lys which are conserved in all the four proteins.

This combinatorial approach encompassing mass spectroscopy, molecular docking and CD spectroscopy unveiled the fact that the conformation changes which take place following molecular recognition process are also likely to significantly perturb the binding affinity between the aptamer and its target protein. Hence, the resulting binding affinity (dissociation constant) may not be a mere translation of the extent of surface coverage of the chemical bonding forces between these two interacting entities as revealed from the current studies. This investigation also highlights the findings that the primer binding regions in the aptamers may also play an equally important role specifically in maintaining the specific 3D binding conformation of the aptamers. This combinatorial method may be used as an alternative investigation into obtaining information on the aptamer binding site for bulky aptamers and the interactions involved, which in turn can

help in determining the minimum aptamer length that binds to the protein to perform co-crystallization for X-ray crystallographic studies. Thus this approach can be of considerable help in initial characterization of aptamer-target interactions especially, in the context of longer aptamers.

Figures

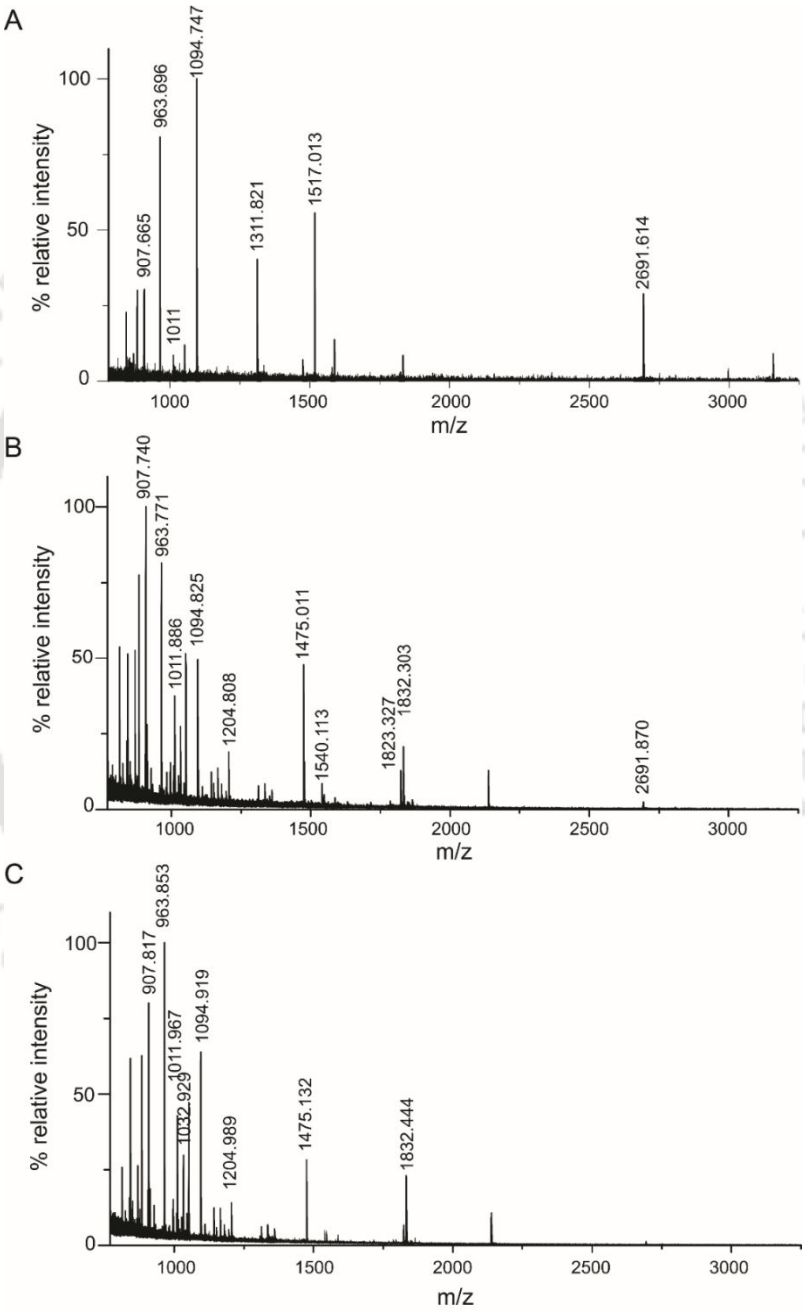

Figure 4.1: MALDI-TOF mass spectrum of a 10 min tryptic digest of (A) recombinant FABP3, (B) 1:4 molar ratio of FABP3:N13 and (C) 1:4 molar ratio of FABP3:N53.

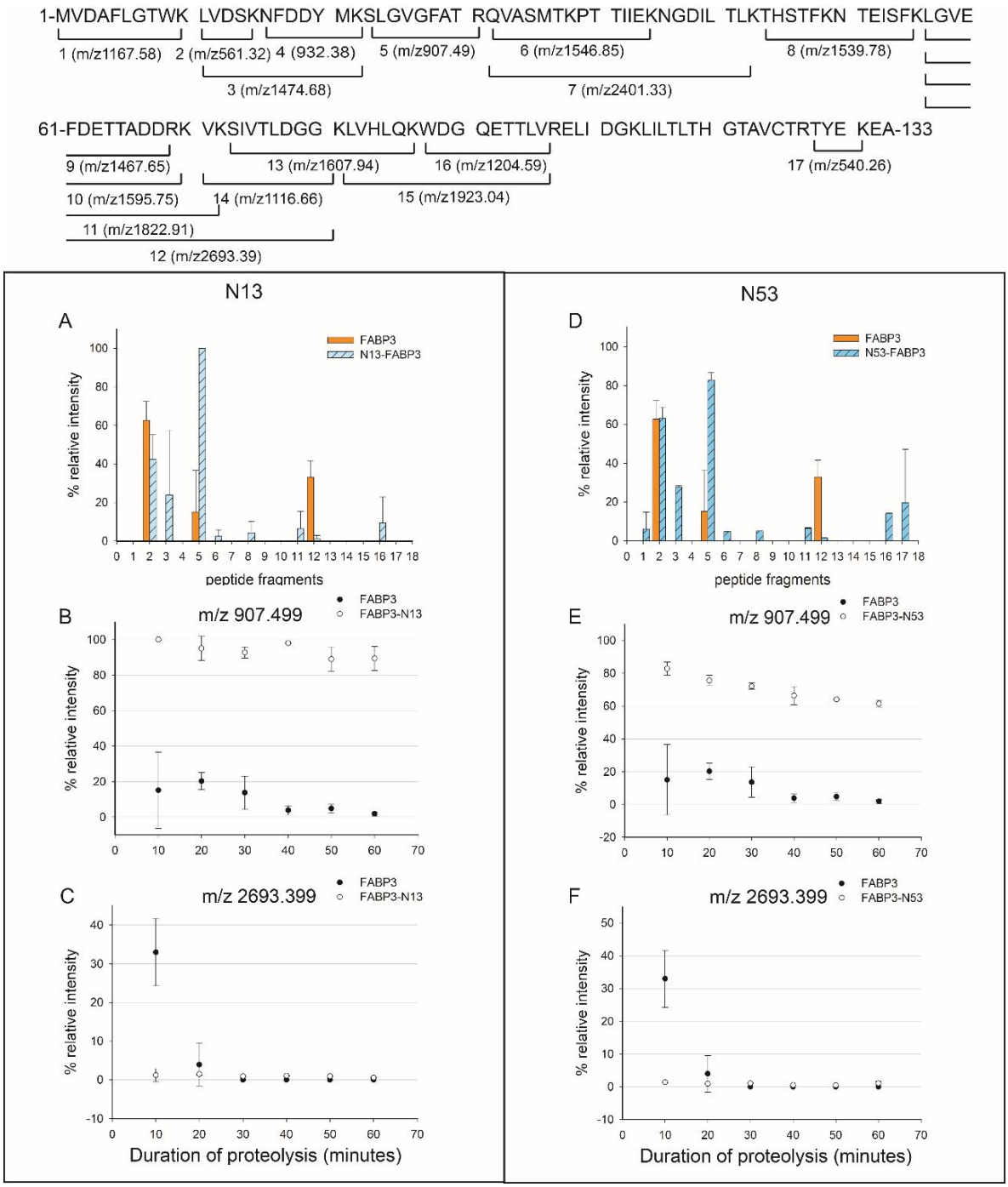

Figure 4.2: Comparison of percent relative intensity of FABP3 peptide fragments in the absence and presence of (A) N13 and (D) N53 after trypsin digestion. Panels B, C, E and F represent the comparison of percent relative ion intensity versus digest time for two peptide ions (m/z 907.499 and 2693.399) observed in the FABP3 and the FABP3:N13 or FABP3:N53 tryptic digests.

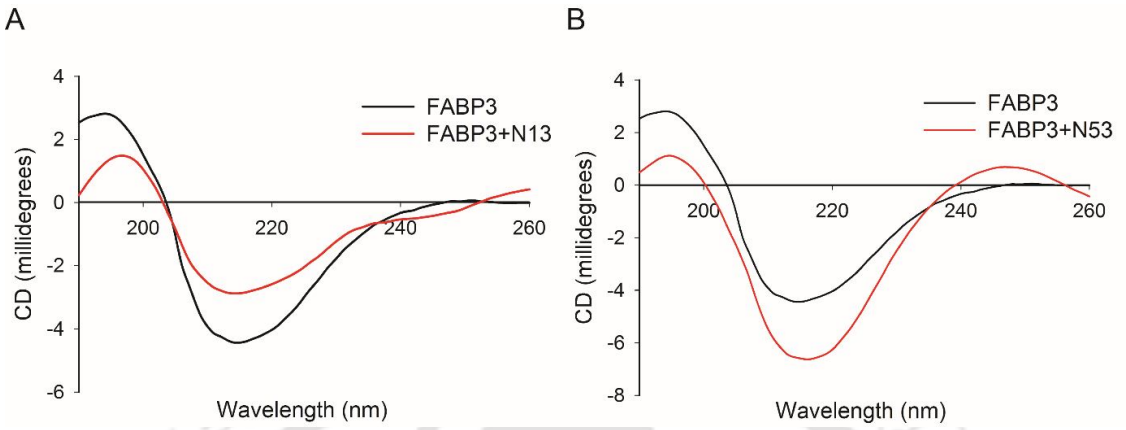

Figure 4.3: Normalized CD spectra of FABP3 in the presence of (A) N13 and (B) N53.

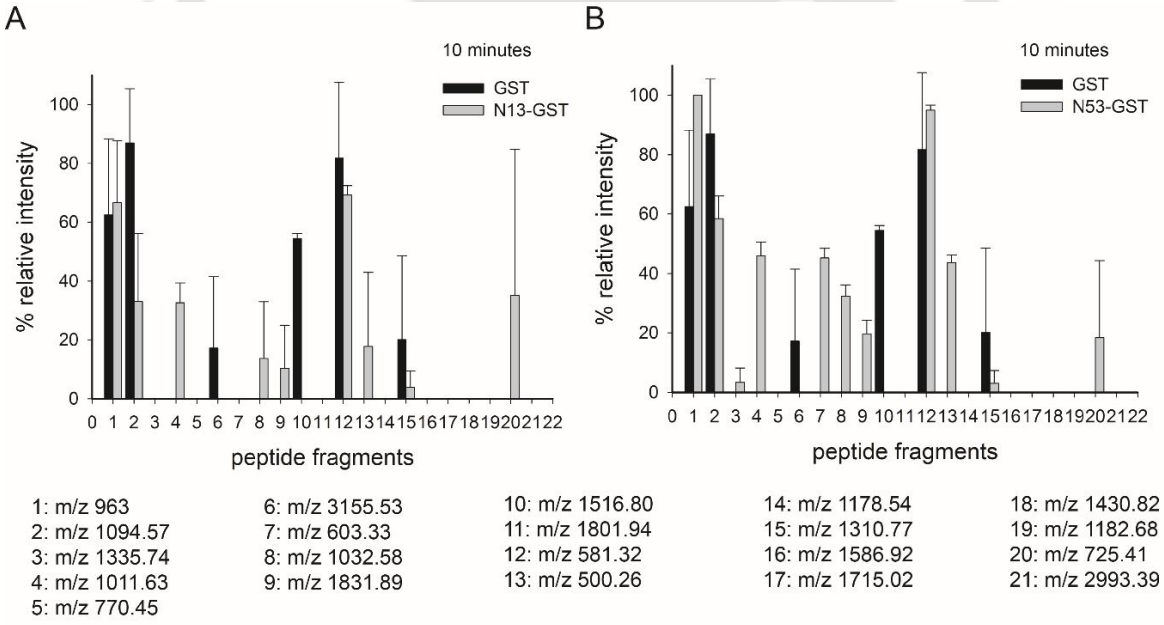

Figure 4.4: Comparison of percent relative intensity of GST peptide fragments in the absence and presence of (A) N13 and (B) N53, respectively after trypsin digestion.

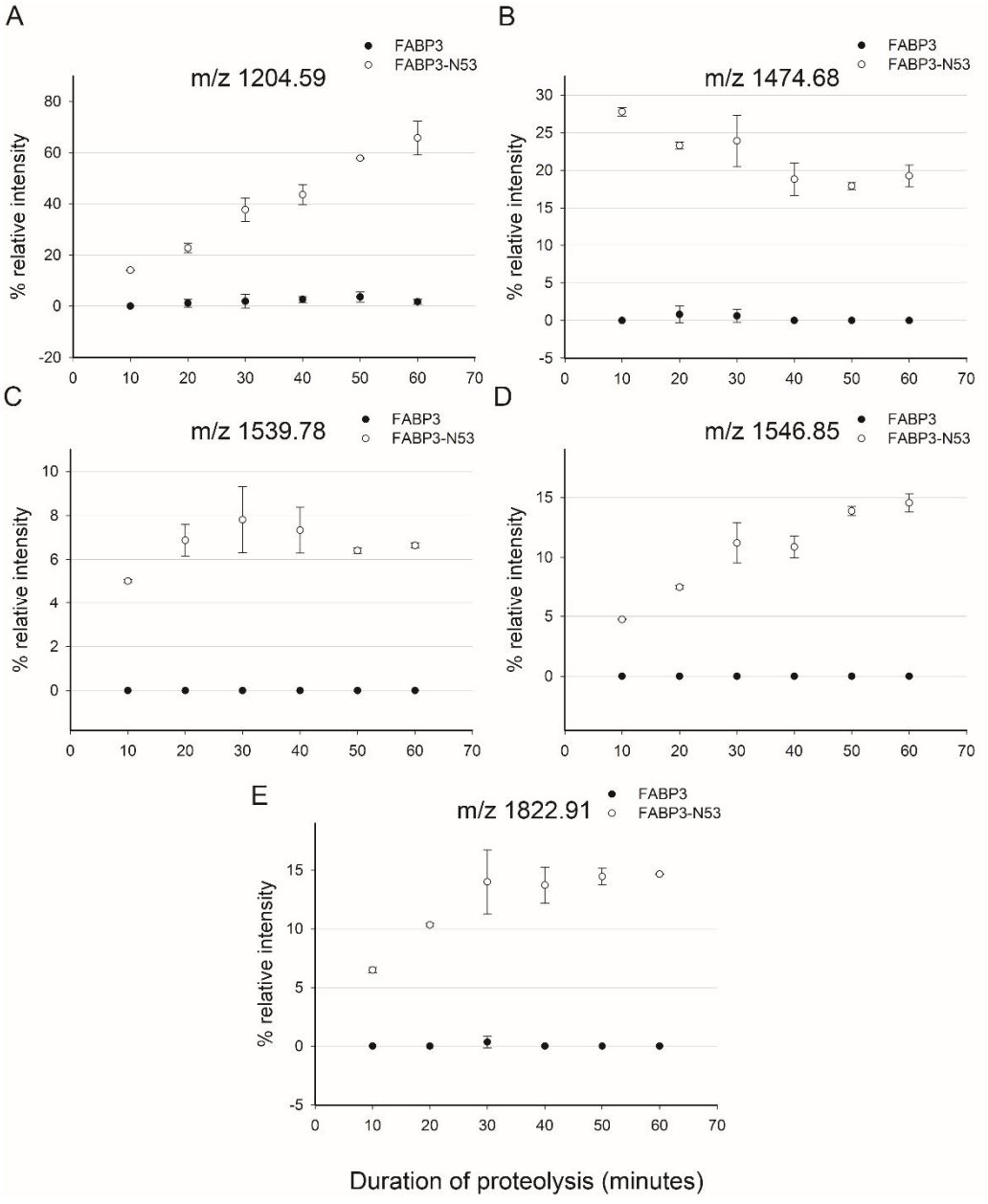

Figure 4.5: Comparison of the relative ion intensity vs proteolysis time for tryptic fragments of FABP3 affected in the presence of N53.

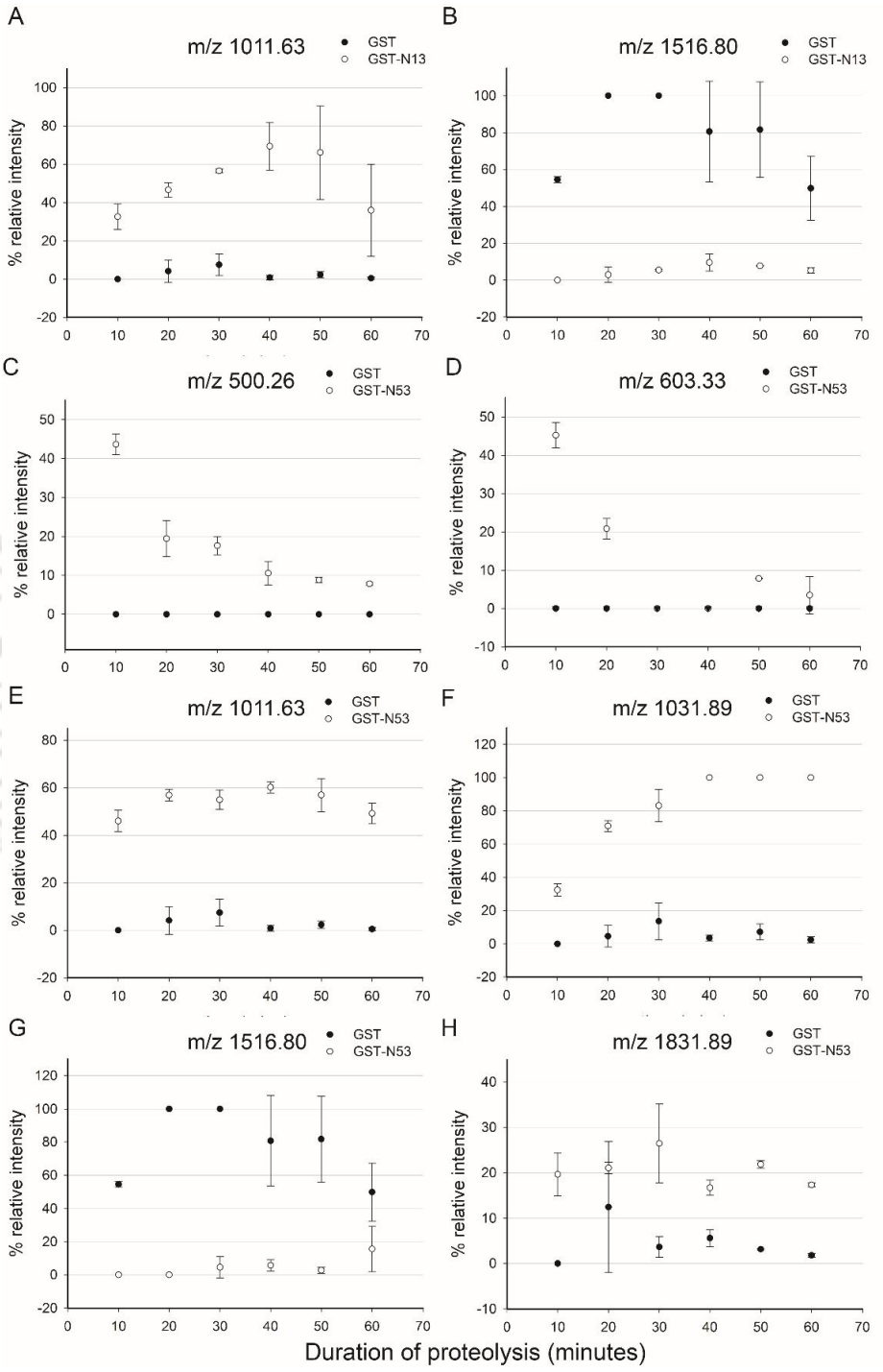

Figure 4.6: Comparison of relative ion intensity vs proteolysis time for tryptic fragments of GST affected in the presence of N13 (A and B) and N53 (C, D, E, F, G and H).

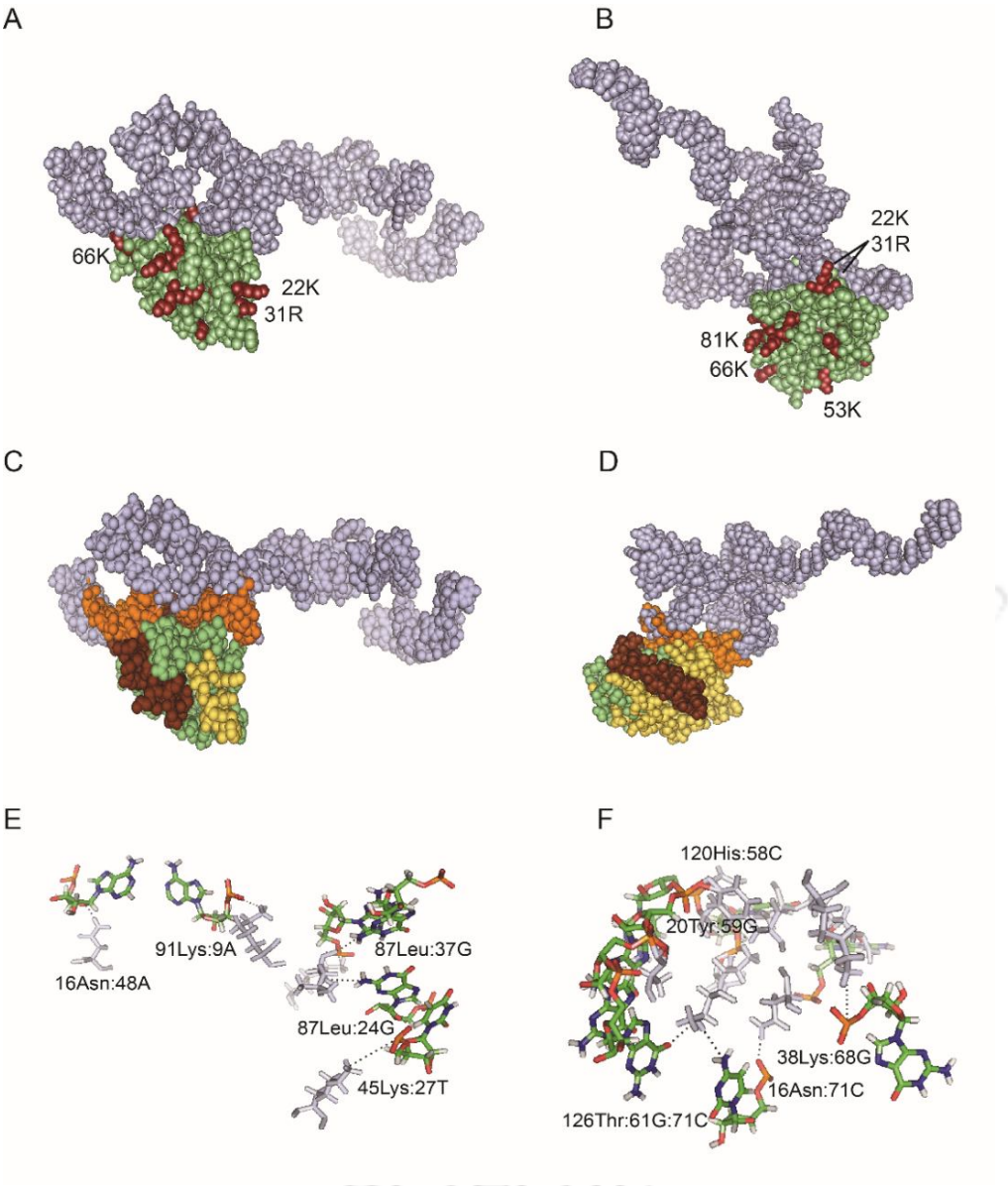

Figure 4.7: The best fit docking model as predicted by NPDock between (A) FABP3 and N13; and (B) FABP3 and N53. The trypsin digestion sites affected by aptamer binding are labelled red (aptamers are colored blue and protein green). (C) and (D) represents the various peptides influenced by the aptamer interaction for N13 and N53, respectively. Orange domain:aptamer residues within binding range; brown domain: peptide fragment with decreased intensity; light yellow: peptide fragment with increased intensity. Few of the proposed bonds formed at the interface of FABP3 with (E) N13 and (F) N53.

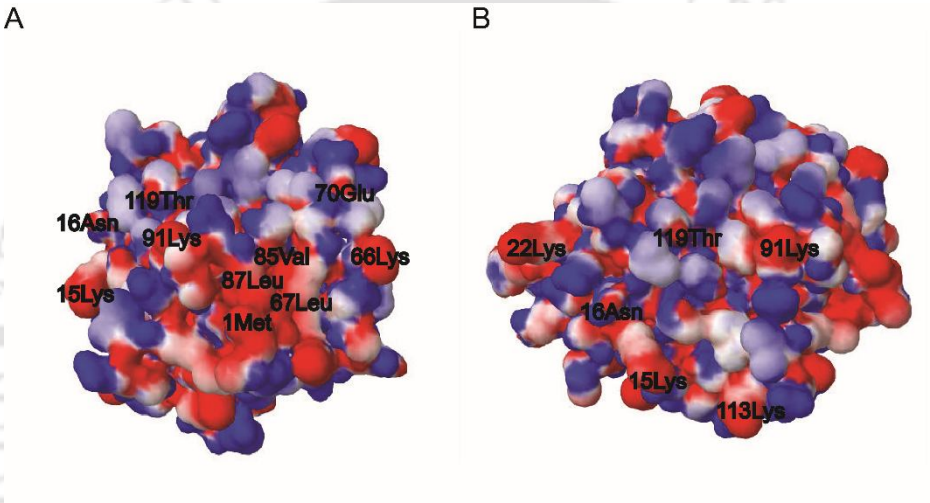

Figure 4.8: Surface electrostatic potential of FABP3 at pH 7.4 displaying electropositive groups in the binding region of (A) N13 and (B) N53 (using APBS).

5

Development of a paper-based microfluidic platform for detection of FABP3

CHAPTER 5

Development of a paper-based microfluidic platform for detection of FABP3

5.1. Overview

Paper as a substrate has been extensively used in analytical and clinical chemistry ranging from paper chromatographic techniques used for the separation of different biomolecules, litmus paper to paper based diagnostic tests (Chin *et al*., 2007; Yetisen *et al*., 2013; Feigel *et al*., 1946; Clegg *et al*., 1950; Jungreis *et al*., 1997; Hossain *et al*., 2009; Oberhofer *et al*., 1982; Zocher *et al*., 1999; Wong *et al*., 2006; Allen *et al*., 1995; Hardman *et al*., 2003; Gussenhoven *et al*., 1997; Wang *et al*., 2006; Deborggraeve *et al*., 2006; Liu *et al*., 2006; Zlateva *et al*., 2005). As a substrate, paper has many advantages over traditional device materials including power–free fluid movement to designated areas, cheap, portable, biologically compatible and modifiable for specific interests. Paper as a substrate for microfluidic devices was first reported by Martinez *et al* in the year 2007 wherein they used a hydrophobic patterning reagent to define hydrophilic channels to direct the movement of sample to a defined area for sample analysis. This development paved the way for use of paper as a substrate for applications where low cost and portability are important.

Paper-based microfluidic systems however suffer from two major drawbacks: first is the leakage of sample from the rear side of the channels during sample analysis and second is the difficulty in precise incorporation of reagents in the test zone without the inherent spreading of reagents to the surrounding areas including the microchannels. Additionally, covalent immobilization of certain detection reagents (e.g. antibodies, aptamers, enzymes etc.) in the test zone require multiple chemical treatment cycles and washing steps, which further aggravates the fabrication handling process. To overcome these problems various efforts have been made starting from clamping the device to plastic or glass, encasing the device in between adhesive tape, printing toner to laminating the device on both sides. Though advantageous, these methods have drawbacks of their own. For example the methods using certain adhesive tapes have the limitation that adhesive bond may weaken with the addition of sample and with time may wear off. Similarly the paper printed with a layer of toner mainly avoids contamination, acts as a thermal adhesive and helps in containing the reagents rather than acting as a mechanical support (Kauffman *et al*., 2010; Fu *et al*., 2010; Schilling *et al*., 2012; Fenton *et al*., 2008; Cassano *et al*., 2013; Canellas *et al*., 2010; Garcia *et al*., 2002; Asahara *et al*., 2003; Murray *et al*., 2003; da Silva *et al*., 2015; Schilling *et al*., 2012; Schilling *et al*., 2013).

Here, we report a fabrication process and design to mitigate the problems mentioned above. We used a fabrication process using negative photoresist instead of using the simple wax or AKD printing technologies since the photolithography technique presented multiple steps wherein the extent of partial polymerization on only one surface of the µPAD can be tuned to offer a leak-proof surface. The current fabrication process (processing time ~1 hr) allows the partial

polymerization of photoresist on the rear of the device, which prevents sample leakage during tests and thereby reduces the cost of laminating both sides of the device from $ 0.036 to $0.018 per device, thus reducing the overall device cost to ~ $ 0.048. We also report a new design and method for preparing the customized test zone with controlled spotting facility of reagents and treatments involving multiple washing and regeneration steps. The customized test zone with embedded reagents specific for respective target analytes can be integrated to the base device at the time of analysis. Finally, a preliminary study was performed for detection of FABP3 on the paper based microfluidic device in a yes/no format using the developed aptamers as bio recognition element. The principle of salt-mediated aggregation of gold nanoparticles was exploited as an optical probe for detection of aptamer binding with the target FABP3 protein.

5.2. Experimental Approaches

5.2.1. Materials

Whatman Chromatography paper No 1 (20 X 20 cm) was obtained from GE Lifesciences (India). Propylene glycol monomethyl ether acetate (PGMEA), triarylsulfoniumhexafluorophosphate salts (photoacid), coomassie brilliant blue G-250, divinyl sulfone, bovine serum albumin (BSA purity ≥ 98 %) and human serum albumin (HSA) were purchased from Sigma Aldrich (USA). EPON SU-8 resin was a gift from MomentiveTM (USA). Tetrabromophenol Blue, phenolphthalein indicator and 30 % hydrogen peroxide (H_2O_2) were purchased from Merck (Germany). Acetone and isopropanol were purchased from Himedia

(India). 3,3'-Diaminobenzidinetetrahydrochloride hydrate (DAB) was purchased from Amresco (USA). Monoclonal rat anti-human FABP3 antibody and goat anti-rat IgG HRP affinity purified polyclonal antibody were obtained from R&D systems (USA). Recombinant heart type fatty acid binding protein (FABP3) was purified in the lab with >= 95 % purity as discussed in Chapter 2. Transparency sheets (polyester with a thickness of 100 micron) were purchased from Oddy India Ltd. All other reagents were of analytical grade and used as received.

5.2.2. Designing of microfluidic channels

Design patterns were drawn with AUTOCAD (Version 2010). The designs consisted of six rows of 12 devices each totaling to 72 devices per sheet. The design of the microfluidic device consisted of a sample zone of 3 mm, an absorbent zone of 5.5 mm with connecting channels 3 mm in length and 1 mm in width. The test zone region was left empty in between the two zones. The designs were printed on a transparent sheet with a RICOH 2030 printer using a black toner cartridge (MP C2551) from RICOH (Japan).

5.2.3. Device fabrication

The microfluidic channels were fabricated on Whatman Chromatography paper No 1 using the FLASH technique with certain modifications (Martinez *et al.*, 2008). Briefly, the photoresist (EPON SU-8 resin: 52 % by mass, triarylsulfoniumhexafluorophosphate salts (photoacid): 5 % by mass, and PGMEA: 43 % by mass, mixed overnight) was poured onto the paper, spread evenly with a glass rod and allowed to soak the photoresist for 5 mins. The photoresist impregnated paper

was then baked on a hotplate set at around 130 ^{o}C for 5 mins or till complete evaporation of the PGMEA. After complete cooling of the paper at room temperature, the paper was covered on one side with a black paper (with 0 % transparency) and the other side with the design printed transparent sheet. The paper surface in contact with the transparency sheet was then exposed to UV light (40 W) at a distance of 3 cm for 25 mins, following which the design sheet and the black paper were removed and the paper was again exposed to UV for 10-15 s on the same surface. The paper was baked at 130 ^{o}C for 5 mins. The unpolymerized photoresist was removed by soaking it in acetone, followed by a rinse in acetone (1x) and finally rinsing the paper with 70 % isopropanol using a squirt bottle. The rinse with isopropanol was done on the surface that was not in direct contact of the UV source. The devices were ready to use after drying at room temperature or were stored covered with aluminum foil. The circular test zone of appropriate sizes from Whatman chromatographic paper No. 1 was prepared by using a punching machine. This untreated test zone was used to load reagents before it was placed on the microfluidic channel. It was then incorporated externally between the sample and absorbent zone partially overlapping the microfluidic channels, followed by laminating the device on one side to hold the test zone in place.

5.2.4. Characterization of the constructed device

The surface morphology of the photoresist modified surface and unmodified surface of the device were analyzed through Atomic force microscopy (AFM) using an ambient air scanning probe microscope (Agilent Technologies 5500, USA) and a silicon nitride probe. Images were recorded with typical contact mode using Picoscan 5 software**.** The scan speed was set at 4.476

µm/s, I Gain-0.7, P Gain-1 and AC Drive of 1.7 %. Images of cross-sections of the modified and unmodified paper were taken using a Field Emission Scanning Electron Microscope (FESEM) (Zeiss) with EHT 1kV and a Nikon-SMZ800 microscope equipped with a Nikon D7000 camera (Japan).

5.2.5. Flow characterization

Flow rates were determined by applying a 10 % Coomassie Brilliant Blue G-250 in methanol to the sample zone and measuring the time for the dye to flow from the sample zone to the absorbent zone. The entire flow process was video graphed using a camera and the time required by the dye to travel from the sample zone to the tip of the absorbent zone was calculated from the video. Multiple experiments were conducted to obtain an average linear velocity.

5.2.6. Quantitative assay for nonspecific detection of protein in artificial urine

Artificial urine was prepared following the protocol of Brooks *et al* (1997). Stock solutions containing BSA were prepared using this artificial urine. Desired concentrations of BSA (10-100 µM) were obtained by diluting the stock.

The external test zone was spotted with 3 µL of 125 mM citric acid buffer at pH 1.8, dried at room temperature followed by addition of 3 µL of 10 mM tetrabromophenol blue (TBPB) in ethanol and allowed to dry at room temperature. Five µL of each sample was dispensed on the sample zone of the micro fluidic device and allowed to flow through the channels to the test zone

and react with the reagents spotted. The reaction was allowed to proceed for 10 mins after which the color development was recorded.

5.2.7. Quantitative detection of base

Different concentrations of sodium hydroxide (NaOH) solution were prepared in MilliQ (18 mΩ) water in the range of 1 mM to 10 mM. The test zone was spotted with a solution of phenolphthalein in ethanol and allowed to dry at room temperature. Five µL of each sample was dispensed on the sample zone and allowed to flow through the channels to react with the reagent spotted on the test zone. The development of color was monitored immediately after migration of sample to the test zone.

5.2.8. Quantitative assay for specific detection of protein

For the quantitative detection of protein (anti-FABP3 antibody), the test zone was covalently modified through DVS (divinylsulfone) chemistry to immobilize FABP3 (capture molecule) following the protocol of Yu *et al*, (2012). The homobifunctional DVS molecule contains electrophilic vinyl groups which exhibit cross-linking activity with nucleophiles. The chemical strategy involves the addition of one of the vinyl groups to the hydroxyl groups on cellulose while the remaining vinyl groups covalently attaches to the nucleophile bearing biomolecules. Briefly 12.0 × 9.0 cm sheets of Chromatography paper 1 were immersed in 20 ml 10 % DVS solution (v/v, 0.1 M sodium carbonate, pH 11) and incubated in separate 400 ml-capacity plastic zip bags, and agitated for 2 hr on a rocking shaker. Following incubation, the DVS-

activated (DVS+) paper was removed from the bags and rinsed in a plastic tray with 100 ml MilliQ water three times. These membranes were dried for 2 hrs in ambient conditions and then punched with a punching machine to obtain circular test zones each of diameter 4 mm. The FABP3 protein prepared in PBS (phosphate buffer saline, pH 7.4) was then spotted on the test zone and allowed to react under ambient conditions overnight. This was followed by three washing steps with PBS to remove any unbound protein. After drying the zone, it was spotted with BSA to block any exposed site. This was followed by three washing steps to remove excess BSA and subsequent drying under normal room conditions. The sample zone was spotted with 5 µM HRP conjugated anti-rat antibodies (detector molecule) and allowed to dry overnight at 4 ^{o}C. Different concentrations of rat anti-FABP3 antibodies (0-3.4 µM) were prepared in PBS and applied to the sample zone. The sample was allowed to migrate to the test zone, dried for 5 mins followed by 5 applications of PBS buffer (20 µl each) at the sample zone to allow unbound antibodies to migrate to the absorbent zone. This was followed by application of DAB substrate (10 ml 0.05 % DAB in PBS with 10 µl 30 % H_2O_2). In the presence of H_2O_2, DAB is converted to an insoluble brown reaction product and water by the enzyme HRP. Color development after 5 mins was monitored to determine the concentration of analyte present in the sample.

5.2.9. Method for digitization of obtained results

To quantify the obtained results the images of the devices were acquired using an Epson Image scanner. The color images were then transferred to a computer, converted to 8-bit gray scale using Adobe Photoshop and the mean pixel intensities noted corresponding to each analyte

concentration. To obtain background corrected data, the mean pixel intensity of each device was subtracted from the intensity of a control device not exposed to any analyte. A similar method was used for the detection of protein with TBPB, where instead of converting the image to grayscale, the cyan channel in the CMYK (cyan, magenta, yellow, and key (black)) format was chosen to quantify the colorimetric response (Martinez *et al*., 2008).

5.2.10. Synthesis of gold nanoparticles

Gold nanoparticles were prepared by the classical citrate reduction method (Turkevich *et al*., 1951). Briefly, colloidal nanoparticles were prepared by rapidly injecting a sodium citrate solution (1 ml, 38.8 mM) to a boiling solution of $HAuCl_4$ (10 ml, 1 mM) with vigorous stirring. The reaction was boiled till the color changed to wine red. It was cooled to room temperature and used for adsorption of aptamers.

5.2.11. Detection of FABP3 using gold nanoparticles on the developed paper based microfluidic device

A total 2 µM of aptamer was incubated with 1nM prepared gold nanoparticles (AuNPs) for 10 mins. Three µl of the aptamer modified AuNPs were spotted on the external test zone, allowed to dry for 5 mins and then the test zone was incorporated with the base device and laminated. This was followed by addition of various concentrations of FABP3 spiked serum (0-120 ng/ml) to the sample zone of the device and allowed to incubate for 10 mins. A control test was also set taking

HSA as the analyte in place of FABP3. Subsequently, 120 mM NaCl was added in the test zone, allowed to incubate for 5 mins and the change in color were recorded with a camera.

5.3. Results and Discussion

5.3.1. Device fabrication process

Detection of different analytes involves the use of different reagents which in traditional paper based microfluidic devices (µPADs) are spotted on the test zones. However, it requires an extremely controlled process to spot since erroneous handling can allow the reagents to cross to the other zones. Furthermore, detection strategies involving the use of sandwich assays demand covalent immobilization of capture molecules on the test zone itself. This adds multiple treatment steps of the test zone, which in the case of traditionally designed µPADs is not feasible. In addition to the above shortcomings, µPADs also suffer from another disadvantage that is the leakage of sample from the back side of the device. As a means of overcoming these drawbacks we designed a device consisting of a sample, absorbent and externally inserted test zone, as well as evolved a fabrication method which adds a leak proof layer at the back side of the device during the fabrication step itself.

The device design and fabrication process is illustrated in scheme as Fig.5.1. For this concept we used the paper surface that was not directly exposed to the UV source. The slight projection of the channels on this side of the patterned paper acted as bridges to connect the test zone to the sample and absorbent zones. The channels were designed in a way that 1 mm length of the channel

overlapped with the test zone to facilitate effective movement of fluid to and from the channels to the test zone. The incorporation of the test zone between the sample and absorbent zones is a simple but critical step and can be manually performed without much difficulty. The different zones varied in size connected by channels: size gradually increased from the sample zone to the absorbent zone which helped to increase the wicking of fluid from the sample zone to the absorbent zone in a controlled manner (Fig 5.2). The addition of the absorbent zone to the design setup helped absorb the unbound detector molecules and reagents, resulting in less nonspecific detection signals. The optimized size ratio of the sample, test and absorbent zone were 1.83:1.33:1.00 (Table 5.1).

Table 5.1: Optimization of device design parameters

Sl No	Sample zone diameter (mm)	Test zone diameter (mm)	Absorbent zone diameter (mm)	Length of channels (mm)	Width of channels (mm)	Ratio of the zones	Flow pattern
1	1	2	3	0.5	0.2	3:2:1	Sample zone too small/sample spillage/flow blocked.
2	2	3	4	0.5	0.3	2:1.5:1	Sample zone small/flow blocked.
3	2	3	5	1.0	0.4	2.5:1.5:1	Sample zone small/flow blocked halfway.
4	3	4	5	1.5	0.4	1.66:1.33:1	Flow blocked halfway.

Continued…

5	3	4	5.5	1.5	0.8	1.83:1.33:1	Flow time ~15mins.
6	3	4	5.5	3.0	1.0	1.83:1.33:1	Flow time decreased (~9mins) with uniform spreading to zones.

Modification of the FLASH (Fast Lithographic Activation of Sheets) technique was carried out at multiple steps for obtaining a device that evades the need for lamination on the rear side to prevent the leakage of sample. The brief exposure of 10-15 s on the rear side of the device during fabrication allowed partial polymerization of the photoresist, thus making the back side of the device hydrophobic. The absence of isopropanol washing on the UV exposed side of the paper prevented leaching of the partial photoresist layer from that side of the paper, thereby preventing sample leakage from the rear side (Fig 5.3).

Furthermore the external placement of the test zone on the hydrophobic base of the prepared device (that is the paper platform consisting of the sample and absorbent zones) enhances the leak proof property of the device. The partial layer of photoresist on the device also limits the sample volume to 7 ± 0.2 µl as compared to devices without the partial photoresist layer which requires a larger sample volume of 10 ± 0.1 µl. The partial photoresist reduces the overall volume of the microfluidic channels which leads to the observed reduction in sample volumes. However, the minor variations in sample volume depend on the level of moisture content of the paper.

5.3.2. Characterization of the constructed device

AFM images of the photoresist modified surface and unmodified surface of the device revealed a rough surface with uneven morphology for the unmodified surface whereas the treated surface appeared to be smoother (Fig 5.4A). The root mean square (RMS) roughness factor for the photoresist modified and unmodified surface were calculated as $44.4x10^{-6}$ and $76.9x10^{-6}$, respectively. The unmodified surface retained the fibrous structure of the paper displaying a rough contour whereas the surface with polymerized photoresist was smooth as the photoresist impregnated the fibrous structure of the paper. Cross sectional images of Whatman Chromatography paper No. 1 with photoresist and with a partial layer of photoresist were analyzed by FESEM (Fig 5.4B). The images revealed a change in the thickness of the papers following photoresist treatment. The thickness of the paper with complete photoresist was an average 271.8 µm, which was greater compared to the untreated (180 µm) and partially layered (200.7 µm) paper. The increase in thickness of the partially layered paper in comparison to the untreated paper indicated the presence of photoresist in its paper structure.

Cross-sectional view of the control and sample device manifests the presence of the partial photoresist layer (white layer) in the sample device as can be seen in Fig 5.4C (II) and the lack of the layer in the control device (Fig 5.4C (I)). The blue layer with dye corresponds to lack of photoresist. The device fabrication process was able to confine the aqueous blue dye preventing it from penetrating through the entire thickness of the paper.

5.3.3. Flow characterization

Comparison of fluid flow rates through the constructed channels on both the devices with externally fabricated and inbuilt test zone were carried out by applying a dye on the sample zone of each device and then recording the time needed for the dye front to reach the end of the absorbent zone. The device with inbuilt test zone had a greater flow rate of 3.3 ± 1.2 mm/min compared to 1.8 ± 0.9 mm/min of the device with externally fabricated test zone. The decreased flow rate of device with prefabricated test zone can be ascribed to the overlapping design and less area of contact between the test zone and the connecting microchannels. The noticeable decline in the flow rate could be advantageous as it would allow increased time for the reagents to interact with the analyte thereby presenting a more sensitive detection signal.

5.3.4. Quantitative detection of protein in artificial urine, base and specific protein (anti-FABP3 antibody)

Three assay methods were chosen to validate the application feasibility of the designed device. The nonspecific detection of protein and base were based on direct color change on interaction of the analyte with the specific reagents. Whereas, the specific detection of protein was based on a variation of the sandwich assay involved the use of a capture and detector molecule. Fig 5.5 shows the correlation of obtained signals to the corresponding analyte concentrations. All datum points are mean intensities of five measurements of each concentration using independent devices while the error bars represent the relative standard deviation. For nonspecific detection of

protein in artificial urine, BSA was used as the analyte in the range 10-100 µM. Quadratic least squares fitting of the data yielded a coefficient of determination (R^2) of 0.99. The responses were linear in the range of 10-40 µM and started deviating from linearity, reaching a plateau at higher concentrations (Fig 5.5A and Fig 5.6A). The device was able to detect protein as low as 2.5 µM to as high as 40 µM. This renders the device useful as protein excretion during proteinuria falls in the range of 2.5-4.5 µM.

Determination of base using the phenolphthalein indicator based detection was carried out in the range of 1-10 mM NaOH. Quadratic least square fitting of the data yielded an R^2 value of 0.97. The graph followed a linear pattern in the range of 1-4 mM (Fig 5.5B and Fig 5.6B). The limit of detection was found to be 1mM.

Specific detection of anti-FABP3 antibody used the HRP catalyzed conversion of DAB into a brown precipitate. The scheme undertaken is demonstrated in Fig 5.7. The assay was carried out with an analyte concentration range of 0-3.4 µM. Quadratic least square fitting of the data yielded an R^2 value of 0.97. The response was linear in the range of 0-0.8 µM, beyond which the signal was saturated (Fig 5.5C). The detection limit for quantifying anti-FABP3 antibody was found to be 0.05 µM. This model assay for indirect ELISA on the designed µPAD reaffirms the feasibility of the device for detecting various antigens and antibodies present in biological fluids during infections, autoimmune diseases etc. The results obtained confirmed the usability of the designed device for simple detection assays as well for complex assays involving antibodies.

5.3.5. Detection of FABP3 using gold nanoparticles on the developed µPAD

Unmodified gold nanoparticles are inherently aggregated in the presence of salt ions but adsorption of aptamers on the surface of gold nanoparticles stabilizes them against salt-induced aggregation. However, on addition of the target protein and subsequent addition of salt solution, the adsorbed aptamer preferentially binds to the target, exposing the gold nanoparticles to salt induced aggregation (Fig 5.8). Both N13 and N53 were able to bind to the target protein specifically and the binding induced a change in color of the solution (Fig 5.9). Though easy to use, this gold nanoparticle based detection of FABP3 on the paper based microfluidic device served best as a yes/no format of detection with a minimum detection limit of 54 ng/ml. It could not be used a quantifiable assay due to the low color intensity change at disease concentration range, which was not prominent enough for quantifying using a camera or scanner.

5.4. Conclusion

The fabrication process used for the development of a µPAD, allows the partial polymerization of photoresist on the rear side of the device, which prevents sample leakage during tests and thereby reducing the cost of laminating both sides of the device. This study also describes a new design and method for preparing the test zone of µPAD with hassle-free spotting of reagents and treatment of the test zone which requires washing and regeneration. Functionality of the device was successfully demonstrated for colorimetric assays using fabricated test zones with different reagents (chemicals, proteins etc). The fabricated device presents the possibility of controlled

loading of varied biomolecules (antibody, protein, aptamers, DNA etc.) as well as chemical reagents on the test zones without any reagent crossover to surrounding sites of the device. Another advantage of the device for detection of FABP3 using aptamer modified gold nanoparticles is the absence of contact between the gold nanoparticles and the partial photoresist layer present in the other zones. This is because, gold nanoparticles tend to aggregate in the presence of photoresist without the addition of analyte or salt. Since the test zone is prepared externally the gold nanoparticles retain their homogeneous behavior and the color change is solely due to the reaction involving analyte, aptamer and salt. However, the gold nanoparticle based assay was not sensitive enough to generate a response curve and served more as a yes/no format for FABP3 presence. The minimum concentration of FABP3 detectable on the device was found to be 54 ng/ml which falls in the mid-range of AMI detection range. The prepared device has the potential for leak proof detection of analyte, requires low sample volume, involves reduced cost of production ($ 0.03, excluding reagent and lamination cost) and enables the integration of customized test zones. Furthermore, the prefabrication test zone approach might reduce the overall costs associated with low temperature storage of the device by minimizing the storage volume for the product as the storage of only prefabricated test zones with embedded heat labile reagents would suffice instead of storing the whole assembly with base device.

Figures

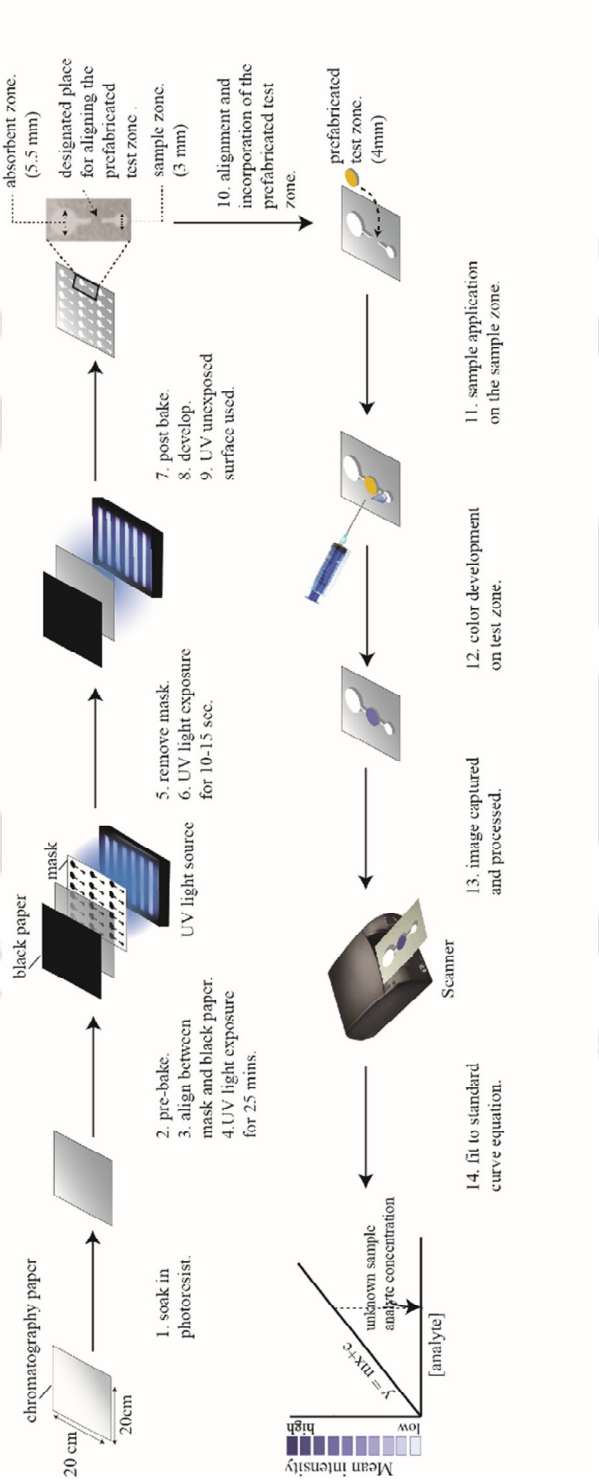

Figure 5.1: Schematic representation of fabrication process used to develop a leak-proof device with prefabricated test zone.

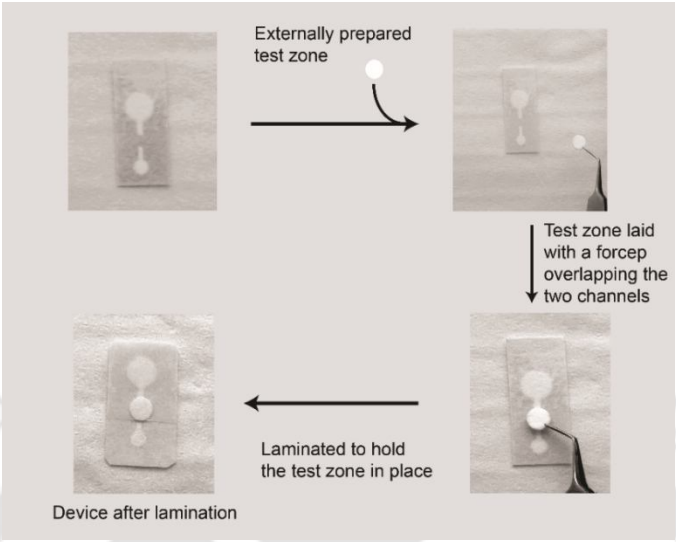

Figure 5.2: Illustration of the procedure followed to construct the device with an externally applied test zone.

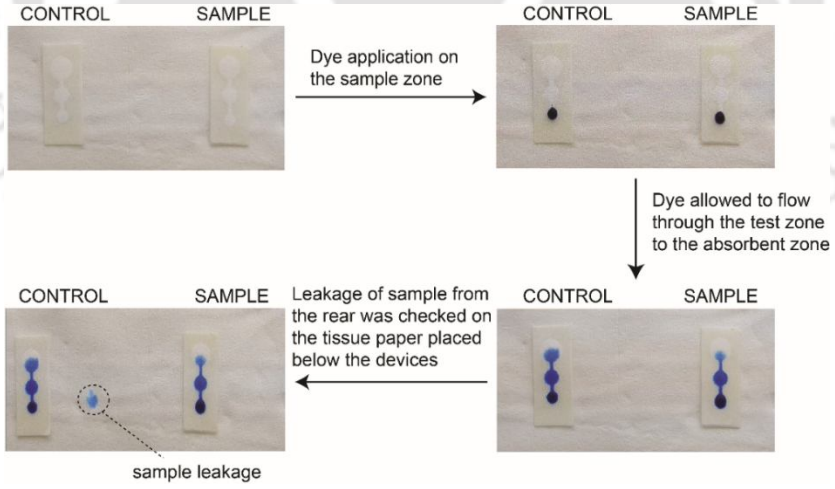

Figure 5.3: Sample device prepared by the conventional (control) and modified (sample) FLASH techniques were compared to demonstrate the impediment of leakage of sample from the rear of the sample device.

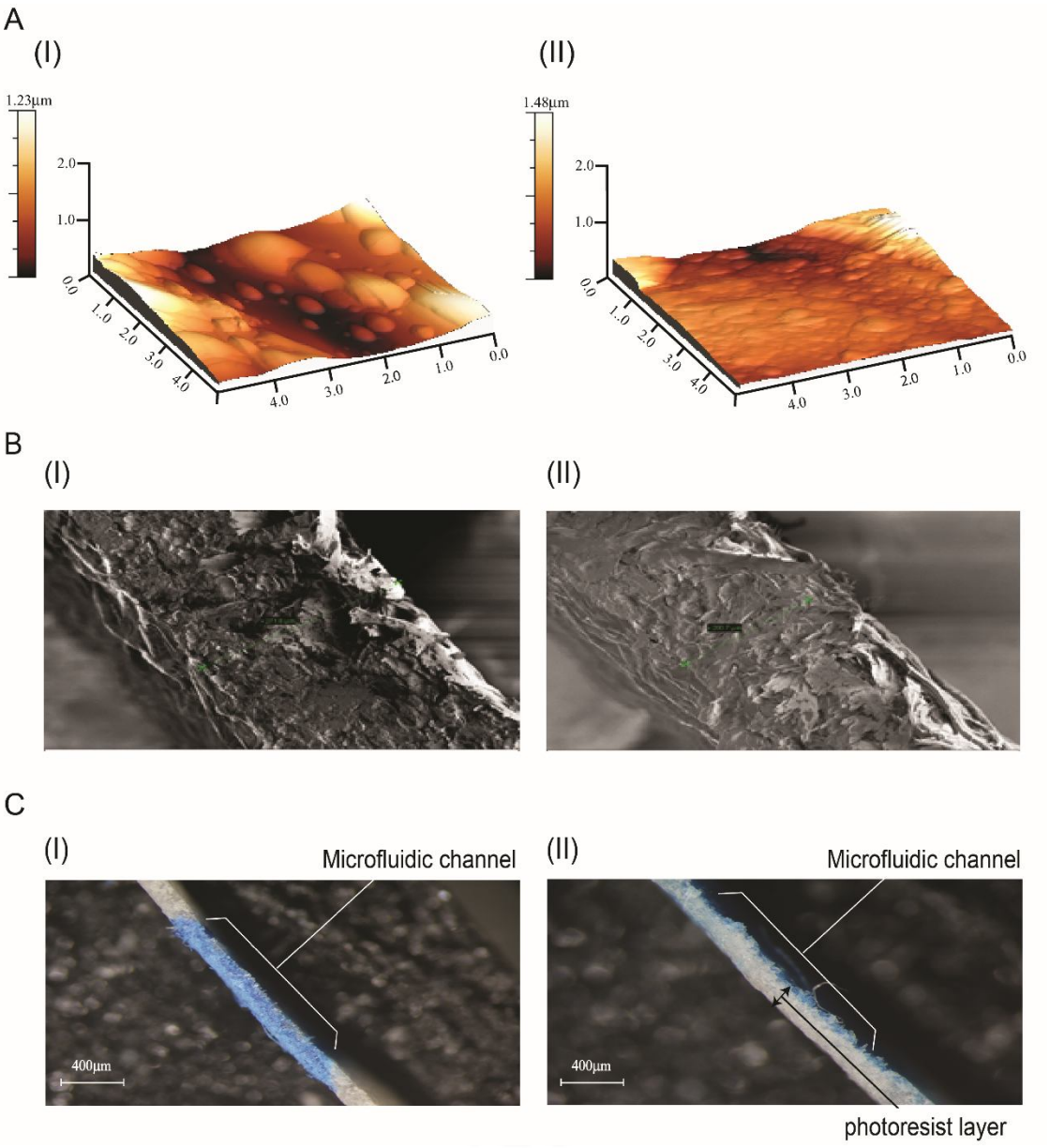

Figure 5.4: (A) AFM images of (I) unmodified surface and (II) photoresist modified surface of the device. (B) FESEM images of Whatman chromatography Paper No. 1 with (I) complete photoresist and (II) partial photoresist. (C) Cross-sectional view of the control (I) and sample (II) device showing the presence of the partial photoresist layer (white layer) in the sample device and the lack of the layer in the control device. The blue layer with dye corresponds to lack of photoresist.

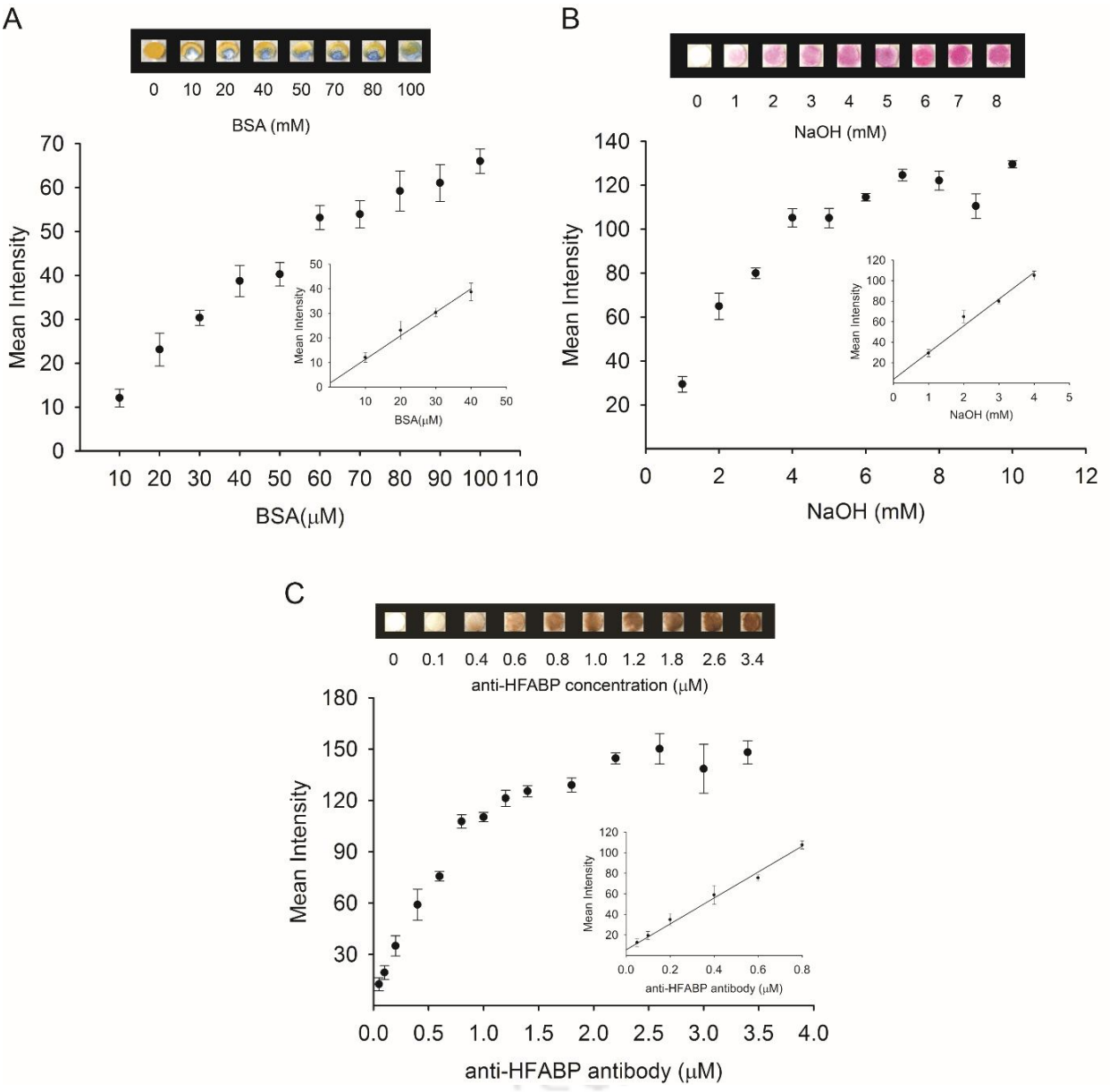

Figure 5.5: Representative images of BSA, NaOH, and anti-HFABP antibody detection are shown on the head of each graph, respectively. The BSA, NaOH, and anti-HFABP antibody concentrations were in the range of 0–100 µM, 0–10 mM, and 0–3.4 µM, respectively. Calibration plots for each analyte are shown. The mean intensity for each data point was obtained from the histogram in Adobe Photoshop. Each datum

is the mean of 5 assays and the error bars represent the relative standard deviations. (A) Calibration curve for different concentrations of BSA in artificial urine. The linear region of the data was fit in a linear equation (shown in inset); the slope (m), intercept (b), and R^2 values are as follows: 1.71, 0.9572, and 0.98, respectively. (B) Calibration plot for different concentrations of NaOH. The linear range of the data when fit into a linear equation (shown in inset) yielded a slope (m): 3.72, intercept (b): 26.0882, and R^2 value: 0.98. (C) Calibration plot for different concentrations of anti-HFABP. The linear region of the data (shown in inset) had a slope (m), intercept (b), and R^2 value of 5.4063, 126.25, and 0.98, respectively.

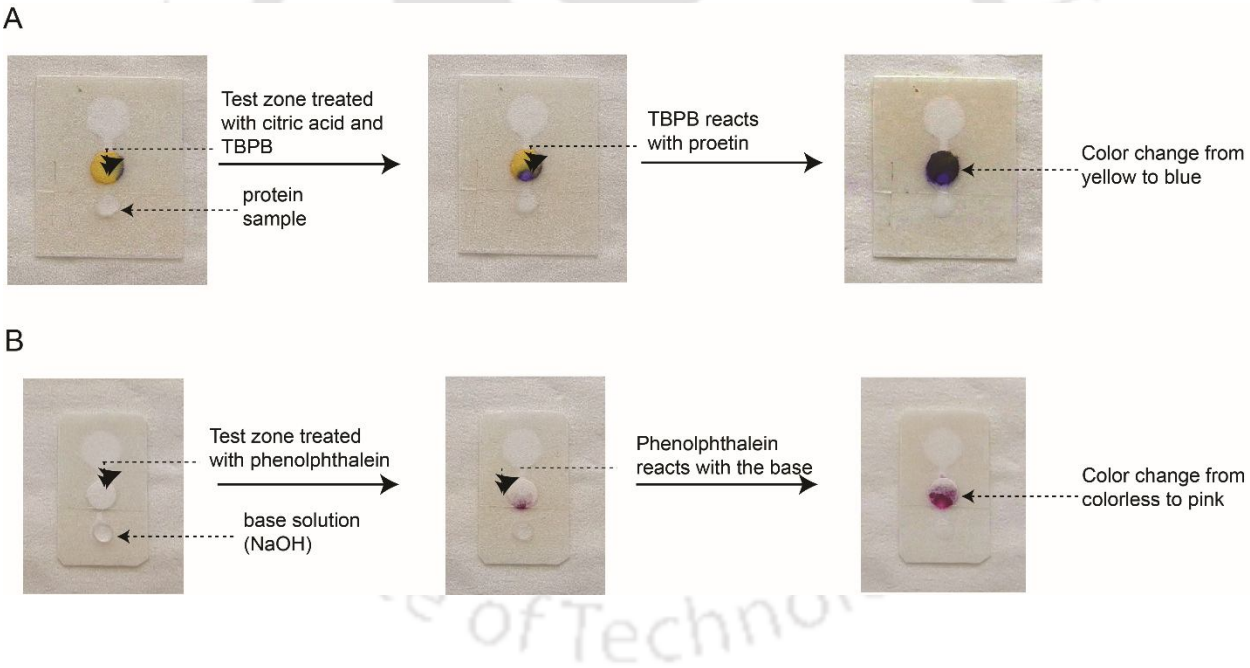

Figure 5.6: Fabricated µPAD for the analysis of (A) protein and (B) base. The circular zone in the middle is the externally added test zone pre-treated with tetrabromophenol blue and phenolphthalein, respectively.

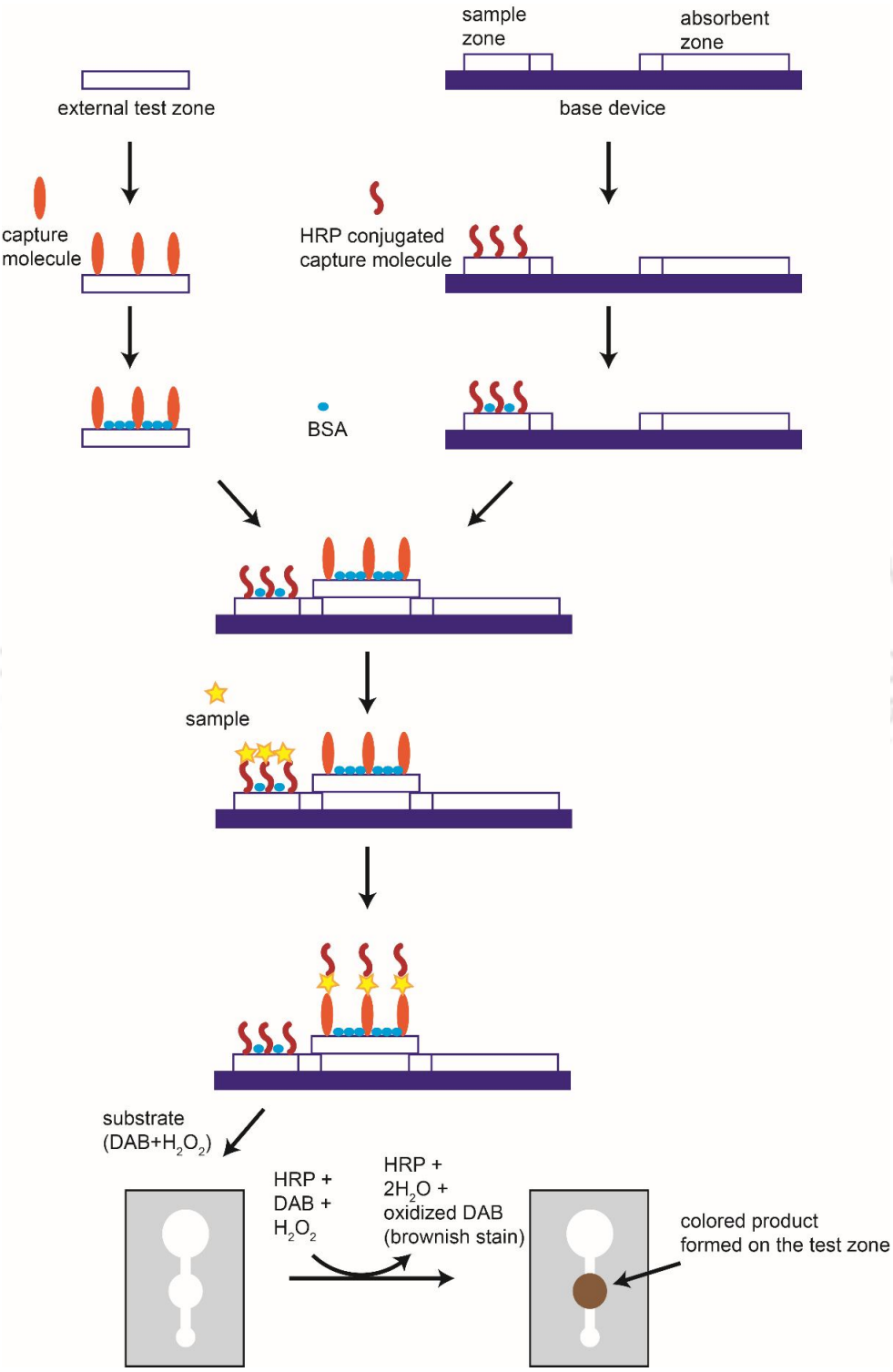

Figure 5.7. Scheme used for the detection of specific protein using HRP-DAB chemistry.

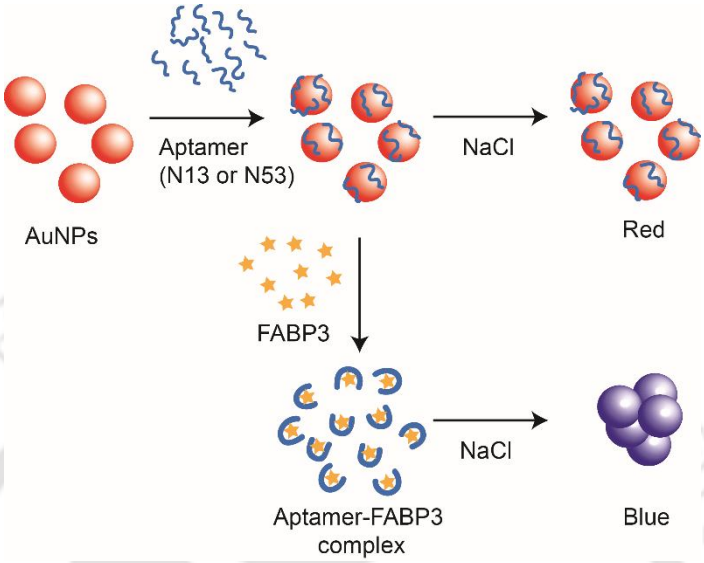

Figure 5.8. Reaction principle used for detection of FABP3 using gold nanoparticles.

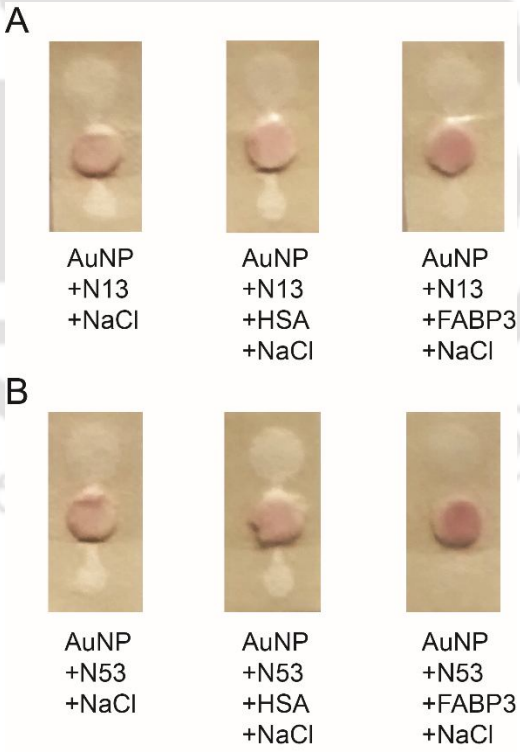

Figure 5.9: Detection of FABP3 using aptamer modified gold nanoparticles. (A) N13 based detection (B) N53 based detection.

Conclusions and future direction of work

Conclusions and future direction of work

Development of aptamers against human FABP3, a novel biomarker for AMI was accomplished for the first time. For the aforementioned work, coding sequences of the target FABP3 and the control proteins were successfully cloned, expressed in bacterial cells and purified. The recombinant proteins were validated through Western blot and their secondary structures were characterized through CD studies. All the proteins displayed secondary structures dominated by β-sheets which conforms to reported data. Employing SELEX, aptamers were generated specifically for FABP3, followed by TA cloning, screening and sequencing. Among the 50 positive clones obtained 7 aptamer sequences demonstrated increased enrichment as compared to other sequences. A combination of EMSA and CD studies revealed that two aptamers (N13 and N53) were specific for FABP3 and bound to FABP3 with different affinities. Both the aptamers exhibited stable behavior at varying ionic conditions, pH and temperature. Furthermore, computational and SVD analysis of melting curves of the aptamers suggested that both the aptamers fold into simple stem loop structures and exist in a simple two state. This study served as a basis for prediction of the 3D structures of the aptamers to understand their interaction with FABP3. Using a combinatorial approach involving limited proteolysis, mass spectrometry and molecular docking, the interaction patterns of the aptamers with the target protein FABP3 were explored. The results indicated towards a larger binding footprint on FABP3 by N53 compared to N13, in contrast to its high dissociation constant. This however can be explained by the observed change in conformation of both the aptamer and protein on binding, as observed in CD studies. The change in conformation of N53 and FABP3 on binding is more pronounced as compared to

N13, which might have a cumulative effect on the bonding pattern at the aptamer-protein interface, which might ultimately lead to loss of stable binding contacts between the protein and N53. Apart from casting light on the interactions involved, this study further suggests the basis of specificity of N13 towards a single amino acid which is conserved in FABP3, while the minor signal change observed for N53 on addition of the control proteins could be attributed to one or more of the 12 amino acids conserved in FABP3 and one or more of the control proteins.

Finally, to achieve detection of FABP3 using aptamers on a paper based microfluidic platform, a device was designed and fabricated. The device so developed had two important characteristics-one is the leak proof property and the other is the facility for controlled spotting of reagents and feasibility of chemical modification on the test zone. The leak proof property is attributed to the partial layer of photoresist on the rear of the device which was achieved through modification of the fabrication process, while the feasibility of controlled application or surface modification of the test zone was achieved through incorporating an external test zone on the base device. Experimental validation of the designed device was conducted with detection assays for protein and base using a nonspecific approach while specific detection of proteins using ELISA was demonstrated on the device. For detection of FABP3 using the aptamers developed (N13 and N53), a salt induced aggregation of aptamer modified gold nanoparticles was used. This assay validated the practical utility of the developed aptamers on the µPAD constructed.

The investigations in this thesis, entails a detailed study from the generation of specific aptamers for FABP3 and the study of their diverse interaction patterns to their practical feasibility in the detection of AMI on a specially designed low cost µPAD. This study will further open

avenues for understanding aptamer-target interactions using alternative methods, validation of the dynamic phenomena involving these interactions and finally for generating highly sensitive aptamer based sensing of AMI for ASSURED diagnostics.

Scope for future work

The present investigation needs further exploration on a few important points to augment the work involving aptamer target interactions and their practical use in sensing. Firstly, the aptamers developed as a part of this thesis work, are the first ones to be reported against FABP3. Therefore, studies on determining the optimum sequence length capable of specific binding to FABP3 needs to be performed. Secondly, obtaining further information on the 3D structure of the aptamers may help in understanding its interaction with the target protein. X-ray crystallographic analysis of the co-crystallized aptamer-protein complexes could paint a more detailed picture of the interactions involved. Thirdly, a detailed investigation of the concurrent conformational change observed on aptamer-protein binding is required to understand the mechanisms involved and how it influences aptamer-protein binding affinity. Finally, use of the aptamers for detection of FABP3 in this thesis has been limited to a preliminary investigation using gold nanoparticles. Colorimetric assays on paper are mainly limited to yes/no or a semiquantitative format. This can be overcome by designing assays for more sensitive detection, so that a response curve can be generated. Additionally, different principles of sensitive detection like electrochemical or chemiluminescence can be implemented for enhancing the signal performance of the developed aptamers on the designed µPAD. Furthermore interference studies involving different components of serum are to be carried

out in the developed µPAD.

Bibliography

Bibliography

Abe, K., Kotera, K., Suzuki, K., Citterio, D. Inkjet-printed paperfluidic immuno-chemical sensing device. Anal. Bioanal. Chem. 398, 885-893 (2010).

Abe, K., Suzuki, K., Citterio, D. Inkjet-Printed Microfluidic Multianalyte Chemical Sensing Paper. Anal. Chem. 80, 6928–6934 (2008).

Abe, S., Siago, M., Yamashita, T., Toda, H., Nomoto, K., *et al*. Heart fatty acid-binding protein is useful in early and myocardial-specific diagnosis of acute myocardial infarction. Circulation. 94, I-323 (1996).

Albada, H. B., Golub, E., Willner, I. Computational docking simulations of a DNA-aptamer for argininamide and related ligands. J. Comput. Aided. Mol. Des 29, 643-654 (2015).

Alhadi, H. A., Fox, K. A. Do we need additional markers of myocyte necrosis: The potential value of heart fatty-acid-binding protein. Q. J. Med. 97, 187-198 (2004).

Allen, M. P. ChemTrack Inc. U.S. Patent 5,409,664, (1995).

Alpert, J. S., Antman, E., Apple, F., Armstrong, P. W., Bassand, J. P., *et al*. Myocardial infarction redefined - A consensus document of The Joint European Society of Cardiology/American College of Cardiology Committee for the redefinition of myocardial infarction. J. Am. Coll. Cardiol. 36, 959-969 (2000).

Apple, F. S., Christenson, R. H., Valdes, R., Andriak, A. J., Berg, A., *et al*. Simultaneous rapid measurement of whole blood myoglobin, creatine kinase MB, and cardiac troponin I by the triage cardiac panel for detection of myocardial infarction. Clin. Chem. 45, 199-205 (1999).

Asahara, J., Hori, N., Takemura, A., Ono, H. Cross-linked acrylic pressure-sensitive adhesives.2. Effect of humidity on the cross-linking reaction. J Apply Polym Sci. 87, 1493-1499 (2003).

Banaszak, L. J., Winter, N., Xu, Z. H., Bernlohr, D. A., Cowan, S., *et al*. Lipid-binding

proteins: A family of fatty acid and retinoid transport proteins. Adv. Prot. Chem. 45, 89-151 (1994).

Binas, B., Danneberg, H., McWhir, J., Mullins, L., Clark, A. J. Requirement for the heart-type fatty acid binding protein in cardiac fatty acid utilization. FASEB. J. 13, 805-812 (1999).

Binas, B., Han, X. X., Erol, E., Luiken, J. J. F. P., Glatz, J. F. C., *et al*. A null mutation in H-FABP only partially inhibits skeletal muscle fatty acid metabolism. Am. J. Physiol. Endocrinol. Metab. 285, E481-E489 (2003).

Body, R., McDowell, G., Carley, S., Wibberley, C., Ferguson, J., *et al*. A FABP-ulous 'rule out' strategy? Heart fatty acid binding protein and troponin for rapid exclusion of acute myocardial infarction. Resuscitation. 82, 1041-1046 (2011).

Bourdoux, P. P., Van Thi, H. V., Courtois, P. A., Ermans, A. M. Superiority of thyrotropin to thyroxine as a tool in the screening for congenital hypothyroidism by the filter paper spot technique. Clin. Chim. Acta. 195, 97–105 (1991).

Bradford, M. M. Rapid and sensitive method for the quantization of microgram quantities of protein utilizing the principle of protein-dye binding. Anal Biochem. 72, 248–254 (1976).

Brooks, T., Keevil, C. W. A simple artificial urine for the growth of urinary pathogens. Letters in Applied Microbiology. 24, 203–206 (1997).

Bruno, J. G., Richarte, A. M., Phillips, T. Preliminary development of a DNA aptamer-magnetic bead capture electrochemiluminescence sandwich assay for Brain Natriuretic Peptide. Microchem. J. 115, 32–38 (2014).

Bruzewicz, D. A., Reches, M., Whitesides, G. M. Low-cost printing of poly (dimethylsiloxane) barriers to define microchannels in paper. Anal. Chem. 80, 3387–3392 (2008).

Burke, D.H., Nickens, D.G. Expressing RNA aptamers inside cells to reveal proteome and ribonome function. Brief. Funct. Genomics Proteomics. 1, 169–188 (2002).

Burton, P. B. J., Hogben, C. E., Joannou, C. L., Clark, A. G. B., Hsuan, J. J., *et al*. Heart Fatty

Acid Binding Protein Is a Novel Regulator of Cardiac Myocyte Hypertrophy. Biochem. Biophys. Res. Commun. 205, 1822-1828 (1994).

Candiano, G., Bruschi, M., Musante, L., Santucci, L., Ghiggeri, G. M., *et al*. Blue silver: a very sensitive colloidal Coomassie G-250 staining for proteome analysis. Electrophoresis. 25, 1327-33 (2004).

Canellas, E., Aznar, M., Mercea, P. Partition and diffusion of volatile compounds from acrylic adhesives used for food packaging multilayers manufacturing. J Mater Chem.20, 5100-5109 (2010).

Cappellini, F., Da Molin, S., Signorini, S., Avanzini, F., Saltafossi, D., *et al*. Heart-type fatty acid-binding protein may exclude acute myocardial infarction on admission to emergency department for chest pain. Acute cardiac care. 15, 83-87 (2013).

Carrilho, E., Martinez, A. W., Whitesides, G. M. Understanding Wax Printing: A Simple Micropatterning Process for Paper-Based Microfluidics. Anal. Chem. 81, 7091-7095 (2009).

Cassano, C. L., Fan, Z. H. Laminated paper-based analytical devices (LPAD): fabrication, characterization, and assays. MicrofluidNanofluid. 15,173–181 (2013).

Chamoles, N. A., Blanco, M. B., Gaggioli, D., Casentini, C. Hurler-like phenotype: enzymatic diagnosis in dried blood spots on filter paper. Clin. Chem. 47, 2098–2102 (2001).

Chan C. P., Sum, K. W., Cheung, K. Y., Glatz, J. F. C., Sanderson, J. E., *et al*. Development of a quantitative lateral-flow assay for rapid detection of fatty acid-binding protein. J. Immunol. Methods. 270, 91-100 (2003b).

Chan, C. P. Y., Wan, T. S. M., Watkins, K. L., Pelsers, M. M. A. L., Van der Voort, D. L., *et al*. Rapid analysis of fatty acid-binding proteins with immunosensors and immunotests for early monitoring of tissue injury. Biosens. Bioelectron. 20, 2566-2580 (2005).

Chan, C. P., Sanderson, J. E., Glatz, J. F. C., Cheng, W. S., Hempel, A., *et al*. A superior early myocardial infarction marker: Human heart-type fatty acid-binding protein. Zeitschrift fur

Kardiologie. 93, 388—397 (2004).

Chan, C. P., Cheng, W. S., Glatz, J. F. C., van der Voort, D., Sanderson, J. E., *et al*. Early diagnosis of acute myocardial infarction using immunosensors and immunotests. Anal. Lett. 36, 1987-2004 (2003a).

Chang, Y. M., Chen, C. K., Hou, M. H. Conformational Changes in DNA upon Ligand Binding Monitored by Circular Dichroism. Int. J. Mol. Sci. 13, 3394-3413 (2012).

Chayen, N. E., Saridakis, E. Protein crystallization: From purified protein to diffraction-quality crystal. Nat. Methods. 5, 147–153 (2008).

Chin, C. D., Linder, V., Sia, S. K. Lab-on-a-chip devices for global health: past studies and future opportunities. Lab Chip.7, 41–57 (2007).

Chitnis, G., Ding, Z., Chang, C. L., Savran, C. A., Ziaie, B. Laser-treated hydrophobic paper: an inexpensive microfluidic platform. Lab Chip 11, 1161-1165 (2011).

Chiu, A., Chan, W. K., Cheng, S. H., Leung, C. K., Choi, C. H. Troponin-I, myoglobin, and mass concentration of creatine kinase-MB in acute myocardial infarction. Q. J. Med. 92, 711-718 (1999).

Chmurzynska, A. The multigene family of fatty acid-binding proteins (FABPs): Function, structure and polymorphism. J. Appl. Genet. 47, 39-48 (2006).

Cho, E. J., Lee, J. W., Ellington, A. D. Applications of aptamers as sensors. Annu. Rev. Anal. Chem (Palo Alto Calif). 2, 241-264 (2009).

Choi, K. H., Park, M. W., Lee, S. Y., Jeon, M. Y., Kim, M. Y., *et al*. Intracellular expression of the t-cell factor-1 rna aptamer as an intramer. Mol. Cancer Ther. 5, 2428–2434 (2006).

Chung, C. T., Niemela, S. L., Miller, R. H. One-step preparation of competent Escherichia coli: Transformation and storage of bacterial cells in the same solution. Proc Natl Acad Sci. 86, 2172-2175 (1989).

Civallero, G., Michelin, K., de Mari, J., Viapiana, M., Burin, M., *et al*. Twelve different enzyme assays on dried-blood filter paper samples for detection of patients with selected inherited lysosomal storage diseases. Clin. Chim. Acta. 372, 98–102 (2006).

Clegg, D. L. Paper Chromatography. Anal. Chem. 22, 48–59 (1950).

Collinson, P. O., Gaze, D. C. Biomarkers of cardiovascular damage. Med. Princ. Pract. 16, 247-261 (2007).

Curto, V. F., Lopez-Ruiz, N., Capitan-Vallvey, L. F., Palma, A. J., Benito-Lopez, F., *et al*. Fast prototyping of paper-based microfluidic devices by contact stamping using indelible ink. RSC Adv. 3, 18811 (2013).

da Silva, E. T. S. G., Santhiago, M., de Souza, F. R., Coltro, W. K. T., Kubota, L. T. Triboelectric effect as a new strategy for sealing and controlling the flow in paper-based devices. Lab Chip. DOI: 10.1039/C5LC00022J (2015).

Daar, A. S., Thorsteinsdottir, H., Martin, D. K., Smith, A. C., Nast, S., *et al*. Top ten biotechnologies for improving health in developing countries. Nat. Genet. 32, 229–232 (2002).

Davies, M. J. Stability and instability: Two faces of coronary atherosclerosis: The Paul Dudley White lecture 1995. Circulation. 94, 2013-2020 (1996).

De Groot, M. J., Wodzig, K. W., Simoons, M. L., Glatz, J. F., Hermens, W. T. Measurement of myocardial infarct size from plasma fatty acid-binding protein or myoglobin, using individually estimated clearance rates. Cardiovasc. Res. 44, 315-24 (1999).

Deborggraeve, S., Claes, F., Laurent, T., Mertens, P., Leclipteux, T., *et al*. Molecular dipstick test for diagnosis of sleeping sickness. J. Clin. Microbiol. 44, 2884–2889 (2006).

Delaney, J. L., Hogan, C. F., Tian, J. F., Shen, W. Electrogenerated chemiluminescence detection in paper-based microfluidic sensors. Anal. Chem. 83, 1300–1306 (2011).

Demirel, G.; Babur, E. Vapor-phase deposition of polymers as a simple and versatile technique

to generate paper-based microfluidic platforms for bioassay applications. Analyst. 139, 2326−2331 (2014).

Dolinsky, T.J., Nielsen, J. E., McCammon, J. A., Baker, N.A. PDB2PQR: an automated pipeline for the setup of Poisson–Boltzmann electrostatics calculations. Nucleic Acids Res. 32, W665-7 (2004).

Dong, L., Tan, Q. W., Ye, W., Liu, D. L., Chen, H. F., *et al*. Screening and Identifying a Novel ssDNA Aptamer against Alpha-fetoprotein Using CE-SELEX. Sci. Rep. 5, 15552 (2015).

Dungchai, W., Chailapakul, O., Henry, C. S. A low-cost, simple, and rapid fabrication method for paper-based microfluidics using wax screen-printing. Analyst (Amsterdam). 136, 77-82 (2011).

Dungchai, W., Chailapakul, O., Henry, C. S. Electrochemical detection for paper-based microfluidics. Anal. Chem. 81, 5821–5826 (2009).

Ellington, A. D., Szostak, J. W. In vitro selection of RNA molecules that bind specific ligands. Nature. 346, 818-822 (1990).

Engelbienne, P. Use of colloidal gold surface plasmon resonance peak shift to infer affinity constants from the interactions between protein antigens and antibodies specific for single or multiple epitopes. Analyst. 123, 1599-1603 (1998).

Erlikh, A. D., Katrukha, A. G., Trifonov, I. R., Bereznikova, A. V., Gratsiansky, N. A., *et al*. Prognostic significance of heart fatty acid binding protein in patients with non-ST elevation acute coronary syndrome: Results of follow-up for twelve months. Kardiologia. 45, 13-21 (2005).

Falomir-Lockhart, L. J., Laborde, L., Kahn, P. C., Storch, J., Corsico, B. Protein-membrane interaction and fatty acid transfer from intestinal fatty acid-binding protein to membranes. Support for a multistep process. J. Biol. Chem. 281, 13979–13989 (2006).

Famulok, M., Blind, M., Mayer, G. Intramers as promising new tools in functional proteomics. Chem. Biol. 8, 931–939 (2001).

Famulok, M., Verma, S. In vivo-applied functional RNAs as tools in proteomics and genomics research. Trends Biotechnol. 20, 462–466 (2002).

Feigel, F. Qualitative Analysis by Spot Tests. Elsevier: New York, (1946).

Fernandez Garcia, M., Chiang, M. Y. M. Effect of hygrothermal aging history on sorption process, swelling, and glass transition temperature in a particle-filled epoxy-based adhesive. J Appl Polym Sci. 84, 1581-1591 (2002).

Flower, D. R., North, A. C., Attwood, T. Structure and sequence relationships in the lipocalins and related proteins. Protein Sci. 2:753–761 (1993).

Fransen, E. J., Maessen, J. G., Hermens, W. T., Glatz, J. F. C. Demonstration of ischemia-reperfusion injury separate from postoperative infarction in coronary artery bypass graft patients. Ann. Thorac. Surg. 65, 48-53 (1998).

G Eyetech Study. Preclinical and phase 1A clinical evaluation of an anti-VEGF pegylated aptamer (EYE001) for the treatment of exudative age-related macular degeneration. Retina. 22, 143-152 (2002).

Gallardo, A., Rawson, K., McNeil, C. Near patient testing: diag-nosing a first world killer. Chem. Eng. 734, 30-32 (2002).

Garbett, N. C., Ragazzon, P. A., Chaires, J. B. Circular dichroism to determine binding mode and affinity of ligand–DNA interactions. Nat. Protoc. 2, 3166-3172 (2007).

Geiger, A., Burgstaller, P., von der Eltz, H., Roeder, A., Famulok, M. RNA aptamers that bind L-arginine with sub-micromolar dissociation constants and high enantioselectivity. Nucleic Acids Res. 24, 1029–1036 (1996).

Gerede, D. M., Gulec, S., Kilickap, M., Kaya, C. T., Vurgun, V. K., *et al*. Comparison of a qualitative measurement of heart-type fatty acid-binding protein with other cardiac markers as an early diagnostic marker in the diagnosis of non-ST-segment elevation myocardial infarction. Cardiovascular Journal of Africa. 26, 204-209 (2015).

Ghani, F., Wu, A. H. B., Graff, L., Petry, C., Armstrong, G., *et al.* Role of heart-type fatty acid-binding protein in early detection of acute myocardial infarction. Clin.Chem. 46, 718-719 (2000).

Giddings, J. C., Keller, R. A. Advances in Chromatography. Marcel Dekker, Inc.: New York, (1965).

Glatz, J. F. C., Haastrup, B., Hermens, W. T., Zwaan, C. D., Barker, J., *et al*. Fatty acid-binding protein and the early detection of acute myocardial infection: the EUROCARDI multicenter trial. Circulation. 96, I-215 (1997).

Glatz, J. F. C., van der Vusse, G. J., Simoons, M. L., Kragten, J. A., van Dieijen-Visser, M. P., *et al*. Fatty acid-binding protein and the early detection of acute myocardial infarction. Clin. Chim. Acta. 272, 87-92 (1998).

Glatz, J. F. C., Kleine, A. H., Vannieuwenhoven, F. A., Hermens, W. T., Vandieijenvisser, M. P., *et al.* Fatty-acid-binding protein as a plasma marker for the estimation of myocardial infarct size in humans. Br. Heart. J. 71, 135-140 (1994).

Glatz, J. F., Vanbilsen, M., Paulussen, R. J. A., Veerkamp, J. H., Vandervusse, G. J., *et al*. Release of fatty acid-binding protein from isolated rat heart subjected to ischemia and reperfusion or to the calcium paradox. Biochim. Biophys. Acta. 961, 148-152 (1988).

Gray, R. D., Chaires, J. B. Analysis of multidimensional G-Quadruplex melting curves. Curr Protoc Nucleic Acid Chem, Chapter 17: Unit 17.4 (2011).

Green, M. R., Sambrook, J. Molecular Cloning: a laboratory manual-4th ed. Cold Spring Harbour Laboratory Press, Cold Spring Harbour, New York, USA (2012).

Gul, O., Calay, E., Sezerman, U., Basaga, H., Gurbuz, Y., *et al.* Sandwich-type, antibody microarrays for the detection and quantification of cardiovascular risk markers. Sens. Actuators B. Chem. 125, 581-588 (2007).

Gussenhoven, G. C., vanderHoorn, M. A. W. G., Goris, M. G. A., Terpstra, W. J., Hartskeerl, R. A., *et al.* LEPTO dipstick, a dipstick assay for detection of Leptospira-specific immunoglobulin

M antibodies in human sera. J. Clin. Microbiol. 35, 92–97 (1997).

Haastrup, B., Gill, S., Kristensen, S. R., Jorgensen, P. J., Glatz, J. F. C., *et al*. Biochemical markers of ischaemia for the early identification of acute myocardial infarction without ST segment elevation. Cardiology. 94, 254-261 (2000).

Hamilton, A. J., Swales, L. A., Neill, J., Murphy, J. C., Darragh, K. M., *et al*. Risk stratification of chest pain patients in the emergency department by a nurse utilizing a point of care protocol. Eur. J. Emerg. Med. 15, 9-15 (2008).

Hansen, S., Tremmel, D., Madhurantakam, C., Reichen, C., Mittl, P. R. E., *et al*. Structure and energetic contributions of a designed modular peptide-binding protein with picomolar affinity. J. Am. Chem. Soc. 10.1021/jacs.6b00099 (2016).

Hardman, J. D., Slater, J. H., Reid, A. G., Lang, W. K., Jackson, R. Diamatrix Ltd. U.S. Patent 6,573,108, (2003).

Hasegawa, T., Yoshimura, N., Oka, S., Ootaki, Y., Toyoda, Y., *et al*. Evaluation of heart fatty acid-binding protein as a rapid indicator for assessment of myocardial damage in pediatric cardiac surgery. J. Thorac. Cardiovasc. Surg. 127, 1697-1702 (2004).

Hayashida, N., Chihara, S., Akasu, K., Oda, T., Tayama, E., *et al*. Plasma and urinary levels of heart fatty acid-binding protein in patients undergoing cardiac surgery. Jpn. Circ. J. 64, 18-22 (2000).

Hodsdon, M. E., Cistola, D. P. Ligand binding alters the backbone mobility of intestinal fatty acid-binding protein as monitored by 15N NMR relaxation and 1H exchange. Biochemistry. 36, 2278-2290 (1997).

Hoffmann, U., Espeter, F., Weiss, C., Ahmad-Nejad, P., Lang, S., *et al*. Ischemic biomarker heart-type fatty acid binding protein (hFABP) in acute heart failure - diagnostic and prognostic insights compared to NT-proBNP and troponin I. BMC Cardiovascular Disorders. 15, 50 (2015).

Hossain, S. M., Luckham, R. E., Smith, A. M., Lebert, J. M., Davies, L. M., *et al*. Development

of a bioactive paper sensor for detection of neurotoxins using piezoelectric inkjet printing of sol-gel-derived bioinks. Anal. Chem. 81, 5474–5483 (2009).

Huang, C. H. Prognostic relevance of plasma heart-type fatty acid binding protein after out-of-hospital cardiac arrest. Clinica Chimica Acta. 435, 7-13 (2014).

Huynh, H. T., Larsson, C., Narod, S., Pollak, M. Tumor suppressor activity of the gene encoding mammary-derived growth inhibitor. Cancer. Res. 55, 2225-2231 (1995).

Ireson, C. R., Kelland, L. R. Discovery and development of anticancer aptamers. Mol. Cancer. Ther. 5, 2957-2962 (2006).

Ishii, J., Ozaki, Y., Lu, J. C., Kitagawa, F., Kuno, T., *et al.* Prognostic value of serum concentration of heart-type fatty acid binding protein relative to cardiac troponin T on admission in the early hours of acute coronary syndrome. Clin. Chem. 51, 1397-1404 (2005).

Ishii, J., Wang, J. H., Naruse, H., Taga, S., Kinoshita, M., *et al.* Serum concentrations of myoglobin vs human heart-type cytoplasmic fatty acid-binding protein in early detection of acute myocardial infarction. Clin.Chem. 43, 1372-1378 (1997).

Ito, T., Ueno, Y., Komatsu, Y., Matsuda, A. Synthesis, thermal stability and resistance to enzymatic hydrolysis of the oligonucleotides containing 5-(n-aminohexyl)carbamoyl-2′-o-methyluridines. Nucleic Acids Res. 31, 2514–2523 (2003).

Jacobs, L. H. J., van Borren, M., Gemen, E., van Eck, M., van Son, B., *et al*. Rapidly rule out acute myocardial infarction by combining copeptin and heart-type fatty acid-binding protein with cardiac troponin. Annals of Clinical Biochemistry.52, 550-561 (2015).

Jarvis, T. C., Davies, D. R., Hisaminato, A., Resnicow, D. I., Gupta, S., *et al*. Non-helical DNA Triplex Forms a Unique Aptamer Scaffold for High Affinity Recognition of Nerve Growth Factor. Structure. 23, 1293-1304 (2015).

Jenison, R. D., Gill, S. C., Pardi, A., Polisky, B. High-resolution molecular discrimination by RNA. Science. 263, 1425-1429 (1994).

Joubert, M. K., Kinsley, N., Capovilla, A., Sewell, B. T., Jaffer, M. A., *et al.* A Modeled Structure of an Aptamer-gp120 Complex Provides Insight into the Mechanism of HIV-1 Neutralization. Biochemistry. 49, 5880-5890 (2010).

Jungreis, E. Spot Test Analysis: Clinical, Environmental, Forensic, and Geochemical Applications, 2nd ed. John Wiley & Sons, Inc: New York, (1997).

Kakoti, A., Goswami, P. Heart type fatty acid binding protein: Structure, function and biosensing applications for early detection of myocardial infarction. Biosens Bioelectronics. 43, 400-411 (2013).

Kaptein, W. A., Korf, J., Cheng, S., Yang, M., Glatz, J. F. C., *et al.* On-line flow displacement immunoassay for fatty acid-binding protein. J. Immunol. Methods. 217, 103-111 (1998b).

Kaptein, W. A., Zwaagstra, J. J., Venema, K., Korf, J. Continuous ultraslow micro-dialysis and ultrafiltration for subcutaneous sampling as demonstrated by glucose and lactate measurements in rats. Anal. Chem. 70, 4696-4700 (1998a).

Kashtanova, E. V., Voevoda, M. I., Kuimov, A. D., Polonskaya, Y. V., Lozhkina, N. G., *et al.* Heart type fatty acid binding protein in acute coronary syndrome. Russian Journal of Cardiology. 1, 31-34 (2012).

Keffer, J. H. Myocardial markers of injury: Evolution and insights. Am. J. Clin. Pathol. 105, 305-320 (1996).

Key, G., Schreiber, A., Feldbrugge, R., McNeil, C. J., Jorgensen, P., *et al.* Multicenter evaluation of an amperometric immunosensor for plasma fatty acid-binding protein: An early marker for acute myocardial infarction. Clin. Biochem. 32, 229-231 (1999).

Kikin, O., D'Antonio, L., Bagga, P. S. QGRS Mapper: a web-based server for predicting G quadruplexes in nucleotide sequences. Nucleic Acids Res.34, W676-682 (2006).

Kilcullen, N., Viswanathan, K., Das, R., Morrell, C., Farrin, A., *et al.* Heart-Type Fatty Acid-Binding Protein Predicts Long-Term Mortality After Acute Coronary Syndrome and Identifies

High-Risk Patients Across the Range of Troponin Values. J. Am. Coll. Cardiol. 50, 2061-2067 (2007).

Kimoto, M., Yamashige, R., Matsunaga, K., Yokoyama, S., Hirao, I. Generation of high-affinity DNA aptamers using an expanded genetic alphabet. Nat. Biotechnol. 31, 453-457 (2013).

Klasner, S. A., Price, A. K., Hoeman, K. W., Wilson, R. S., Bell, K. J., *et al*. Paper-based microfluidic devices for analysis of clinically relevant analytes present in urine and saliva. Anal. Bioanal. Chem. 397, 1821–1829 (2010).

Kleine, A. H., Glatz, J. F. C., Van Nieuwenhoven, F. A., Van der Vusse, G. J. Release of heart fatty acid-binding protein into plasma after acute myocardial infarction in man. Mol. Cell. Biochem. 116, 155-162 (1992).

Kool, E.T. Preorganization of DNA: Design principles for improving nucleic acid recognition by synthetic oligonucleotides. Chem. Rev. 97, 1473–1488 (1997).

Kraemer, S., Vaught, J. D., Bock, C., Gold, L., Katilius, E., *et al*. From SOMAmer-based biomarker discovery to diagnostic and clinical applications: a SOMAmer-based, streamlined multiplex proteomic assay. PLos One. 6, e26332 (2011).

Kricka, L.J., Fortina, P. Analytical ancestry: "Firsts" in fluorescent labeling of nucleosides, nucleotides, and nucleic acids. Clin. Chem. 55, 670–683 (2009).

Kroger, D., Katerkamp, A., Renneberg, R., Cammann, K. Surface investigations on the development of a direct optical immunosensor. Biosens. Bioelectron. 13, 1141-1147 (1998).

Kunz, U., Katerlamp, A., Renneberg, R., Spener, F., Cammann, K. Sensing fatty acid bind protein with planar and fiber-optical surface plasmon resonance spectroscopy devices. Sens. Actuators. 32, 129-155 (1996).

Kwak, H., Hwang, I., Kim, J. H., Kim, M. Y., Yang, J. S., *et al*. Modulation of transcription by the peroxisome proliferator-activated receptor δ-binding RNA aptamer in colon cancer cells. Mol. Cancer Ther. 8, 2664–2673 (2009).

Laemmli, U. K. Cleavage of structural proteins during the assembly of the head of bacteriophage T4. Nature. 227, 680–685 (1970).

Lao, Y. H., Chiang, H. Y., Yang, D. K., Peck, K. & Chen, L. C. Selection of aptamers targeting the sialic acid receptor of hemagglutinin by epitope-specific SELEX. Chem. Commun (Camb).50, 8719-8722 (2014).

Leung, V., Shehata, A. A. M., Filipe, C. D. M., Pelton, R. Streaming potential sensing in paper-based microfluidic channels. Colloids Surf. A. 364, 16-18 (2010).

Li, W., Li, M., Ge, S. G., Yan, M., Huang, J. D., *et al.* Battery-triggered ultrasensitive electrochemiluminescence detection on microfluidic paper-based immunodevice based on dual-signal amplification strategy. Anal. Chem. Acta, 767, 66-74 (2013).

Li, X. J., Nie, Z. H., Cheng, C. M., Goodale, A. B., Whitesides, G. M., *et al.* Paper-based electrochemical ELISA. Proc. Micro Total Analysis Systems. 14, 1487-1489 (2010).

Li, X., Tian, J., Garnier, G., Shen, W. Fabrication of paper-based microfluidic sensors by printing. Colloids Surf. B. 76, 564-570 (2010).

Li, X., Tian, J., Nguyen, T., Shen, W. Paper-Based Microfluidic Devices by Plasma Treatment. Anal. Chem. 80, 9131- 9134 (2008).

Li, X., Tian, J., Shen, W. Progress in patterned paper sizing for fabrication of paper-based microfluidic sensors. Cellulose. 17, 649-659 (2010).

Liberman, J. A., Suddala, K. C., Aytenfisu, A., Chan, D. L., Belashov, I. A., *et al.* Structural analysis of a class III preQ1 riboswitch reveals an aptamer distant from a ribosome-binding site regulated by fast dynamics. Proc. Natl. Acad. Sci. U S A. 112, E3485-3494 (2015).

Lin, P. H., Chen, R. H., Lee, C. H., Chang, Y., Chen, C. S., *et al.* Studies of the binding mechanism between aptamers and thrombin by circular dichroism, surface plasmon resonance and isothermal titration calorimetry. Colloids Surf. B Biointerfaces. 88, 552-558 (2011).

Lin, P. H., Tsai, C. W., Wu, J. W., Ruaan, R. C., Chen, W. Y. Molecular dynamics simulation

of the induced-fit binding process of DNA aptamer and L-argininamide. Biotechnol. J. 7, 1367-1375 (2012).

Lin, S., Yokoyama, H., Rac, V. E., Brooks, S. C. Novel biomarkers in diagnosing cardiac ischemia in the emergency department: A systematic review. Resuscitation. 83, 684-691 (2012).

Liou, H. L., Kahn, P. C., Storch, J. Role of the helical domain in fatty acid transfer from adipocyte and heart fatty acid-binding proteins to membranes: Analysis of chimeric proteins. J. Biol. Chem. 277, 1806-1815 (2002).

Lippi, G., Mattiuzzi, C., Cervellin, G. Critical review and meta-analysis on the combination of heart-type fatty acid binding protein (H-FABP) and troponin for early diagnosis of acute myocardial infarction. Clinical Biochemistry. 46, 26-30 (2013).

Liu, J., Mazumdar, D., Lu, Y. A simple and sensitive "dipstick" test in serum based on lateral flow separation of aptamer-linked nanostructures. Angew. Chem., Int. Ed. 45, 7955–7959 (2006).

Lollo, B., Steele, F., Gold, L. Beyond antibodies: New affinity reagents to unlock the proteome. Proteomics. 14, 638–644 (2014).

Lu, Y., Shi, W., Jiang, L., Qin, J., Lin, B. Rapid prototyping of paper-based microfluidics with wax for low-cost, portable bioassay. Electrophoresis. 30, 1497-1500 (2009).

Luck, G., Zimmer, C., Snatzke, G., Sondgerath, G. Optical Rotatory Dispersion and Circular Dichroism of DNA from various sources at alkaline pH. Eur. J. Biochem. 17, 514-522 (1970).

Lucke, C., Rademacher, M., Zimmerman, A. W., van Moerkerk, H. T. B., Veerkamp, J. H., *et al*. Spin-system heterogeneities indicate a selected-fit mechanism in fatty acid binding to heart-type fatty acid-binding protein (H-FABP). Biochem. J. 354, 259-266 (2001).

Ma, S.; Tang, Y.; Liu, J.; Wu, J. Visible paper chip immunoassay for rapid determination of bacteria in water distribution system. Talanta. 120, 135−140 (2014).

Mabey, D., Peeling, R. W., Ustianowski, A., Perkins, M. D. Diagnostics for the developing world. Nat. Rev. Microbiol. 2, 231–240 (2004).

Macek, K., Becvarova, H. Papers ready for use plates, and flexible sheets for chromatography. Chromatogr. Rev.15, 1–28 (1971).

Marangoni, K., Neves, A. F., Rocha, R. M., Faria, P. R., Alves, P. T., *et al*. Prostate-specific RNA aptamer: promising nucleic acid antibody-like cancer detection. Sci. Rep. 5, 12090 (2015).

Martinez, A. W., Phillips, S. T., Carrilho, E., Thomas, S. W., Sindi, H., *et al*. Simple telemedicine for developing regions: camera phones and paper-based microfluidic devices for real-time, off-site diagnosis. Anal. Chem. 80, 3699–3707 (2008).

Martinez, A. W., Phillips, S. T., Butte, M. J., Whitesides, G. M. Patterned paper as a platform for inexpensive, low-volume, portable bioassays. Angew. Chem. Int. Ed. 46, 1318–1320 (2007).

Martinez, A. W., Phillips, S. T., Whitesides, G. M. Diagnostics for the developing world: microfluidic paper-based analytical devices. Anal. Chem. 82, 3–10 (2010).

Martinez, A. W., Phillips, S. T., Whitesides, G. M. Three-dimensional microfluidic devices fabricated in layered paper and tape. Proc. Natl. Acad. Sci. USA. 105, 19606–19611 (2008).

Martinez, A. W., Phillips, S. T., Wiley, B. J., Gupta, M., Whitesides, G. M. FLASH: a rapid method for prototyping paper-based microfluidic devices. Lab Chip. 8, 2146–2150 (2008).

Martinez, O., Bellard, E., Golzio, M., Mechiche-Alami, S., Rols, M. P., *et al*. Direct validation of aptamers as powerful tools to image solid tumor. Nucleic Acid Ther. 24, 217-225 (2014).

Matheson, I. B. C. The Method of Successive Integration: A General Technique for Recasting Kinetic Equations in a Readily Soluble Form Which Is Linear in the Coefficients and Sufficiently Rapid for Real Time Instrumental Use. Analytical Instrumentation, 16, 345-373 (1987).

McCann, C. J., Glover, B. M., Menown, I. B. A., Moore, M. J., McEneny, J., (t al. Novel biomarkers in early diagnosis of acute myocardial infarction compared with cardiac troponin T. Eur. Heart. J. 29, 2843-2850 (2008).

McMahon, C. J., Lamont, J. V., Curtin, E., McConnell, R. I., Crockard, M., *et al*. Diagnostic accuracy of heart-type fatty acid-binding protein for the early diagnosis of acute myocardial

infarction. American Journal of Emergency Medicine. 30, 267-274 (2012).

Melancon, M. P., Zhou, M., Zhang, R., Xiong, C., Allen, P., *et al.* Selective uptake and imaging of aptamer- and antibody-conjugated hollow nanospheres targeted to epidermal growth factor receptors overexpresses in head and neck cancer. ACS Nano. 8, 4530-4538 (2014).

Miao, Y. Q. Thin-layer Impedimetric biosensorsfor the free label immunoassay. Pak. J. Biol. Sci. 8, 1544-1547 (2005).

Mion, M. M., Novello, E., Altinier, S., Rocco, S., Zaninotto, M., *et al*. Analytical and clinical performance of a fully automated cardiac multi-markers strategy based on protein biochip microarray technology. Clin. Biochem. 40, 1245-1251 (2007).

Murphy, E. J., Barcelo- Coblijn, G., Binas, B., Glatz, J. F. Heart fatty acid uptake is decreased in heart fatty acid-binding protein gene-ablated mice. J. Biol. Chem. 279, 34481-34488 (2004).

Murphy, E. J., Owada, Y., Kitanaka, N., Kondo, H., Glatz, J. F. Brain arachidonic acid incorporation is decreased in heart fatty acid binding protein gene-ablated mice. Biochemistry. 44, 6350-6360 (2005).

Murray, S., Hillman, C., Pecht, M. Environmental aging and deadhesion of siloxane-polyimide-epoxy adhesive. IEEE Trans Compon Packag technol. 26,524-531 (2003).

Mwaba, P., Cassol, S., Pilon, R., Chintu, C., Janes, M., *et al*. Use of dried whole blood spots to measure CD4+ lymphocyte counts in HIV-1-infected patients. Lancet. 362, 1459–1460 (2003).

Nakata, T., Hashimoto, A., Tsuchihashi, K., Shimamoto, K. Human heart-type fatty acid-binding protein as an early diagnostic and prognostic marker in acute coronary syndrome. Cardiology. 99, 96-104 (2003).

Newby, L. K., Storrow, A. B., Gibler, W. B., Garvey, J. L., Tucker, J. F., *et al.* Bedside multimarker testing for risk stratification in chest pain units: The chest pain evaluation by creatine kinase-MB, myoglobin, and troponin I (CHECKMATE) study. Circulation.103, 1832-1837 (2001).

Ng, E. W., Adamis, A. P. Anti-VEGF aptamer (pegaptanib) therapy for ocular vascular diseases. Ann. N. Y. Acad. Sci. 1082, 151-171 (2006).

Niemeyer, C. M. The developments of semisynthetic DNA-protein conjugates. Trends Biotechnol. 20, 395–401 (2002).

Nizeki, T., Takeishi, Y., Arimoto, T., Nozaki, N., Hirono, O., *et al*. Persistently increased serum concentration of heart-type fatty acid-binding protein predicts adverse clinical outcomes in patients with chronic heart failure. Circ. J. 72, 109-114 (2008).

Nurak, T.; Praphairaksit, N.; Chailapakul, O. Fabrication of paper-based devices by lacquer spraying method for the determination of nickel (II) ion in waste water. Talanta. 114, 291−296 (2013).

O'Donoghue, M., *et al*. Prognostic utility of heart-type fatty acid binding protein in patients with acute coronary syndromes. Circulation. 116, 550-557 (2006).

O'Regan, T. M., Pravda, M., O'Sullivan, C. K., Guilbault, G. G. Development of a disposable immunosensor for the detection of human heart fatty-acid binding protein in human whole blood using screen-printed carbon electrodes. Talanta. 57, 501-510 (2002).

Oberhofer, T. R., Towle, D. W. Evaluation of the rapid penicillinase paper strip test for detection of beta-lactamase. J. Clin. Microbiol. 15, 196–199 (1982).

Ockner, R. K., Manning, J. A., Poppenhausen, R. B., Ho, W. K. A binding protein for fatty acids in cytosol of intestinal mucosa, liver, myocardium, and other tissues. Science. 177, 56-58 (1972).

Ohkaru, Y., Asayama, K., Ishii, H., Nishimura, S., Sunahara, N., *et al*. Development of a sandwich enzyme-linked immunosorbent assay for the determination of human heart type fatty acid-binding protein in plasma and urine by using two different monoclonal antibodies specific for human heart fatty acid-binding protein. J. Immunol. Methods. 178, 99-111 (1995).

Okamoto, F., Sohmiya, K., Ohkaru, Y., Kawamura, K., Asayama, K., *et al*. Human heart-type

cytoplasmic fatty acid-binding protein (H-FABP) for the diagnosis of acute myocardial infarction. Clinical evaluation of H-FABP in comparison with myoglobin and creatine kinase isoenzyme MB. Clin. Chem. Lab. Med. 38, 231-238 (2000).

Olkkonen, J., Lehtinen, K., Erho, T. Flexographically Printed Fluidic Structures in Paper. Anal. Chem. 82, 10246-10250 (2010).

Orban, M., Katerkamp, A., Renneberg, R., Spener, F., Cammann, K. Kinetic analysis of immunointeractions with covalently immobilized fatty acid-binding protein using a grating coupler sensor. Immunol. Methods. 215, 17-26 (1998).

Ornatska, M., Sharpe, E., Andreescu, D., Andreescu, S. Paper Bioassay Based on Ceria Nanoparticles as Colorimetric Probes. Anal. Chem. 83, 4273-4280 (2011).

Otaki, Y., Watanabe, T., Takahashi, H., Hirayama, A., Narumi, T., *et al*. Association of Heart-Type Fatty Acid-Binding Protein with Cardiovascular Risk Factors and All-Cause Mortality in the General Population: The Takahata Study. PLoS One. 9, e94834 (2014).

Pagani, F., Bonara, R., Bonetti, G., Panteghini, M. Evaluation of a sandwich enzyme-linked immunosorbent assay for the measurement of serum heart fatty acid-binding protein. Ann. Clin. Biochem. 39, 404-405 (2002).

Panteghini, M. Role and importance of biochemical markers in clinical cardiology. Eur. Heart. J. 25, 1187-1196 (2004).

Panteghini, M., Bonora, R., Pagani, F., Brothers, G., Mangion, J., *et al*. Heart fatty acid-binding protein in comparison with myoglobin for the early detection of acute myocardial infarction. Clin. Chem. 43, S-157 (1997).

Parekh, P., Kamble, S., Zhao, N. X., Portier, B. P. and Zu, Y. L. Immunotherapy of CD30-expressing lymphoma using a highly stable ssDNA aptamer. Biomaterials. 34, 8909-8917 (2013).

Peeling, R. W., Holmes, K. K., Mabey, D., Ronald, A. Rapid tests for sexually transmitted infections (STIs): the way forward. Sex. Transm. Infect. 82, 1–6 (2006).

Pelsers, M. M. A. L., Chapelle, J. P., Knapen, M., Hermens, W. T., Glatz, J. F. C. Influence of age and sex and day-to-day and within-day biological variation on plasma concentrations of fatty acid-binding protein and myoglobin in healthy subjects [5]. Clin.Chem. 45, 441-443 (1999).

Pelsers, M. M. A. L., Hermens, W. T., Glatz, J. F. C. Fatty acid-binding proteins as plasma markers of tissue injury. Clin. Chim. Acta. 352, 15-35 (2005).

Pelton, R. Bioactive paper provides a low-cost platform for diagnostics. Trends Anal. Chem. 28, 925–942 (2009).

Penner, G. Commercialization of an aptamer-based diagnostic test. IVD Technol. 18, 31–37 (2012).

Petzold, T., Feindt, P., Sunderdiek, U., Boeken, U., Fischer, Y., *et al.* Heart-type fatty acid binding protein (hFABP) in the diagnosis of myocardial damage in coronary artery bypass grafting. Eur. J. Cardio-Thorac. Surg. 19, 859-864 (2001).

Phelan, C. M., Larsson, C., Baird, S., Futreal, P. A., Ruttledge, M. H., *et al.* The human mammary-derived growth inhibitor (MDGI) gene: Genomic structure and mutation analysis in human breast tumors. Genomics. 34, 63-68 (1996).

Pirrung, M. C. How to make a DNA chip. Angew. Chem. Int. Ed. 41, 1276–1289 (2002).

Popenda, M., Szachniuk, M., Antczak, M., Purzycka, K. J., Lukasiak, P., *et al.* Automated 3D structure composition for large RNAs. Nucleic Acids Res. 40, e112. doi: 10.1093/nar/gks339 (2012).

Potyrailo, R. A., Murray, A. J., Nagraj, N., Pris, A. D., Ashe, J. M., *et al.* Towards maintenance-free biosensors for hundreds of bind/release cycles. Angew. Chem. Int. Ed. Engl. 54, 2174-2178 (2015).

Prinsen, C. F. M., Veerkamp, J. H. Fatty acid binding and conformational stability of mutants of human muscle fatty acid-binding protein. Biochem. J. 314, 253-260 (1996).

Qian, Q., Kuo, L., Yu, Y. T., Rottmann, J. N. A concise promoter region of the heart fatty acid-

binding protein gene dictates tissue-appropriate expression. Circ. Res. 84, 276-289 (1999).

Qin, C. F., Li, G. C. Mammalian cell display technology coupling with AID induced SHM in vitro: An ideal approach to the production of therapeutic antibodies. Int. Immunopharmacol. 23, 380–386 (2014).

Radom, F., Jurek, P. M., Mazurek, M. P., Otlewski, J., Jeleń, F. Aptamers: molecules of great potential. Biotechnol. Adv. 31, 1260-1274 (2013).

Ramzaeva, N., Rosemeyer, H., Leonard, P., Muhlegger, K., Bergmann, F., *et al.* Oligonucleotides functionalized by fluorescein and rhodamine dyes: Michael addition of methyl acrylate to 2′-deoxypseudouridine. Helv. Chim. Acta. 83, 1108–1126 (2000).

Ren, L., Wang, J. C., Liu, W., Tu, Q., Liu, R. An enzymatic immunoassay microfluidics integrated with membrane valves for microsphere retention and reagent mixing. Biosens.Bioelectron. 35, 147-154 (2012).

Reshetnikov, R. V., Golovin, A. V., Kopylov, A. M. Comparison of Models of Thrombin-Binding 15-mer DNA Aptamer by Molecular Dynamics Simulation. Biochemistry (Mosc). 75, 1017-1024 (2010).

Rhinehardt, K. L., Srinivas, G., Mohan, R. V. Molecular Dynamics Simulation Analysis of Anti-MUC1 Aptamer and Mucin 1 Peptide Binding. J. Phys. Chem. B. 119, 6571-6583 (2015).

Richieri, G. V., Ogata, R. T., Kleinfeld, A. M. Equilibrium constants for the binding of fatty acids with fatty acid- binding proteins from adipocyte, intestine, heart, and liver measured with the fluorescent probe ADIFAB. J. Biol. Chem. 269, 23918-23930 (1994).

Robers, M., Van der Hulst, F. F., Fischer, M. A. J. G., Roos, W., Salud, C. E., *et al.* Development of a rapid microparticle-enhanced turbidimetric immunoassay for plasma fatty acid-binding protein, an early marker of acute myocardial infarction. Clin. Chem. 44, 1564-1567 (1998).

Robertson, D. L., Joyce, G. F. Selection in vitro of an RNA enzyme that specifically cleaves

single stranded DNA. Nature. 344, 467-468 (1990).

Roos, W., Eymann, E., Symannek, M., Duppenthaler, J., Wodzig, K. W. H., *et al.* Monoclonal antibodies to human heart fatty acid-binding protein. J. Immunol. Methods. 183, 149-153 (1995).

Ropson, I. J., Frieden, C. Dynamic NMR spectral analysis and protein folding: Identification of a highly populated folding intermediate of rat intestinal fatty acid-binding protein by19F NMR. Proc. Natl. Acad. Sci. USA. 89, 7222-7226 (1992).

Ruigrok, V. J. B., van Duijn, E., Barendregt, A., Dyer, K., Tainer, J. A., *et al.* Kinetic and stoichiometric characterization of streptavidin-binding aptamers. ChemBioChem. 13, 829–836 (2012).

Sacchettini, J. C., Gordon, J. I., Banaszak, L. J. Refined apoprotein structure of rat intestinal fatty acid binding protein produced in Escherichia coli. Proc. Natl. Acad. Sci. USA. 86, 7736-7740 (1989).

Salentin, S., Schreiber, S., Haupt, V. J., Adasme, M. F., Schroeder, M. PLIP: fully automated protein–ligand interaction profiler. Nucleic Acids Res. 43, W443-447 (2015).

Samanta, A., Das, D. K., Jones, R., George, A., Prasad, M. R. Free radical scavenging by myocardial fatty acid binding protein. Free. Radic. Res. Commun. 7, 73-82 (1989).

Sassolas, A., Leca-Bouvier, B. D., Blum, L. J. DNA biosensors and microarrays. Chem. Rev. 108, 109–139 (2008).

Schaap, F. G., Binas, B., Danneberg, H., van der Vusse, G. J., Glatz, J. F. Impaired long-chain fatty acid utilization by cardiac myocytes isolated from mice lacking the heart-type fatty acid binding protein gene. Circ. Res. 85, 329-337 (1999).

Schena, M., Shalon, D., Davis, R.W., Brown, P.O. Quantitative monitoring of gene expression patterns with a complementary DNA microarray. Science. 270, 467–470 (1995).

Schilling, K. M., Jauregui, D., Martinez, A. W. Paper and toner three-dimensional fluidic devices: programming fluid flow to improve point-of-care diagnostics. Lab Chip. 13(4), 628-631

(2013).

Schilling, K. M., Lepore, A. L., Kurian, J. A., Martinez, A. W. Fully enclosed microfluidic paper-based analytical devices. Anal Chem. 84, 1579–1585 (2012).

Schneider, C., Sühnel, J. A Molecular Dynamics Simulation of the Flavin Mononucleotide–RNA Aptamer Complex. Biopolymers. 50, 287-302 (1999).

Schoetzau, T., Langner, J., Moyroud, E., Roehl, I., Vonhoff, S., *et al.* Amino modified nucleobases: Functionalized nucleoside triphosphates applicable for selex. Bioconjugate Chem. 14, 919–926 (2003).

Siegmann-Thoss, C., Renneberg, R., Glatz, J. F. C., Spener, F. Enzyme immunosensor for diagnosis of myocardial infarction. Sens. Actuators. 30, 71-76 (1996).

Snyder, D. A., Chen, Y., Denissova, N. G., Acton, T., Aramini, J. M., *et al.* Comparisons of NMR spectral quality and success in crystallization demonstrate that NMR and X-ray crystallography are complementary methods for small protein structure determination. J. Am. Chem. Soc. 127, 16505–16511 (2005).

Schreiber, A., Feldbrugge, R., Key, G., Glatz, J. F. C., Spener, F. An immunosensor based on disposable electrodes for rapid estimation of fatty acid-binding protein, an early marker of myocardial infarction. Biosens. Bioelectron. 12, 1131-1137 (1997).

Seino, Y., Ogata, K., Takano, T., Ishii, J., Hishida, H., *et al.* Use of a whole blood rapid panel test for heart-type fatty acid-binding protein in patients with acute chest pain: comparison with rapid troponin T and myoglobin tests. Am .J. Med. 115, 185-190 (2003).

Seino, Y., Tomita, Y., Takano, T., Ohbayashi, K. Office cardiologists cooperative study on whole blood rapid panel tests in patients with suspicious acute myocardial infarction: comparison be-tween heart-type fatty acid-binding protein and troponin T tests. Circ. J. 68, 144-148 (2004).

Sharma, M., Bulusu, G., Mitra, A. MD simulations of ligand-bound and ligand-free aptamer: Molecular level insights into the binding and switching mechanism of the add A-riboswitch. RNA.

15, 1673-1692 (2009).

Shirakabe, A. Prognostic impact of the serum heart-type fatty acid-binding protein (H-FABP) levels in patients admitted to the non-surgical intensive care unit. Clinical Research in Cardiology. 103, 791-804 (2014).

Sia, S. K., Linder, V., Parviz, B. A., Siegel, A., Whitesides, G. M. An integrated approach to a portable and low-cost immunoassay for resource-poor settings. Angew. Chem. Int. Ed. 43, 498–502 (2004).

Spitsberg, V. L., Matitashvili, E., Gorewit, R. C. Association and coexpression of fatty-acid-binding protein and glycoprotein CD36 in the bovine mammary gland. Eur. J. Biochem. 230, 872-878 (1995).

Stoltenburg, R., Nikolaus, N., Strehlitz, B. Capture-SELEX: Selection of DNA Aptamers for Aminoglycoside Antibiotics. J. Anal. Methods. Chem. 2012, 415697 (2012).

Storch, J., Thumser, A. E. The fatty acid transport function of fatty acid-binding proteins. Biochim. Biophys. Acta. 1486, 28-44 (2000).

Sun, H., Zhu, X., Lu, P. Y., Rosato, R. R., Tan, W., *et al*. Oligonucleotide aptamers: new tools for targeted cancer therapy. Mol. Ther. Nucleic Acids. 5, e182 (2014).

Sun, H., Zu, Y. A Highlight of Recent Advances in Aptamer Technology and Its Application. Molecules. 20, 11959-11980 (2015).

Sun, L., Jin, H. W., Zhao, X. Y., Liu, Z. M., Guan, Y. F., *et al*. Unfolding and Conformational Variations of Thrombin-Binding DNA Aptamers: Synthesis, Circular Dichroism and Molecular Dynamics Simulations. ChemMedChem. 9, 993-1001 (2014).

Sund, J., Lind, C., Åqvist, J. Binding Site Preorganization and Ligand Discrimination in the Purine Riboswitch. J. Phys. Chem. B. 119, 773-782 (2015).

Suzuki, K., Sawa, Y., Kadoba, K., Takahashi, T., Ichikawa, H., *et al*. Early detection of cardiac damage with heart fatty acid-binding protein after cardiac operations. Thorac. Surg. 65, 54-58

(1998).

Tan, N. S., Shaw, N. S., Vinckenbosch, N., Liu, P., Yasmin, R., *et al.* Selective Cooperation between Fatty Acid Binding Proteins and Peroxisome Proliferator-Activated Receptors in Regulating Transcription. Mol. Cell. Biol. 22, 5114-5127 (2002).

Tanaka, T., Hirota, Y., Sohmiya, K. I., Nishimura, S., Kawamura, K. Serum and urinary human heart fatty acid-binding protein in acute myocardial infarction. Clin. Biochem. 24, 195-201 (1991).

Tang, M. K., Kindler, P. M., Cai, D. Q., Chow, P. H., Li, M., *et al.* Heart-type fatty acid binding proteins are upregulated during terminal differentiation of mouse cardiomyocytes, as revealed by proteomic analysis. Cell. Tissue. Res. 316, 339-47 (2004).

Tatarinova, O., Tsvetkov, V., Basmanov, D., Barinov, N., Smirnov, I., Timofeev, E., *et al*. Comparison of the 'Chemical' and 'Structural' Approaches to the Optimization of the Thrombin-Binding Aptamer. PLoS One. 9, e89383 (2014).

Tennilä, T., Antopolsky, M., Azhayev, A., Azhayeva, E. Peptide-oligonucleotide conjugates form stable and selective complexes with antibody and DNA. Bioconjugate Chem. 19, 1361–1367 (2008).

Thygesen, K., Alpert, J. S., White, H. D., Jaffe, A. S., Apple, F. S., *et al.* Universal definition of myocardial infarction. Circulation. 116, 2634-2653 (2007).

Tuerk, C., Gold, L. Systematic evolution of ligands by exponential enrichment: RNA ligands to bacteriophage T4 DNA polymerase. Science. 4968, 505-510 (1990).

Tung, C. H., Stein, S. Preparation and applications of peptide-oligonucleotide conjugates. Bioconjugate Chem. 11, 605–618 (2000).

Turkevich, T., Stevenson, P. C., Hillier, J. A study of the nucleation and growth processes in the synthesis of colloidal gold. Discuss. Faraday Soc. 11, 55-75 (1951).

Tuszynska, I., Magnus, M., Jonak, K., Dawson, W., Bujnicki, J. M. NPDock: a web server for

protein–nucleic acid docking. Nucleic Acids Res. 43, W425-30 (2015).

Unterberg, C., Heidl, G., von Bassewitz, D. B., Spener, F. Isolation and characterization of the fatty acid binding protein from human heart. J. Lipid. Res. 27, 1287-1293 (1986).

Van der Laarse, A. Rapid estimation of myocardial infarct size. Cardio Res. 44, 247-248 (1999).

Van der Voort, D., Pelsers, M. M. A. L., Korf, J., Hermens, W. T., Glatz, J. F. C. Development of a displacement immunoassay for human heart-type fatty acid-binding protein in plasma: the basic conditions. Biosens. Bioelectron. 19, 465-471 (2003).

Van Nieuwenhoven, F. A., Willemsen, P. H., Van der Vusse, G. J., Glatz, J. F. Co-expression in rat heart and skeletal muscle of four genes coding for proteins implicated in long-chain fatty acid uptake. Int. J. Biochem. Cell Biol. 31, 489-498 (1999).

Vance, S. A., Sandros, M. G. Zeptomole detection of C-reactive protein in serum by a nanoparticle amplified surface plasmon resonance imaging aptasensor. Sci. Rep. 4, 5129 (2014).

Viswanathan, K., Kilcullen, N., Morrell, C., Thistlethwaite, S. J., Sivananthan, M. U., *et al*. Heart-type fatty acid-binding protein predicts long-term mortality and re-infarction in consecutive patients with suspected acute coronary syndrome who are troponin-negative. J. Am. Coll. Cardiol. 55, 2590-2598 (2010).

Viswanathan, K., Hall, A. S., Barth, J. H. An evidence-based approach to the assessment of heart-type Fatty Acid binding protein in acute coronary syndrome. The Clinical biochemist. Reviews / Australian Association of Clinical Biochemists. 33, 3-11 (2012).

Vork, M. M., Glatz, J. F. C., van der Vusse, G. J. On the mechanism of long chain fatty acid transport in cardiomyocytes as facilitated by cytoplasmic fatty acid-binding protein. Mol. Cell. Biochem. 123, 175-184 (1993).

Wallukat, G., Boehmer, F., Engstroem, U., Langen, P., Hollenberg, M., *et al*. Modulation of the beta-adrenergic-response in cultured rat heart cells. II. Mammary-derived growth inhibitor (MDGI) blocks induction of beta-adrenergic supersensitivity. Dissociation from lipid-binding

activity of MDGI. Mol. Cell. Biochem. 102, 49-60 (1991).

Wang, J., Wang, Q., Ren, L., Wang, X. Q., Wan, Z. F., *et al.* Carboxylated magnetic microbead-assisted fluoroimmunoassay for early biomarkers of acute myocardial infarction. Colloids. Surf B. Biointerfaces. 72, 112-120 (2009a).

Wang, J., Wang, X. Q., Ren, L., Wang, Q., Li, L., *et al.* Conjugation of biomolecules with magnetic protein microspheres for the assay of early biomarkers associated with acute myocardial infarction. Anal.Chem. 81, 6210-6217 (2009b).

Wang, J., Ren, L., Wang, X. Q., Wang, Q., Wan, Z. F., *et al.* Superparamagnetic microsphere-assisted fluoroimmunoassay for rapid assessment of acute myocardial infarction. Biosens. Bioelectron. 24, 3097-3102 (2009c).

Wang, S., Liu, J., Dong, Y., Su, H., Tan, T. Conformational structure-dependent molecular recognition of two aptamers for tetracycline. RSC Advances. 5, 53796 (2015).

Wang, W., Wu, W. Y., Wang, W., Zhu, J. J. Tree-shaped paper strip for semiquantitative colorimetric detection of protein with self-calibration. J. Chromatogr. A. 1217, 3896–3899 (2010).

Wang, X. Y., Ansaruzzaman, M., Vaz, R., Mondlane, C., Lucas, M. E. S., *et al.* Field evaluation of a rapid immunochromatographic dipstick test for the diagnosis of cholera in a high-risk population. BMC Infect. Dis. 6, 17 (2006).

Watanabe, T., Ohkubo, Y., Matsuoka, H., Kimura, H., Sakai, Y., *et al.* Development of a simple whole blood panel test for detection of human heart-type fatty acid-binding protein. Clin. Biochem. 34, 257-263 (2001).

Webber, J., Stone, T. C., Katilius, E., Smith, B. C., Gordon, B., *et al.* Proteomics analysis of cancer exosomes using a novel modified aptamer-based array (SOMAscan™) platform. Mol. Cell. Proteomics. 13, 1050–1064 (2014).

Widstrom, R. L., Norris, A. W., Spector, A. A. Binding of cytochrome P450 monooxygenase and lipoxygenase pathway products by heart fatty acid-binding protein. Biochemistry. 40, 1070-

1076 (2001).

Willemsen, R. T. A., van Severen, E., Vandervoort, P. M., Grieten, L., Buntinx, F., *et al*. Heart-type fatty acid binding protein (H-FABP) in patients in an emergency department setting, suspected of acute coronary syndrome: Optimal cut-off point, diagnostic value and future opportunities in primary care. European Journal of General Practice. 21, 156-163 (2015).

Williams, B. A. R., Chaput, J. C. Synthesis of peptide-oligonucleotide conjugates using a heterobifunctional crosslinker. In Current Protocols in Nucleic Acid Chemistry; John Wiley &

Wobus, A. M., Zschiesche, W., Grosse, R. Differentiation-promoting effects of mammary-derived growth inhibitor (MDGI) on pluripotent mouse embryonic stem cells. Virchows. Arch. B Cell. Pathol. 59, 339-342 (1990).

Wodzig, K. W. H., Pelsers, M. M. A. L., Van der Vusse, G. J., Roos, W., Glatz, J. F. C. One-step enzyme-linked immunosorbent assay (ELISA) for plasma fatty acid-binding protein. Ann. Clin. Biochem. 34, 263-268 (1997b).

Wodzig, K. W., Kragten, J. A., Hermens, W. T., Glatz, J. F., van Dieijen-Visser, M. P. Estimation of myocardial infarct size from plasma myoglobin or fatty acid-binding protein. Influence of renal function. Eur. J. Clin. Chem. Clin. Biochem. 35, 191-198 (1997a).

Wong, T. S., Schwaneberg, U., Sturmer, R., Hauer, B., Breuer, M. A filter paper-based assay for laboratory evolution of hydrolases and dehydrogenases. Comb. Chem. High Throughput Screening. 9, 289–293 (2006).

World Health Organization. World Health Report, 2012. Geneva, Switzerland.

Wu, Y., Xue, P., Hui, K. M., Kang, Y. A paper-based microfluidic electrochemical immunodevice integrated with amplification-by-polymerization for the ultrasensitive multiplexed detection of cancer biomarkers. Biosens Bioelectron. 52, 180-187 (2014).

Xiong, X. L., Lv, Y. F., Chen, T., Zhang, X. B., Wang, K. M., *et al*. Nucleic acid aptamers for living cell analysis. Annu. Rev. Anal. Chem (Palo Alto Calif). 7, 405-426 (2014).

Yager, P., Edwards, T., Fu, E., Helton, K., Nelson, K., *et al*. Microfluidic diagnostic technologies for global public health. Nature. 442, 412–418 (2006).

Yang, Q., Goldstein, I. J., Mei, H. Y., Engelke, D. R. DNA ligands that bind tightly and selectively to cellobiose. Proc. Natl. Acad. Sci. U S A. 95, 5462-5467 (1998).

Yang, Y., Spitzer, E., Kenney, N., Zschiesche, W., Li, M. L., *et al*. Members of the fatty acid binding protein family are differentiation factors for the mammary gland. Cell. Biol. 127, 1097-1109 (1994).

Yatime, L., Maasch, C., Hoehlig, K., Klussmann, S., Andersen, G. R., *et al*. Structural basis for the targeting of complement anaphylatoxin C5a using a mixed L-RNA/L-DNA aptamer. Nat. Commun. 6, 6481 (2015).

Yee, A. A., Savchenko, A., Ignachenko, A., Lukin, J., Xu, X. H., *et al*. NMR and X-ray crystallography, complementary tools in structural proteomics of small proteins. J. Am. Chem. Soc. 127, 16512–16517 (2005).

Yetisen, A. K., Akram, M. S., Lowe, C. R. Paper-based microfluidic point-of-care diagnostic devices. Lab Chip.13, 2210-2251 (2013).

Yu, A., Shang, J., Cheng, F., Paik, B. A., Kaplan, J. M., *et al*. Biofunctional paper via the covalent modification of cellulose. Langmuir. 28(30), 11265-11273 (2012).

Zanotti, G., Scapin, G., Spandon, P., Veerkamp, J. H., Sacchettini, J. C. Three-dimensional structure of recombinant human muscle fatty acid-binding protein. J. Biol. Chem. 267, 18541-18550 (1992).

Zhang, C. Hybridoma technology for the generation of monoclonal antibodies. In Antibody Methods and Protocols; Proetzel, G., Ebersbach, H., Eds.; Humana Press: New York, NY, USA, Volume 901, pp. 117–135 (2012).

Zhao, W., van der Berg, A. Lab on paper. Lab Chip. 8, 1988–1991 (2008).

Zhao, Y., Hao, C. L., Ma, W., Yong, Q. Q., Yan, W. J., *et al*. Magnetic bead-based multiplex

DNA sequence detection of genetically modified organisms using quantum dot-encoded silicon dioxide nanoparticles. J. Phys. Chem. C. 115, 20134–20140 (2011).

Zimmerman, A. W., Rademacher, M., Ruterjans, H., Lucke, C., Veerkamp, J. H. Functional and conformational characterization of new mutants of heart fatty acid-binding protein. Biochem. J. 344, 495-501 (1999).

Zlateva, K. T., Maes, P., Rahman, M., Van Ranst, M. Chromatography paper strip sampling of enteric adenoviruses type 40 and 41 positive stool specimens. Virol. J. 2, 6 (2005).

Zocher, F., Enzelberger, M. M., Bornscheuer, U. T., Hauer, B., Schmid, R. D. A colorimetric assay suitable for screening epoxide hydrolase activity. Anal. Chim. Acta. 391, 345–351 (1999).

Zschiesche, W., Kleine, A., Spitzer, E., Veerkamp, J. H., Glatz, J. F. C. Histochemical localization of heart-type fatty-acid binding protein in human and murine tissues. Histochem. Cell Biol. 103, 147-156 (1995).

Zuker, M. Mfold web server for nucleic acid folding and hybridization prediction. Nucleic Acids Res. 31, 3406-3415 (2003).

List of Publications

Publications in refereed journals

1. **Ankana Kakoti**, Pranab Goswami. Multifaceted analyses of the interactions between human heart type fatty acid binding protein and its specific aptamers, BBA General Subject DOI: 10.1016/j.bbagen.2016.08.011
2. **Ankana Kakoti**, Mohd Farhan Siddiqui, Pranab Goswami. Low cost design and fabrication method for developing a leak proof paper based microfluidic device with customized test zone, Biomicrofluidics 2015; 9:1-11.
3. Somasekhar R. Chinnadayyala, **Ankana Kakoti**, Mallesh Santhosh, Pranab Goswami A novel amperometric alcohol biosensor developed in a 3rd generation bioelectrode platform using peroxidase coupled ferrocene activated alcohol oxidase as biorecognition system. Biosensors and Bioelectronics 2014; 55: 120-126.
4. Mallesh Santhosh, Somasekhar R. Chinnadayyala, **Ankana Kakoti**, Pranab Goswami, Selective and sensitive detection of free bilirubin in blood serum using human serum albumin stabilized gold nanoclusters as fluorometric and colorimetric probe. Biosensors and Bioelectronics 2014; 59: 370–376.
5. **Ankana Kakoti**, Pranab Goswami. Heart type fatty acid binding protein: Structure, function and biosensing applications for early detection of myocardial infarction. Biosenors and Bioelectronics 2013; 43:400–411.

6. Pranab Goswami, Soma Sekhar R. Chinnadayyala, Mitun Chakraborty, Adepu Kiran Kumar, **Ankana Kakoti**. Applied Microbiology and Biotechnology 2013; 97:4259-4275.
7. **Ankana Kakoti**, Adepu Kiran Kumar, Pranab Goswami. Microsome-bound alcohol oxidase catalyzed production of carbonyl compounds from alcohol substrates. Journal of Molecular Catalysis B: Enzymatic 2012; 78:98-104.

Patents Filed

1. **Ankana Kakoti**, Pranab Goswami (2015). Title of the invention: DNA aptamers specifically binding to human heart type fatty acid binding protein (FABP3). Application No. 1287/KOL/2015.
2. **Ankana Kakoti**, Mohd Farhan Siddiqui, Pranab Goswami (2015). Title of the invention: Paper based microfluidic analytical device with prefabricated customized test zone. Application No. 1365/KOL/2014.
3. **Ankana Kakoti**, Mohd Farhan Siddiqui, Pranab Goswami (2014). Title of the invention: Leak proof paper based analytical microfluidic device and process for its preparation. Application No. 1126/KOL/2014.

Abstracts published in Conferences

1. **Ankana Kakoti**, Pranab Goswami. Aptamer based detection of HFABP in clinical samples for assessment of myocardial infarction, Asian Congress on Biotechnology-2013 organized by The Asian Federation of Biotechnology, 15-19 December, 2013 in New Delhi, Abstract No. 341.

2. **Ankana Kakoti**, Pranab Goswami. Alcohol oxidase from Aspergillus terreus as a potential biocatalyst for the production of fragrance compounds. International Conference on New Horizons in Biotechnology (NHBT-2011), Trivandrum, November 21-24, 2011, Abstract No IB-9, p 88.
3. Mallesh Santhosh, Somasekhar R. Chinnadayyala, **Ankana Kakoti**, Pranab Goswami. Human serum albumin stabilized gold nanoclusters as a novel fluorescent and colorimetric probe for the detection of bilirubin-IX. 24th Anniversary World Congress on Biosensors (Biosensors 2014) organized by Elsevier in association with Biosensors & Bioelectronics, at Melbourne, Victoria, Australia 3001, during 27-30 May 2014. Abstract No.P2-148.

Appendix

Table A1: List of Bacterial Strain

Strain	Description
Escherichia coli DH5α (Novagen)	F'ϕ80dlacZΔM15 Δ (lacZYA-argF) U169 endA1 recA1 hsdR17 (rk^-mk^+) deoR thi-1 phoA supE44 λ^- gyrA96 relA1
Escherichia coli BL21 (DE3) (Novagen)	F^- ompT $hsdS_B$ (r_B- m_B-) gal dcm (DE3). Derivation of B834. (Parental strain: B834; Resistance: none)

Table A2: Culture medium for bacteria

Luria Bertani broth (LB) (1 L)	Casein enzymic hydrolysate 10 g, Yeast extract 5 g, NaCl 10 g, pH 7.5±0.2
Luria Bertani agar (LB) (1 L)	Casein enzymic hydrolysate 10 g, Yeast extract 5 g, NaCl 10 g, Agar 15 g, pH 7.5±0.2

Table A3: List of Buffers and Solutions

Buffers /solutions for protein purification

Binding buffer	50 mM sodium phosphate, 500 mM NaCl, pH 8.0
Washing buffer	50 mM sodium phosphate, 500 mM NaCl, pH 8.0
Elution buffer	50 mM Tris-HCl, 10 mM L-glutathione, pH 9.0

Buffers/solutions for SDS-PAGE

30 % acrylamide-bisacrylamide solution (100 ml)	29.2 g Acrylamide, 0.8 g Bisacrylamide
Tris-HCl, pH 6.8, 0.5 M 100 ml)	6.06 g Tris base, pH adjusted to 6.8 with 2 N HCl
Tris-HCl, pH 8.8, 1.5 M (100 ml)	18.18 g of Tris base, pH adjusted to 8.8 with 2 N HCl
Gel running buffer (10X)	30.0 g of Tris base, 144.0 g of glycine, and 10.0 g of SDS in 1000 ml of water.
SDS gel loading buffer (2X)	100 mM Tris/HCl (pH 6.8), 4% (w/v) SDS, 0.2% (w/v) Bromophenol blue, 20% (v/v) glycerol, 200 mM DTT or β-mercaptoethanol
Staining solution (blue silver staining) (100 ml)	10 ml ortho phosphoric acid, 10 g w/v ammonium sulfate, 0.12 g w/v CBB G250, 20 ml methanol and 70 ml water.

Buffers/solutions for Western Blot

Phosphate buffer saline (PBS)	11.5 g Di-sodium hydrogen orthophosphate, 2.96 g Sodium dihydrogen orthophosphate, 5.84 g Sodium chloride, pH 7.5.
Phosphate buffer saline with Tween 20 (PBST)	PBS containing 0.1 % Tween 20
Transfer buffer	25 mM Tris base, 39 mM glycine, 20% (v/v) methanol
Ponceau solution (Sigma)	0.1 % PonceauS in 5 % acetic acid
Blocking solution	5 % BSA in PBST

Solution for competent cell preparation

Transformation and storage solution (TSS)	10 % (wt/v) polyethylene glycol, 5 % (v/v) dimethyl sulfoxide and 50 mM $MgCl_2$ in LB broth, pH 6.5

Solutions for Plasmid Isolation

Solution I	50 mM glucose, 25 mM Tris/HCl buffer (pH 8.0), 10 mM EDTA (pH 8.0)
Solution II	0.2 N NaOH, 1 % SDS

Solution III	5 M potassium acetate, pH adjusted to 4.8 with acetic acid

Solutions for SELEX

Binding buffer	50 mM sodium phosphate buffer, pH 7.4, 50 mM NaCl, 5 mM KCl, 2.5 mM MgCl2
Coupling buffer	20 mM Tris HCl, pH 7.5, 0.5 M NaCl, 1 mM EDTA
TBE buffer (5X)	54 g of Tris base, 27.5 g of boric acid, 20 mL of 0.5 M EDTA (pH 8.0)
6 % TBE gel (12 ml)	3.4 ml 30 % acrylamide-bisacrylamide solution, 2.4 ml of 5X TBE, 200 µl APS, TEMED 10 µl and 6.4 ml water.

Table A4: List of Antibody

Name	Source/Type	Working condition	Working dilution	Use
Monoclonal Anti-Glutathione-S-Transferase (GST), IgG_{2A} (Sigma)	Rat/ monoclonal	Room temperature	1:1000	Immunoprecipitation, ELISA, WB

Monoclonal Anti-human FABP3, IgG_{2A}, (R&D Systems, MAB1678)	Rat/monoclonal	Room temperature	1: 1000	WB, Immunohistochemistry
Anti-rat IgG HRP conjugated (R&D Systems HAF005)	Goat/polyclonal	Room temperature	1: 3000	WB, ELISA

Table A5: List of Primers

Name	Sequence
Primers for cloning	
FABP3	Forward: 5'CATGGATCCATGGTGGACGCTTTCCTGG3'
	Reverse: 5'CGCCTCGAGTCACAATGCCTCTTTCTCATA3'
FABP1	Forward: 5'CATGGATCCATGAGTTTCTCCGG CAAGT3'
	Reverse: 5'CGCCTCGAGTTAAATTCTCTTGCTGAT3'
FABP4	Forward: 5'CATGGATCCATGTGTGATGCTTTTGTAG3'
	Reverse: 5'CGCCTCGAGTTATGCTCTCTCATAAACTCT3'
FABP7	Forward: 5'CATGGATCCATGGTGGAGGCTTTCT GT3'
	Reverse: 5'CGCCTCGAGTCACAATGCCTTCTCATAGTG3'
Primers for PCR during SELEX	

F1	5’-CAC CTA ATA CGA CTC ACT ATA GCG GA-3’
R1	5’-biotin-GCA AGC TTG TTC GAG CCA G-3’
	5’-GCA AGC TTG TTC GAG CCA G-3’

Table A4: List of Antibiotic

Name	Stock Conc. (mg/ml)	Solvent	Working Conc. (µg/ml)
Ampicillin	100	Water	100